A STUDY OF PRECIPITATION OVER THE U.K. AND IRAQ USING SATELLITE PHOTOGRAPHS

BY

Mudhaffar Abbas Al-Ta'ee

MASTER OF PHILOSOPHY

University of Edinburgh

January, 1983

ABSTRACT

The main objective of this thesis is to develop a model to estimate daily rainfall over a meso-scale area of Iraq using satellite photographs.

The model depends on a statistical comparison between six parameters, three of which are determined subjectively from satellite photographs, namely cloud type, cloud amount and cloud-top temperature, and the other three are calculated numerically from conventional observations i.e. Rackliff Index, relative humidity and synoptic weather pattern.

Algebraic manipulation of these parameters is then carried out to produce a measure of rainfall prediction index and a statistical analysis is made of a set of rainfall prediction index values evaluated against daily values of rainfall to formulate a linear regression equation for the daily rainfall estimation.

The model has been applied first over Scotland because of the availability of the data and also because a similar work (not identical) has been carried out by Barrett (1973) in the British Isles and the results were encouraging.

The model was adopted for Iraq for December 1978 and February 1979 and the linear correlation coefficient between the prediction index and daily rainfall was .90 .

The verification of the model was applied for January 1979 and the results were encouraging showing that the number of correct estimation/forecast exceeds the number of those incorrect by the ratio 3:1. Defects are discussed and guidelines for improving the model suggested.

ACKNOWLEDGEMENTS

I would like to express my sincere thanks to Dr. D. H. McIntosh (Head of Meteorology Department) for giving me the chance to pursue my studies in the Department of Meteorology and for his continuous encouragement and suggestions.

I wish to thank Dr. K. J. Weston for his supervision of this thesis and for his patience, assistance, constructive criticism and detailed correction.

Thanks also to Dr. R. S. Harwood for his invaluable comments, interest and computer programming help.

Special thanks to the late Dr. A. S. Thom for his crucial advice at the first stage of this work.

Thanks to all members of the Department of Meteorology.

Thanks to my friend Graham for reading the manuscript.

Sincere thanks to the Government of Iraq for giving me the financial support during my studies in the Department of Meteorology, University of Edinburgh.

CONTENTS

LIST OF FIGURES

CHAPTER ONE

A REVIEW OF DIFFERENT METHODS OF RAINFALL ESTIMATION USING SATELLITE DATA.

1.1 Introduction

A review of different methods for estimating and forecasting the precipitation over a station (point) and an area using geostationary and polar-orbiting meteorological satellite data is presented in this chapter.

Precipitation estimations have to meet a variety of requirements in the different fields of the national economy. Thus, for agricultural purposes rainfall data are mainly needed over long periods of time such as weeks or months, and over fairly large areas. In this case the data collecting efficiency is of secondary importance. On the other hand, for normal operation of hydropower installations of hydraulic structures, and for the solution of some hydrological problems, data are required on the precipitation occurring over rather shorter time intervals (days), and often over limited areas, such as river basins of a few hundreds or even tens of square kilometers; in this case the information has to be secured as quickly as possible, especially if the precipitation intensity is high. Similar data are also required even more quickly, in connection with dangerous natural phenomena - floods, sudden rises in the level of rivers and reservoirs, lakes, etc.

The requirements of the weather forecasting services for the general public are different. Here the main object is to collect, in a simple and efficient manner, simultaneous precipitation data on a country-wide scale for a short period of time such as a few hours.

The hydrometeorological services of the U.S.A. U.K. and elsewhere are currently carrying out technical improvement in the observational network. The aim of these improvements is to establish an overall system of observation and of data collection, transmission and processing, which would efficiently provide detailed meteorological information on a country wide scale.

The prevailing method of measuring precipitation at a surface network of raingauges and pluviographs, which requires much instrumentation, is highly inefficient and does not easily lend itself to automated collection, processing and transmission of the information. Furthermore, a dense network of this type requires large investments, operational cost and manpower. Even then processing, transmission and centralization of information are difficult.

Studies carried out in the U.K. and other countries have shown, in principle, that it is possible to estimate rainfall at a station or over an area by using satellite images.

The satellite methods of measurement provide the means of obtaining, from a single image, precipitation

data of one station and/or covering an area of synoptic scale or meso-scale, and therefore offers an economic advantage and simplifies the collection, transmission and processing of the data.

The following is a review of different methods for estimating and measuring the precipitation over a station (point) and an area using satellite data.

1.2 Committee on Space Research (COSPAR).

In COSPAR (1967) there are described three methods for inferring precipitation from radiation measurements.

a. Passive methods: The differentiation of precipitating cloud and underlying water or land surfaces, exploiting differences in the emitted radiation of the cloud (raindrops) and background surfaces.

b. Active methods: The differentiation of precipitating cloud and underlying water or land surfaces, exploiting differences in reflection characteristics of the cloud (raindrops) and the background surfaces.

c. The differentiation of space characteristics (emissivity, temperature) of surfaces exposed to precipitation and those over which precipitation did not occur.

Since all precipitation is accompanied by cloud, it is important to operate at wavelengths at which clouds can be partly penetrated, or at least where precipitating clouds can be distinguished from non-

precipitating clouds. This is not the case in the visible portion of the spectrum nor in the commonly used infrared portion of the spectrum. At these wavelengths only the top part of the cloud is sensed.

1.2.1 Microwave Radiation from Precipitating Clouds.

At wavelengths longer than 1.6cm. a cloud-free area is almost transparent. Moreover, cirrus clouds as well as fog and haze will in general be transparent and radiation will, therefore, be received from the underlying surface.

Reflected radiation from precipitating and non-precipitating cloud was investigated by Dennis (1963) using a technique which allows identification of rain areas using satellite-based radar. It is a specific active method for detecting rain.

The emitted radiation from clouds has been investigated by Lethbridge (1967) and Lethbridge and Panofsky (1969) who came to the conclusion that the probability of precipitation from a cloud field increases:

i) with decreasing temperature as measured in the infrared wave band (8-12 μm), or

ii) with increasing cloud brightness in the visible wave band (4-7 μm).

They made no attempt to estimate actual amount of rainfall although they did discriminate between the amounts greater and less than 0.1cm.

Dense rain clouds, on the other hand, will appear rather opaque (Kellogg et al (1964)) but microwaves at 3cm wavelengths and longer will typically penetrate several kilometers into the cloud's mass, so that the cloud temperature measured will be an average over a good fraction of cloud thickness. Since most land surfaces have rather high emissivities but are not completely "black", it is extremely difficult to distinguish the colder, but "black" rain clouds from somewhat warmer but less "black" land surfaces.

There have also been many attempts to use satellite-borne passive microwave radiometers to measure emission in the centimetre region from minor atmospheric constituents. These methods are rather costly and they have limitations which will be discussed in chapter two. The first satellite carrying a multi-channel radiometer with the four wavelengths of 8.5, 3.4, 1.35 and 0.8cm was COSMOS-243, launched in 1968. The long wavelength channels (8.5, 3.4cm.) were used to determine the surface temperature, and the short wavelengths for estimating integrated water vapour content and cloud water content. No explicit attempt was made to separate raining from non-raining clouds, although regions with integrated cloud water content exceeding $0.5 kgm^{-2}$ were regarded as regions likely to produce precipitation (Akvilonova et al. 1971). The physical reason for the difficulty in separating rain-size drops from cloud-size drops is that they both yield comparable attenuation

per unit of integrated liquid water, except for a slight enhancement for drops with diameters comparable with the wavelenghts.

In addition, the Electrically Scanning Microwave Radiometers (ESMR) which was launched on Nimbus-5 and operated at 1.55cm. with resolution of about 25 x 25km. and radar PPI (Plan Position Indicator) with resolution of about 4 x 4km. at McGill University (Montreal) were used to evaluate rainfall rate (Smith and Kidder,1978). Radar signal calibration and satellite orbit attitude are not taken into account in their technique.

Allison et al. (1974), used the ESMR Temperature Humidity Infrared Radiometer (THIR) and DMSP (Defence Meteorological Satellite Program) satellite imagery to study a group of 1973 cyclones. Using a storm model consisting principally of a constant rain rate below the freezing level, no cloud, and saturated air below the freezing level, they delineated three categories (light, moderate and heavy) of rainfall rates. Rao et al. (1976) and Alder and Rodgers (1977) used the ESMR only to evaluate the rainfall rate over the oceanic areas by distinguishing between the microwave attenuation over a vast area of cloud and cloud free over ocean. This method has been developed by Kilonsky and Ramage (1976) and Scofield (1977) by using the ESMR and ground based observation. They have come to the conclusion that the ESMR and the ground based observation can give a direct physical indication of rainfall not only over ocean

but also over land. Details of the method of Rao et al. (1976) and its extension by Kilonsky and Ramage (1976) will be discussed in chapter two.

Wilheit et al. (1977) continued the same work of Allison et al. (1974) but with a slightly different rainfall model. They obtained a quantitative relationship between microwave temperature and rainfall rate. Using radar as ground truth, they obtained agreement to within $\pm$ 100% for rainfall in the range of $1\text{-}25 mm hr^{-1}$, when comparing with averaged radar data for four satellite passes. In 1975 the Nimbus-6 satellite was launched, using the long wavelength channel (0.81cm) with a resolution on the ground of 44 x 20km. The higher frequency was used to increase the contrast between water vapour and liquid water, and this improves the ice identification (Wilheit, 1975). Lovejoy and Austin (1980) have attempted to examine the accuracy of radiometer based techniques, for measuring instantaneous rainfall rates. Using some GATE (Global Atmospheric Research Programme (GARP) Atlantic Tropical Experiment), radar-based computer simulations, Nimbus-7 microwave radiometers products and Thermodynamic data, they were able to estimate the potential accuracy of a microwave brightness-temperature to rainfall rate conversion as $\pm$ 70%.

Satellite microwave radiometers have been used also to detect areas of earlier rainfall through the relatively low reflectivity of wet surface (Hope, 1966).

Quantitative estimates of rainfall using Hope's technique would, however, be difficult to obtain because of the different wettability and radiation 'signature' of soil, rock and vegetation surfaces.

As a consequence of the limitations and difficulties mentioned above (some more limitations and difficulties will be discussed in detail in chapter two) another method of study has evolved. This is the one using statistical techniques which has generally provided results not only acceptable and encouraging but at a lower cost. These methods are of special value to developing countries. Most of these methods (statistical methods) need simple satellite images (visible and infrared), a certain number of raingauge measurements and some skills and experience in analysing satellite images.

1.3 Satellite Images and Rainfall Estimates.

There have been many attempts to use sattelite images to estimate and forecast the rainfall over a station and an area.

In 1967, it was thought that during the period 1968-1971, satellite observations would allow 12-hourly estimates of rainfall intensity to be made on a scale of "light", "moderate" or "heavy" (WMO, 1967).

The satellite observations of rainfall estimates fall in two groups:

(a) Studies of emitted and reflected radiation from precipitating and non precipitating clouds using

microwave radiometers and ground based observations (as has been mentioned in item (1.2.1))

(b) Studies of satellite images (visible and infrared) and conventional observations in order to make a statistical relationship between them.

The author is going to follow this aspect in his work.

Let us now consider group (b) in some detail. The statistical techniques generally involve the following four important steps:

(i) Determination of total extent of cloudiness

(ii) Types of clouds and the percentage area occupied by each.

(iii) The probability and intensity of rain that can be expected from each type of cloud, and

(iv) An integration of all the above three factors into a rainfall model.

What is involved in this procedure is:

(a) a somewhat subjective assessment of the main types of clouds and their extent from either satellite cloud pictures or from the nephanalysis, and

(b) assessment of the rainfall potential of different types of clouds over the area or station (point) concerned based on comparison with actual rainfall values.

Studies seeking to estimate daily and longer period rainfall over a station and an area in different parts of the world have used data in four ways:

(1) the graphical time series relationships between daily values of total cloud cover obtained from nephanalysis and daily averaged rainfall over a network of stations were studied. Johnson (1969), examined the relationship between an index of cloudiness (based upon satellite observations for a single 5^{o} grid square covering East Pakistan) and the average daily rainfall at stations within the area. Cloud indices were derived from ESSA products showing more details than those available for operational uses.

(2) the total monthly precipitation at selected points from nephanalyses using values of mean monthly cloud cover and cloud type categories was estimated, to each of which were ascribed a probability and intensity of rainfall (Barrett, 1970, 1971). Barrett uses satellite nephanalyses to estimate monthly rainfall for the area 90^{o} to 180^{o}E, 15^{o}N to 15^{o}S. He derived an overall rainfall coefficient based on three criteria:

a. mean monthly percentage of cloud cover derived from nephanalyses

b. probabilities of rainfall from the neph cloud types "drawn up to quantify scientific intuition", and

c. intensities of rainfall from the different cloud categories drawn up in the same way. Barrett's contingency table relating estimated precipitation to recorded precipitation, on a monthly average

basis, shows considerable skill and it is for operational purposes.

(3) Meteorological data have been employed to estimate the daily rainfall over a network of stations from satellite pictures using the percentage cover of certain cloud types, to each of which are attributed a probability and intensity of rainfall (Follansbee, 1973). Simple techniques for estimating the average daily rainfall over sub-synoptic areas in the tropics and subtropics are described by Follansbee. The procedure is to determine the percentage of a given area covered by each of three rain-producing cloud types (cumulonimbus, nimbostratus, and cumulus congestus); these percentages are multiplied by empirically established coefficients to obtain the rainfall contribution to be expected from each cloud type. The method was tested for Zambia, Thailand, California, Florida and south Central United States; results were encouraging. Follansbee's technique is for operational purposes. He has also derived weighting factors for the adaptation of the technique to the heavy rainfall stations in India.

(4) The fourth use of data has been to estimate total daily precipitation at extra-tropical stations using wind vectors on a fixed surface to define an area in which the following three variables are determined (Barrett, 1972, 1973).

a. The conventionally-viewed dominant macroscale organisation of advected weather

b. The proportion of the advancing atmosphere covered by cloud

c. The predominant nephanalysis cloud type category occurring within item (b).

Gerrish (1970) obtained significant correlation between average cloud cover, as determined from once-daily satellite mosaics, and mean daily rainfall over south Florida for June 14 to October 22, 1978. The average cloud cover also correlated well with the number of stations receiving rain and with the average relative humidity between the 700 and 500mb. levels.

Scherer and Hudlow (1971) developed a technique to estimate rainfall from weather radar echo characteristics (ie., area of iso-echo at different pressure heights). Their scheme was designed to extend the range of two 3cm weather radars across the Barbados oceanic area (Barbados Oceanographic and Meteorological Experiment "BOMEX"). It builds upon a relationship between echo characteristics and precipitation established for that area of interest. The characteristics of the radar echos over an area beyond the radars ranges is inferred from NIMBUS 3 satellite images (infrared) which have been converted from temperature to equivalent pressure height using near-by temperature soundings. Their data are divided into three weather regimes, undisturbed,

intermediate and disturbed. The undisturbed regime - no appreciable cloud area higher than a height of 450mb above Mean Sea Level (MSL); the intermediate regime - no appreciable cloud area higher than 650mb above MSL; and the disturbed regime - appreciable cloud area at the 650mb above MSL and above. Total iso-echo area for each weather regime is taken as ½ of the cloud amount observed by NIMBUS 3 infrared images. Precipitation over the area beyond the radars ranges is estimated from the derived echo characteristics and a three-dimensional echo model that relates precipitation to the echo isoline areas.

Gruber (1971) used a simple relation in which the percentage of a synoptic area covered by deep convection is the principal contributor to short-period rainfall estimation (about one hour or less). His method did not necessarily require satellite imagery; however, in the single case for which Gruber used satellite pictures to delineate the active convection areas, he obtained reasonable short-period rainfall estimates.

Woodly and Sancho (1971) and Woodly, Sancho and Miller (1972) related enhanced brightness in satellite cloud pictures to rainfall echo from ground radar and conventional rainfall measurements. It was found for meso-scale areas, that the correlation between echo intensity and satellite images of the same area was best when a cloud mass was young and poorest when it was old.

In an extensive study of the South Asian summer monsoon which was carried out by Hamilton (1973), a model has been developed to forecast daily rainfall over Madras

(80° 11′E, 13° 00′N), and Calcutta (88° 20′E, 22° 32′N). Cloud features were analysed (cloud cover, cloud texture, cloud brightness, cloud size and day-to-day persistence) using ESSA digital products. Hamilton then found the statistical relationship between the cloud features and daily rainfall in order to formulate regression equations for daily rainfall estimates. The correlation coefficients were higher than 80% and more than three quarters of all the forecast were in the correct category (right or wrong). This model uses detailed digital satellite cloud data which cannot be derived easily from simple satellite cloud photographs.

Barrett (1975) realised that in many instances better results could be obtained by combining information from different types of sensor sources.

Several schemes using visible and infrared imagery have been devised and have been reviewed, summarized and criticised by Martin and Scherer (1973) and Barrett (1974, 1981). Since 1973, most of these schemes have been improved and modified.

Reynolds et al. (1978) and Lovejoy and Austin (1979) exploited the fact that whereas the cloud top temperature is a measure of cloud height, the visible brightness tends to be more a measure of cloud thickness. Consequently a low (cold) temperature value together with high brightness is indicative of precipitating cloud while low (cold) temperature coupled

with low brightness is indicative of cirrus alone.

Similarly, a diagnostic method to estimate rainfall over large space and time scales by the use of geostationary (GOES) visible or infrared satellite imagery has been derived by Griffth et al. (1978). This method is based on the finding that areas of active convection and rainfall in the tropics are brighter or colder on the satellite visible or infrared images than inactive regions. It has been argued quite plausibly that the rainfall intensity from convective clouds can be determined from a life history of the area of convective cloud.

Scofield and Oliver (1977) used a sophisticated decision-tree method of rainfall estimation. This method, called a man-machine mix technique, enables a meteorologist to estimate point rainfall rates on the basis of the two preceding half-hour sets of Geostationary Operational Environmental Satellite (GOES) infrared, visible data and the synoptic charts. With some skill, the areas of more intense rain can be determined. They include, as determinants of rainfall, cloud-top temperature, rate of anvil growth, and over-shooting tops.

Stout et al (1979) estimated rainfall during the Global Atmospheric Research Program (GARP), Atlantic Tropical Experiment (GATE) from either visible or infrared images of a geostationary satellite. Rain is estimated from cumulonimbus cloud or cloud ensemble area by a

correlation equation, namely $R = a_o A + a_1 (dA/dt)$. R is volumetric rainrate (m^3/s) for a particular cloud, A is the area of the cloud at time t (t in second), (dA/dt) is cloud area change, and a_o and a_1 are empirical constants.

Browning (1979) described a method of short range (0-6 hr) forecasting of rainfall using satellite and radar data with the help of simulated computer model together with man's experience and skills.

The most frequently used variables in precipitation forecasting models are the type and amount of clouds at the beginning of the forecasting period. Ideally, areas where these variables do not change significantly during the first 12-18 hours of the 24 hour forecast period should be considered. However, over the Middle East, wintertime precipitation is advectional and convectional and associated with relatively small diurnal variation in the field of cloudiness.

During winter in the subtropical zone of Iraq, the convective clouds are associated with cyclones and active fronts approaching from the Mediterranean sea and neighbouring areas. Therefore the convective cloud over this area is embedded in the advectional system (see chapter 4). Basically, convectional systems over Iraq in this respect are different from the isolated convection that develops in the lower latitudes where diurnal variations are dominant.

In the next chapter, the rationale behind the choice of the statistical method adopted for this study will be discussed.

CHAPTER TWO

CRITICAL APPRAISAL OF DIFFERENT METHODS.

2.1 Introduction

In order to develop a suitable model for estimation of daily rainfall over a meso-scale area of Iraq using satellite data, one should review and critically assess the merits and demerits of the existing methods. Since the model is meant to be used operationally, it is important to bear in mind the technical and scientific infrastructure as well as facilities for reception of satellite data available in Iraq. While it is difficult to assess precisely in all cases, it is desirable not to ignore the cost-benefit ratio. A critical review of the existing methods leading to the choice of one of them for further development is presented below.

2.2 Microwave Radiometry.

2.2.1 Merits.

The various possibilities for remote sounding observation of some important atmospheric and oceanic parameters by means of microwave instrumentation are discussed in this section.

Historically there is no doubt that meteorological radar was in use for instantaneous rainfall rate estimation in many advanced countries before the satellites arrived on the scene. But it is a fact that many developing

countries still do not have such facilities.

Meteorological radar sees micro- and meso- scale areas only, but provides quite accurate rainfall rate evaluation and identifies areas of precipitating and non-precipitating clouds (Browning, 1980).

Quantitative estimates of rainfall using satellite-microwave radiometers also show reasonable accuracy (see chapter one). So, sattelite-microwave radiometers have to share the scene with radars in order to produce better results.

A Scanning Multichannel Microwave Radiometer (SMMR) was flown on Nimbus-7, launched in 1979. The SMMR can be applied to the extraction of quite a large number of parameters: in the case of the ocean, sea surface temperature and near surface wind; in the case of atmosphere, water vapour content, cloud liquid water content and instantaneous rainfall intensity; in polar regions, various ice parameters, and in the case of land surface, snow and soil moisture parameters. Measurements by the SMMR are expected to give an accuracy of $\sim$1.5 deg.k for sea surface and 2.0 m/s for surface wind speed (see Cracknell, 1981).

Microwave radiometers have been particularly successful in delineating sea ice and open water at certain frequencies because of their different emissivities. The Electrically Scanning Microwave

Radiometer (ESMR) of Nimbus-5 has been used successfully to map open water in the Antarctic. Ice bergs and sea ice appear in strong contrast against the sea background. It is also possible to differentiate between first-year ice and older ice.

Having presented a birds eye view of different potentialities of satellite borne microwave radiometers and radar for extraction of useful atmospheric and oceanic parameters, estimation of rainfall from satellite data, which is the topic of this thesis, will be discussed below.

Wilheit et al (1977) have used the ESMR and Temperature and Humidity Infrared Radiometer (THIR) to obtain a quantitative relationship between microwave temperature and rainfall rate. The "Freezing Level" forms the key feature of their work. It is assumed that up to this level, there is a constant lapse rate (6.5 K/Km) and a linear relative humidity profile varying from 80% at the surface to 100% at the freezing level. There is a small cloud component 0.5 Km thick, of density 0.5 g/m^3 below the freezing level, with a constant rainfall attenuation per unit length from the surface to the bottom of the cloud layer. Results were shown in chapter one. The above assumption will be compared with other cloud model assumptions in order to judge their relative merits.

A cloud water content of 0.5 g/m^3 was found

for an average non-raining cumulus (Fletcher 1962) although Kessler and Atlas (1959) get values between 0.1 g/m^3 and 0.3 g/m^3 depending on the rain rate (2 and 20 mm/hr respectively), and Stepanenko (1968) takes the value as 0.2 g/m^3 for a fair weather cumulus (0.1 g/m^3 for non-raining stratus) and 0.2 g/m^3 and 1 g/m^3 for cumulonimbus with rainfall rate of 1 and 20 mm/hr respectively.

For the purposes of microwave characteristics however, it is clearly the total integrated liquid water content that matters. It is here that Wilheit et al. (1977) are in disagreement with other researchers. They assume a 0.5 km cloud with 0.5 g/m^3 water density which yields an integrated liquid water content of 0.25 Kg/m^2, independent of rain rate. The Kessler and Atlas (1959) model contains a large cloud component above 0^o. If it is assumed that this is all ice (which they do not), it is unimportant in radiometry since ice is virtually transparent to microwave wavelengths. This however, is an important assumption in the Wilheit et al. (1977) model. Because it is possible for supercooled water to exist, particularly in cumulonimbus clouds, right up - 15^oc it is unrealistic to assume that the layers above the freezing level do not contribute to the integrated water content. In fact the integrated water content may have to be increased from 1 to 10 Kgm^{-2} if we provide for supercooled water in the cloud above

the freezing level. Thus the assumption of Wilheit et al. (1977) that the layers above the freezing level consist of ice only and do not therefore contribute to the microwave attenuation is not justified. A provision has therefore to be added to the model to take into account adequately the liquid water content above the freezing level.

The ESMR sensors have been used also to evaluate rain over the oceanic areas, for example, Rao et al. (1976). The basis of their work is to use the ESMR operating at 1.55cm (19.35 GHz) carried on board Nimbus-5, because the emissivity of the water in the vicinity of this frequency is low ($\sim$0.4) and is inversely proportional to the thermodynamic temperature, whereas the brightness temperature as observed by the ESMR is proportional to the product of emissivity and thermodynamic temperature.

Thus the ocean presents a convenient nearly uniform background for the satellite-borne radiometer. This technique only yields instantaneous rainfall rate.

It is feasible to apply the above technique for estimating instantaneous rainfall rate over the continent also. Kilonsky and Ramage (1976) and Scofield (1977) have improved the techniques of Rao et al (1976). They used Nimbus-6 (ESMR) operating

at 0.81cm (37.0 GHz) to evaluate the rainfall rate not only over ocean, but also over land, because the underlying oceans and land present nearly uniform backgrounds for the satellite-borne radiometer.

Methods of deriving rainfall from radar and satellite radiometer observations should still be considered as experimental, since there are many limitations which have to be overcome before they can be utilized operationally. These limitations will be discussed in the next section.

2.2.2 Demerits

The aim of the author is to develop an operational model for deriving 24-hour rainfall over Iraq, largely utilizing the available infrastructure. From this point of view the satellite based microwave radiometer techniques are unsuitable for the following reasons:

i) The processed radiometer data are not regularly disseminated over the Global telecommunication network for utilization by different countries

ii) It will be necessary to set up statistical data receiving station with computers and other peripheral equipment required to process the raw radiance data. At the present stages of development of

the method, it is difficult to justify on the cost-benefit ratio.

iii) Several well trained scientists and technicians with different specializations will be required. This is not immediately feasible in many of the developing countries, where there is a shortage of scientific and technical manpower.

iv) In order to develop methods like this, it is also necessary to set up a suitable radar network for quantitative estimation of rainfall as well as a dense network of conventional observations to provide the ground truth.

It will thus be seen that very elaborate facilities and infrastructure have to be developed before such methods can be adopted for operational use. They cannot yet be justified on consideration of cost effectiveness, but they should still be considered as research routes.

The other categories of methods are those which utilize satellite cloud imagery (visible and infrared) regularly available in many parts of the world and easily accessible. Useful information is derived from these images and is quantified. These derived data together with those obtained from conventional meteorological observation are subjected to statistical analyses to result in the operationally required estimate of daily rainfall. They also take into account the

synoptic features and indirectly incorporate the local peculiarities of the area concerned. Methods of interpreting satellite cloud imagery and extraction of useful information from them have recently received much attention from researchers for the simple reason that they have the widest application. This situation encouraged the author to study in depth the available methods in this category and develop a method most suited to Iraq.

2.3 Statistical Methods.

The aim of the present review is to arrive at the selection of a method most suitable for utilization operationally in Iraq. The two factors that have therefore to be kept prominently in mind are:

1. The characteristics of weather systems that cause precipitation over Iraq, and
2. The technical facilities available in Iraq for this purpose.

Satellite images and image data are nowadays used by meteorologists in so many different ways, that it would be difficult, perhaps impossible, to list them all. Much ingenuity in analysis and application of the data is being shown in many countries with widespread enthusiasm and determination that exist to extract as much benefit from that data as possible. There is little doubt that the number and range of applications will continue to grow.

There have been two main lines of approach; one designed primarily for routine, continuous application and the other for application in selected situations, notably those in which severe storms occur.

a. In the first approach, cloud data (cloud type and amount) are related to the actual rainfall measured on the ground, typically for 24-hour periods. In an area or an occasion when conventional rainfall measurement are not available, such relationships can be utilized to estimate the likely rainfall amounts. Rainfall estimates derived in this way are supplied regularly to various international agencies for use in connection with agricultural and hydrological projects in developing countries, and also as a means of converting into potential floods or droughts, requiring emergency relief action.

b. The second approach utilizes the relationship between image brightness and rainfall. One of the most successful methods extracts cloud top temperature from enhanced infrared images and uses them in conjunction with general appearances of the same clouds to produce rainfall estimates. The underlying idea is that the higher (and colder) the cloud top temperature, the heavier the rain.

Geostationary satellite images at 30-minute intervals are used, and with various refinements the method is now capable of giving, quite quickly, a remarkably good estimate of rainfall in the vicinity of a storm (see Scofield and Oliver, 1977; Reynolds et al. 1978; Stout et al. 1979, and Lovejoy and Austin, 1979).

Image data are also being used in various methods for short- and long-period estimates of rainfall. For short-periods estimation of rainfall (up to 6-hr), the basic tool employed is radar, which can provide direct observation of rainfall intensity and rain areas, but only within a limited range. By merging satellite data with that of radar, it is possible in effect to extend the range in both space and time over which observation of rainfall can be made (Woodley and Sancho, 1971; Woodley, Sancho and Miller, 1972, and Browning, 1979). These methods depend heavily on careful control of satellite picture enhancement and precise radar signal calibration. Such control would be feasible only at centres where the sophisticated equipment required is available.

Methods for estimation of rainfall for long-periods basically depend upon average cloudiness (amount, type and other characteristics) over periods of a month or even a season. The cloud characteristics are translated into rainfall estimates. Such models,

developed by Barrett (1970, 1971), Follansbee and Oliver (1975) and Follansbee (1976), are for use in studies of regional climatology and the precipitation component of the global hydrological cycles.

2.3.1 The Method Adopted.

On the basis of a careful examination of all the available methods for rainfall estimation referred in chapter 1 and earlier on in chapter 2, the author crystalized his approach and narrowed down the choice of methods to two, namely: Follansbee (1973) and Barrett (1973). As a logical consequence the merits and demerits of these two methods will be examined in order to arrive at a method for application in Iraq. In this connection, it is worth repeating that rain-producing clouds in winter over Iraq are advectional and convective and have a relatively small diurnal variation. They are a combination of some of the features of the tropical clouds (convective clouds) and the higher latitude clouds (mainly advectional). A detailed discussion of these aspects will be presented in chapter 4.

Follansbee's method (1973) for estimation of the daily rainfall is one of the earliest operational methods based on the easily available satellite cloud imagery (Automatic Picture Transmission "APT"). This evolved from the original method of Barrett (1971) for estimation of monthly rainfall. Amongst the important modifications that Follansbee made are the

following:

a. the original stratiform category of Barrett (1971) was replaced with nimbostratus on the assumption that neither low stratus nor cirrostratus produce appreciable rain

b. similarly the cumuliform was replaced with the cumulus congestus on the basis that cumulus humilis does not make any significant contribution to rainfall. Fortunately it is easy to distinguish between cumulus congestus and cumulus humilis from the APT cloud imagery.

c. Follansbee retained the category of cumulonimbus, but by trial and error he found that the coefficient of the cumulonimbus in the Barrett's equation (1971) should be raised from 0.72 to 1.0. The coefficient of 0.25 for the stratiform and 0.02 for cumuliform originally suggested by Barrett (1971) were retained.

Among the major differences in the approach of Follansbee (1973) and Barrett (1973) is the fact that Follansbee utilized the readily available APT cloud imagery, whereas Barrett utilized a centrally produced nephanalyses prepared by the U.S. National Weather Record Centre in the U.S.A. While it is true that there is some advantage in using centrally

produced nephanalyses, which are products of experienced satellite analysts, it has also the following disadvantages.

a. A local meteorologist with long experience of observing the clouds of a particular area is certainly at an advantage in identifying the cloud categories from the satellite imagery.

b. The satellite analysts at a meteorological centre in the USA do not always have access to the ground truth that is regularly available to a local meteorologist at or near real time. This is very important in ensuring that cloud identification is as accurate as possible.

The other important difference between the two methods is in the number of cloud categories considered by them. Follansbee, whose main goal was to arrive at an easily adaptable operational method mostly for the tropics, considered only three cloud categories, but Barrett, who utilized the nephanalyses and applied his method in higher latitudes, considered a more elaborate categorisation. Follansbee's approach has the advantage that it is much easier to distinguish his three categories for the APT cloud imagery than the elaborate classification of Barrett. It should be stated that the three categories of Follansbee are adequate for the tropical

area where local convection has rapid development and dissipation and is largely responsible for heavy rain. However, in the higher latitude considered by Barrett, the rain-producing disturbances are associated with a larger number of categories of cloud system than in the tropics which have a rather small diurnal variation.

Follansbee's method utilizes afternoon satellite pictures to estimate rain amount for the period beginning on the morning of the current day and ending the next morning. This normally would prove to be a serious disadvantage for estimating 24-hour rainfall. But in the tropics where rainfall is largely convective and occurs in the afternoon and evening, the afternoon satellite pictures were able to catch the significant convective activity responsible for the rainfall of that day. However, this procedure is likely to fail in other areas where rainfall does not have such a marked diurnal variation. In areas where the advective weather systems are responsible for rainfall it is not enough if the cloud cover over the area required at a particular time is related to the rainfall over that area during the next 24 hours. It is obvious that at the commencement of the forecast period we should identify those areas of cloud most likely to affect the area concerned during the next 24 hours and then interpret them in terms of expected rainfall.

Barrett (1973) has taken this into account by selecting the appropriate quadrant of a circle up wind from the station concerned and determining the cloud in the quadrant. The choice of an appropriate wind for this purpose is the most difficult aspect of this method. In addition, Barrett had the problem that the different data required by him were not synchronized. Barrett (1973) used the forecasting for mainly advectional rain-producing clouds.

It therefore appears that a modification of Barrett's method, taking into account the fact that rainfall over Iraq is caused by a combination of advectional and convectional rain-producing clouds, will be most appropriate for the estimation of daily rainfall over Iraq.

The input to Barrett's (1973) technique was strictly limited to cloud types and amounts shown by nephanalyses and synoptic patterns from synoptic charts. However, it should be supported and modified by any tool available in order to be used operationally for Iraq. This, for example, includes temperature of the tops of clouds that may affect the area under consideration. Stability and relative humidity can also be incorporated into the Barrett technique. This aspect (modification) will be discussed in chapter 3.

Some other considerations have encouraged the author to adapt Barrett's technique for use in Iraq, namely:

a. It is easy to obtain simple satellite images (visible and infrared) for developing and verifying the model (i.e. satellite images not at or near real time).

b. METEOSAT-1 satellite images every 30 minutes make it possible to synchronize observations involved in the adapted model (see chapter 5) of rainfall estimation over Iraq.

c. The type of conventional meteorological data and satellite images (visible and infrared) required for the adapted model are easily obtainable from Baghdad Meteorological Office.

CHAPTER THREE

RAINFALL ESTIMATION FROM SATELLITE PHOTOGRAPHS OVER SCOTLAND

3.1 Introduction

In this chapter an attempt is made to develop a method of estimating daily rainfall at a selected area (Scotland) using enlarged NOAA - 5 satellite photographs (received at Dundee) and conventional observations.

Until recently, few satellite-based studies have investigated patterns of precipitation, despite their obvious importance to man, although many have sought to interpret satellite picture data in terms of other atmospheric variables measured by surface observations.

This work, is similar, but not identical, to Barrett's work in 1973. Barrett (1973) estimated the daily rainfall over Valentia ($51^{o}65'N$, $10^{o}15'W$), in the Irish Republic. He used a model involving satellite nephanalyses and certain conventional weather data, for application in a region where the rain-bearing clouds are mainly advectional, rather than convectional. Essentially, the scheme depended upon the daily selection of an appropriate cloud quadrant for the station in question and the evaluation of a "Rainfall Prediction Index" for that quadrant, embracing its synoptic weather

organisation, its mean cloud cover, and its included cloud types. The rainfall prediction index was then used to forecast a class of rainfall for the day ahead in terms of "no rain", "light", "moderate", or "heavy rain". The essential Barrett indices were specified for Valentia using data for January to June 1967. Rainfall "Estimate" were then made for July to December 1967. Verification of these forecasts indicates a ratio of approximately 3:1, when classified on a simple right:wrong basis.

The author has added three other independent parameters to Barrett's index; cloud top temperature, Rackliff index and relative humidity, which are well correlated with rainfall as we can see in the next article.

3.2 Development of the Model to Estimate Rainfall

3.2.1 Picture Analysis

To analyse any features of cloudiness around a station using satellite pictures taken once each day, a sample area must be defined.

Areal sampling is preferred to a point sample because point sampling may produce unrepresentative results in cases where the type and amount of cloudiness undergo rapid diurnal and day to day changes. The rainfall amount varies considerably with locality for the same cloudiness. With areal sampling local inhomogeneities will, to a large extent, be averaged out.

To simplify analysis of picture data and rainfall measurements, daily rainfall will be not related entirely to only one independent variable (parameter) as shown in table 3.1. This table of April 1977 data for Scotland shows some of the results of the linear correlation coefficients between the independent variables themselves and between the daily rainfall and the independent variables also. The lowest correlation coefficient is .01 between the Rackliff Index and the relative humidity. The maximum correlation of .39 is shown between cloud-top temperature and Rackliff Index. Each independent variable has been correlated with each of the five independent variables individually and shows the correlation coefficient value ranges from .1 to .39 . The daily rainfall has been correlated with each one of the six parameters individually and shows acceptable correlation ranging from .51-.69 .

The extraction of the six independent variables (parameters) mentioned above will be discussed in detail in the next article.

The present attempt is to develop a model of combined, independent variables (rainfall prediction index) for an operational use to estimate daily rainfall over a meso-scale area. The success of this model should be judged by the accuracy of results of rainfall estimates and not by its theoretical basis.

Scotland, April, 1977.

Parameters	A	B	R
Rainfall and Rackliff Index	-4.356	0.211	0.51
Rainfall and relative humidity (1000-500mb)	-6.010	0.140	0.69
Rackliff Index and relative humidity	57.035	0.025	0.01
Rainfall and cloud top temperature	-1.757	-0.634	0.58
Cloud top temperature and Rackliff Index	41.867	0.513	0.39
Relative humidity and cloud top temperature	2.623	0.059	0.32

Table 3.1 To show the linear correlation coefficient (R) between the independent (variables) parameters.

The development of a system involving satellite pictures and in situ observation for estimation of daily rainfall may be divided into the following steps:

a. The probability of daily rainfall over a meso-scale area in relation to each one of the following parameters was estimated separately: synoptic weather pattern, cloud type, cloud amount, relative humidity, cloud top temperature and Rackliff index.

b. These individual probabilities were combined to produce an overall rainfall prediction index.

c. The rainfall prediction index was related to the average daily rainfall over the chosen meso-scale area. This resulted in a model for rainfall estimation.

d. The fourth and final step consisted of applying and testing the model by estimating the rainfall for a period which had not been used in the derivation of the model.

In fact, once developed and tested, such a model might be improved as short-comings become apparent during its operational use.

3.2.2 Derivation of the Prediction Index

To simplify analysis of pictures and rainfall recordings, daily rainfall data must be correlated with each of Barrett's parameters (ie. synoptic weather pattern, cloud type and cloud cover)

and the author's parameters (ie. Rackliff index, cloud top temperature and relative humidity) (see table 3.1)

The equation of the rainfall prediction index (RR24) will thus be:

$$RR24 = Sw.Ct.C.\ (RI).(CTT).(RH\%) \quad \ldots\ldots\ldots\ldots (1)$$

$$RR24 = Sw.Ct.C.(Barrett,1973) \quad \ldots\ldots\ldots\ldots\ldots (2)$$

Where

Sw is synoptic weather pattern index;

$$Ct = \frac{I}{a}_1 + \frac{I}{b}_2 + \ldots\ldots\ldots + \frac{I}{j}_{10},$$

where $I_1, I_2 \ldots\ldots\ldots I_{10}$ are cloud type or rainfall intensity indices specifying the types of clouds observed within areas $\frac{1}{a}, \frac{1}{b} \ldots\ldots\ldots \frac{1}{j}$, of the quadrant respectively such that $\frac{1}{a} + \frac{1}{b} \ldots\ldots\ldots \frac{1}{j} = 1$; C is a cloud cover index expressing mean cloudiness within a particular cloud quadrant; (RI) is a Rackliff index; CTT cloud top temperature index and RH% is the index of the average relative humidity of 1000-500 mb. layer.

RR24 is the resulting rainfall prediction index from which rainfall can be made.

The synoptic weather pattern, cloud type and cloud cover have been explained by Barrett (1973). For example, 9 days out of 10 recorded rain at Valentia when the passage of an occluded front was indicated on the synoptic charts of the Daily Weather Report (DWR), so that the probability of rainfall is 90% for the occluded front (see table 3.2).

Synoptic weather pattern (Sw)	Rainfall probability (%)	Synoptic weather (rainfall probability index)
Frontal succession	90	9
Occluded front	90	9
Trailing cold sector	80	8
Warm front	70	7
Cold front	70	7
Warm sector	70	7
Non-frontal trough	60	6
Leading cold sector	60	6
Ridge of high pressure	30	3
Cell of high pressure	30	3
Col	20	2

Table 3.2 Rainfall probability index, synoptic weather pattern, based on the observed ratios of rain versus no-rain day associated with specific synoptic weather patterns.(after Barrett 1973).

The method of evaluation of the rainfall probability and intensity is presented by Barrett, 1970, and is called Bristol method . The idea of this method is to locate a certain cloud type over a period of time at a grid area (see Barrett 1981).

It was easy for Barrett in 1971 to locate a single cloud type in a grid area (ie. cumulonimbus, stratiform ... etc.) over a period of time in order to ascribe an index of probability and intensity to each cloud type category. The same work was done by Barrett 1973 for the Irish Republic (Valentia) and the results are listed in table 3.3.

The cloud cover/amount involved in this model is listed in table 3.4, and derived by Barrett in 1970 from ESSA nephanalysis produced in the U.S. Weather Bureau. The cloud amounts represent the average amount of cloud in percentage in the sky or a portion of sky. Barrett (1971, 1973) used the same data listed in table 3.4 to estimate rainfall over the tropical Far East and Valentia respectively.

The author here estimated the percentage of the cloud cover to the nearest 5% from the cloud quadrants projected on the NOAA-5 photographs. The idea of the author in cloud amount estimation is generally similar to that of Barrett (1970).

The Rackliff index, cloud top temperature and relative humidity which are added to Barrett's (1973)

Nephanalysis and cloud categories	Rainfall Intensity Index	Index No.
Cumulonimbus with cirrus	10	I_{10}
Cumulonimbus	9	I_9
Cumulonimbus with cumuliform	8	I_8
Cumulonimbus with stratiform	7	I_7
Layerd stratiform, stratiform with cirrus, stratiform with cumuliform and cirrus	6	I_6
Stratiform, stratiform with cumuliform	5	I_5
Cumuliform with cirrus scattered cumulonimbus	4	I_4
Cumuliform	3	I_3
Cirrus	2	I_2
Stratocumuliform	1	I_1
No cloud	0	I_0

Table 3.3 Nephanalysis cloud categories and the cloud type"rainfall intensity"(after Barrett 1973).

Key letter	% Range of cloud cover	Mean cloudiness in each category %	Nephanalysis of cloud cover category
C	80 - 100	90	Closed(or Coverd)
MCO	50 - 80	65	Mostly Closed(or Mostly Covered)
MOP	20 - 50	35	Mostly Open
O	0 - 20	10	Open
Clear	0	0	Clear Skies

Table 3.4 Nephanalysis indications of the amount of cloud cover.

model are explained below:

a. Instability Index (Rackliff Index "R.I").

Precipitation is a result of vertical motion in the troposphere; hence the vertical instability of the troposphere is of great importance. Several methods of estimating instability using the tephigram (TØ-gram), are described in McIntosh and Thom (1975). Here we are dealing only with the Rackliff index (instability index) using the TØ-gram.

Showalter (1953) introduced the "instability index" with relatively simple parameters to be used as an aid in predicting cumulus congestus and cumulonimbus. This instability index is a static measure of latent instability, computed by lifting a parcel or bubble of air adiabatically from 850 to 500 mb. The theoretical temperature of the lifted parcel is then subtracted algebraically from the environment temperature at 500 mb. Positive numbers indicate stability and negative numbers indicate instability. Galway (1956) introduced a similar index, but in which a forecast is made of temperature in the lowest layer.

Rackliff (1962) introduced an index which is little different from that of Showalter. The differences are that 900 mb. rather than 850 mb. is the level from which air is assumed to be lifted and that a 900 mb. wet-bulb potential temperature (θw 900) is used in place of the dry-bulb temperature obtained by lifting the air to the 500 mb. The formula used by

Rackliff is:

$$R.I = \Theta w_{900} - T_{500} \quad \ldots\ldots\ldots (3)$$

Where T_{500} is the 500 mb dry bulb temperature, and R.I is the Rackliff index (the threshold value over UK of R.I = 29, above which deep convective cloud are likely to occur and below which they are unlikely "see HWF, 1975". An example of the extraction of the Rackliff index from a radiosonde sounding plotted on a TØ-gram is given in figure 3.1a. The Rackliff index is preferred to Showalter's because it assumes that air is lifted from 900 mb rather than 850 mb. layer. The 850 mb layer is too high out of the moist layer at or near the surface. The 900 mb layer is more representative of air at low levels and would not be affected to any degree at night by outgoing terrestial radiation. At pressures higher than 900 mb. temperature and humidity fluctuations arising from nocturnal radiation and stratification, will be reflected in the lowest readings of midnight soundings.

b. Cloud Top Temperature

Three elements that will obviously have an important bearing on which particular mechanism is likely to be dominant in the release of precipitation from a particular cloud, or cloud system, are the cloud base temperature, the cloud thickness, and the cloud top temperature. The temperature of the base will largely control the liquid water content of the cloud, which, together with the cloud thickness will largely

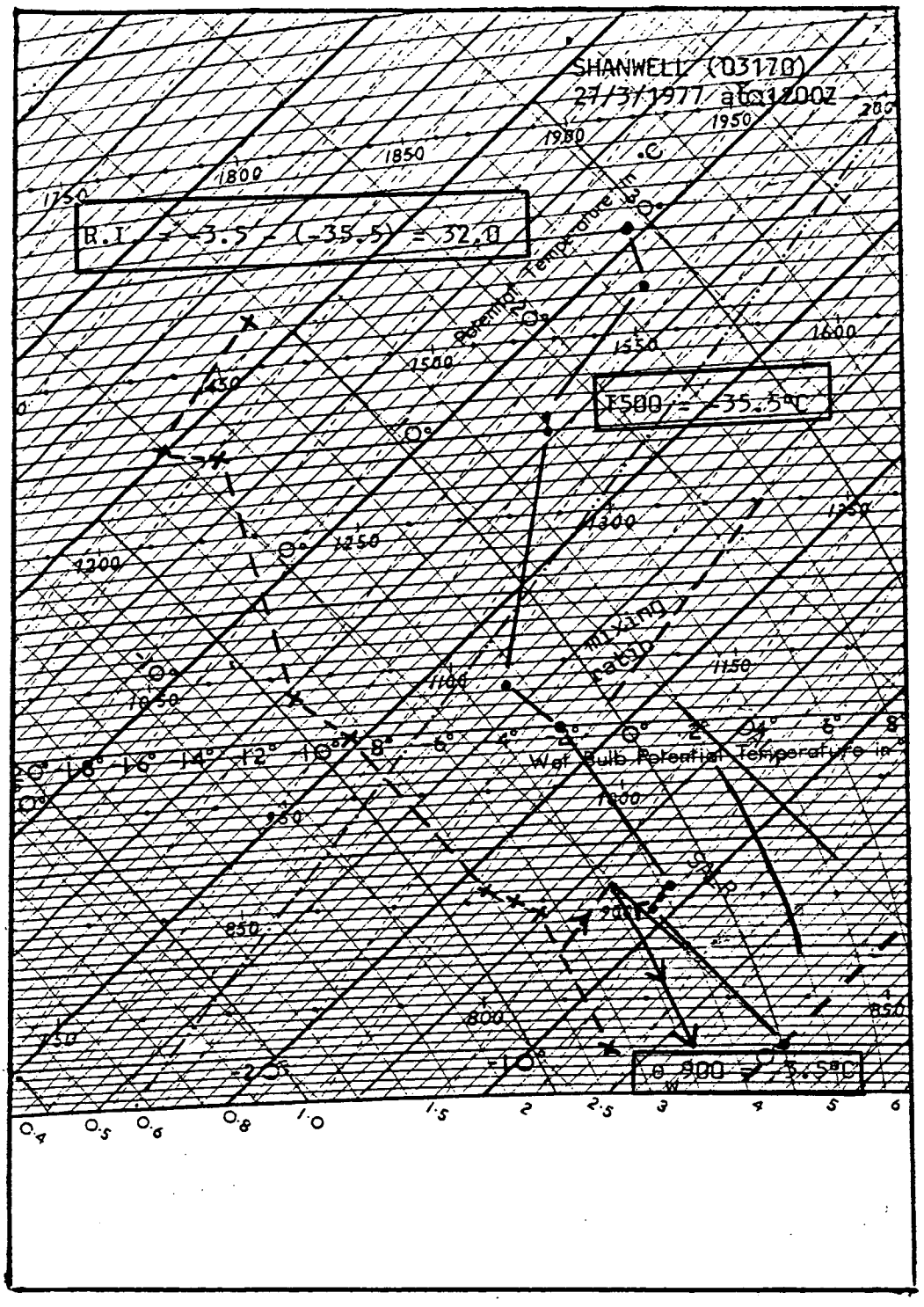

Figure 3.1a Shanwell's TØ-gram of 27/3/1977 at 1200Z. To show example of calculating Rackliff Index (RI) from the wet-bulb potential temperature at 900mb. (θ_{w900}) and the dry-bulb temperature at 500mb. (T_{500}.)

determine whether or not raindrops may be produced by coalescence, while the cloud top temperature will indicate the likely presence or absence of ice crystals.

By means of infra-red satellite photographs, the temperature of the top of clouds can be estimated. Since temperature varies with height, the infra-red essentially supplies the third dimension, namely height of cloud tops, since the visible pictures of weather satillite give only cloud coverage. Lethbridge (1967) showed that there is a negative correlation between the probability of precipitation and cloud top temperature.

April 1977 were used to estimate cloud top temperature from NOAA-5 photographs in 2^{o} square of latitude over Shanwell (03170) and midday upper-air ascent from Shanwell. April 1977 data were used for the model development and March 1977 data have been used for testing and verification.

Cumulonimbus clouds are vividly presented on satellite imagery. These cloud systems routinely extend to the tropopause height. Anvil clouds or plumes, indicating wind flow, can be seen on top of these cumulonimbus. Cumulonimbus usually form clusters (in tropics) and appear very white on satillite imagery. Sometimes, cirrus can be seen on the top of the cumulonimbus.

The cumulonimbus clouds top heights were calculated by the parcel method (for parcel method see Hess, 1959) in which a parcel of air is lifted from 950 mb. (950 mb. is used in order to avoid the super adiabatic layer or surface cooling). An example is shown in Fig. 31b for Shanwell at 1200GMT on 1 April 1977, in which that the top of the cloud reached above 6,890 metres by the parcel method and the NOAA-5 photograph (IR) shows very white spots inside the 2^{o} square latitude area over Shanwell. This is supported by the 12 GMT actual surface observation of Shanwell which reported cumulonimbus (low cloud (cl) = 9), see figures 3.1b and c.

Cumulus clouds are a very common cloud type seen on satellite imagery. These small, puffy, fair weather clouds are detected by the new very high-resolution meteorological satellites. The earlier meteorological satellite could not resolve each and every cumulus cloud.

Cumulus clouds usually have cloud tops anywhere between 1500 and 3000 metres. Cumulus clouds can form "open cell" patterns in contrast to stratocumulus "closed cell" patterns. These patterns resemble geometric shapes such as polygons or ellipses. These patterns behind cold fronts in the higher latitudes are marked as cumulus, which are easily identified on the high-resolution visual data.

Cumulus cloud top heights have been

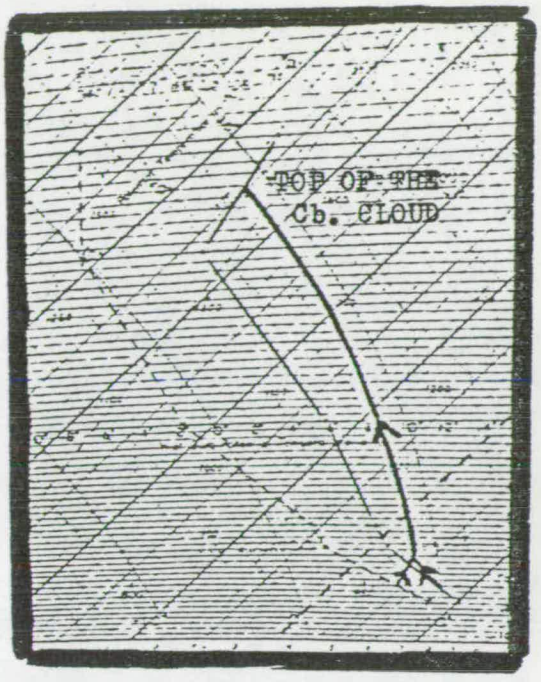

Figure 3.1b. Parcel method to extract the temperature of the cumulonimbus cloud top from Shanwell TØ - gram at 1200GMT On 1 April 1977.

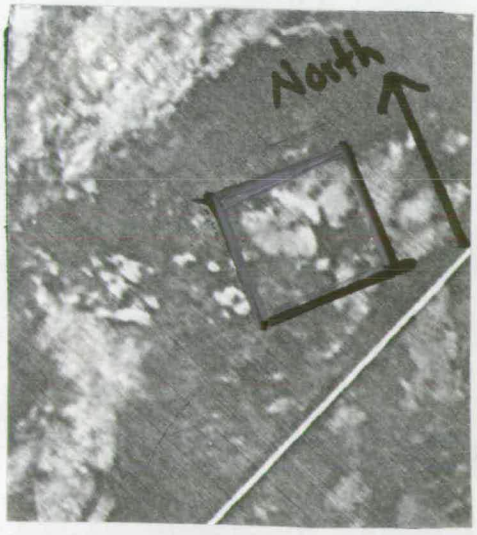

Figure 3.1c. NOAA-5 (IR), shwos very bright spots (cumulonimbus) inside the 2° square of latitudes projected on Shanwell at 1108GMT on 1 April 1977.

estimated by the identification of the level of the minimum saturation wet-bulb potential temperature (θ_s) (see Weston, 1980), for example on 17 April 1977 at Shanwell. The TØ-gram at 12 GMT showed that the minimum θ_s was at 785 mb. and the NOAA-5 photograph showed a grey shade of patchy cumulus in the 2^{o} square latitide projected over Shanwell and the actual surface observation was cumuliform cloud (low cloud (cl) = 8) see figures 3.1d and e.

Stratiform clouds are usually uniform and textured, white or grey, depending on the density and sun angle on the visible,and grey or dark grey on the infrared images. Boundaries are sharply defined and the stratiform cloud often outline the topography, such as coast lines, mountains and valleys. Figures 3.1f and g show the top of the stratus cloud.

For the stratus cloud cases the author has used his experience with the aid of TØ-grams and NOAA-5 photographs. The indicators of the top of the stratus were a distinct increase in dew point depression starting at 750 mb. for the example shown in figure 3.1f and NOAA-5 (figure 3.1g) showed very dark grey shade and the actual surface observation showed stratiform cloud (low cloud CL = 5). Rain may be expected to fall most frequently from the brightest (VIS) and coldest (IR) cloud, since this probably often has the greatest thickness and top height. Very bright cloud usually consists either of cumulonimbus cloud

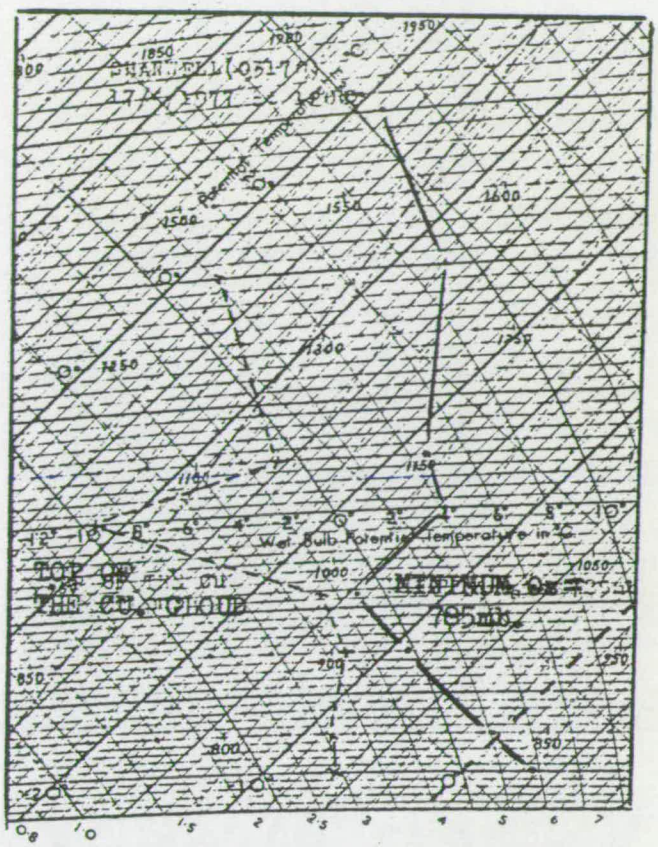

Figure 3.1d. Minimum saturation wet-bulb potential temperature(θ_s) at 785mb.represents the height of the cumulus cloud top ... (Shanwell on 17/4/1977 at 1200Z.)

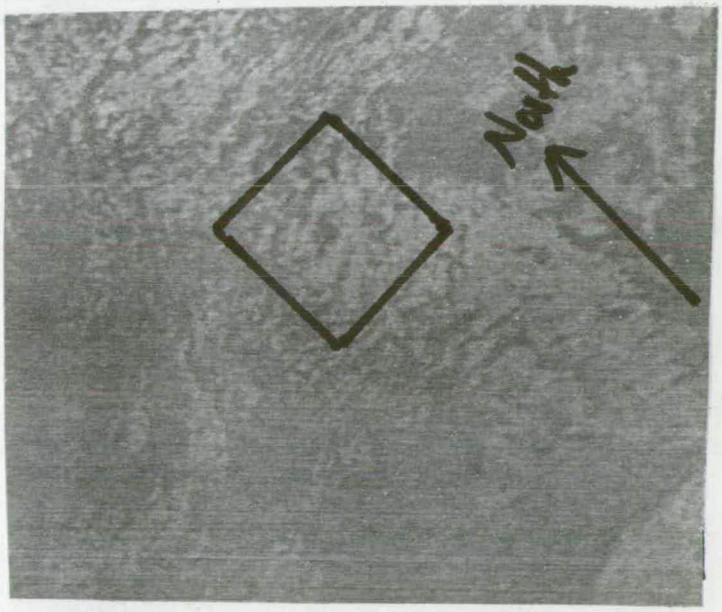

Figure 3.1e. NOAA-5(IR)- Patches of cumulus convective cloud(light grey)inside the 2^{o} square of latitudes projected over Shanwell at 0908Z on 17/4/1977.

Figure 3.1f. Shanwell TØ-gram, at 1200Z on 25/4/1977, to show the decrease of dew-point depression with height starting at the top of stratiform cloud (i.e., at 750mb).

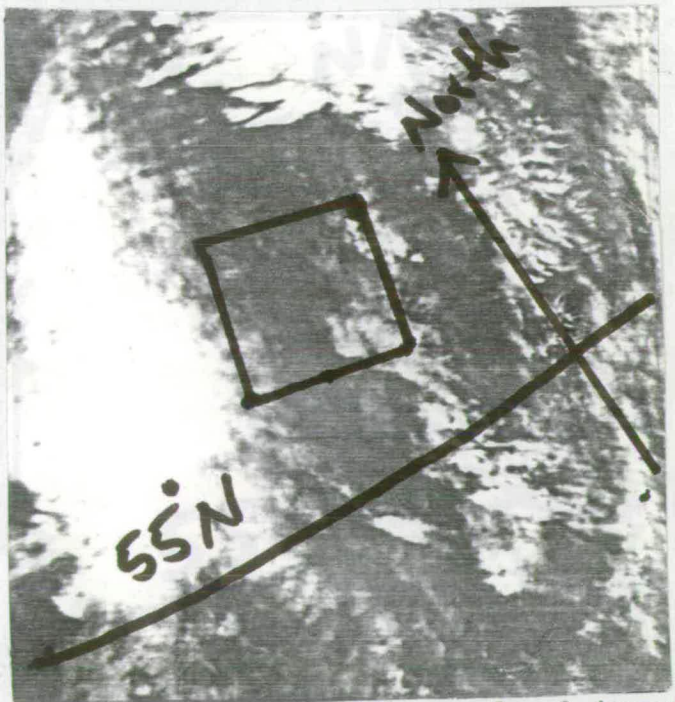

Figure 3.1g. NOAA-5(IR) shows stratiform cloud tops(dark grey)inside the square over Shanwell(0900Z, 25/4/1977).

overlain by cirriform shields, or vigorous convective towers shooting up through relatively inactive cloud debris with fuzzy edges (Skidar and Suomi, 1971). These areas seem likely to produce rain.

In our 30 observations of April 1977, six occurrences of very bright cloud top (-51 to -60°c) gave rain on six occasions, and five occurrences of very dark grey cloud top (0.0 to -10°c) gave no rain five times. The index of the cloud top temperature from zero per cent probability to 100% probability has been interpolated linearly between the six grey shades shown in table 3.5.

The author performed the cloud top temperature probability interpolation linearly between the very bright (100%) probability and very dark (0%) probability and intermediate shades and corresponding probabilities were then calculated. This was because calculating the percentage for each grey shade requires a large number of observations, in order to be statistically reliable.

c. Average Relative Humidity ($\overline{RH}$%) 1000-500

The relative humidity (RH%) can be obtained easily and quickly from the TØ-gram, by the following equation:

$$(RH\%) = \frac{r}{rw} \times 100\% \quad \ldots\ldots\ldots\ldots\ldots\ldots (4)$$

Where, r is the saturation mixing ratio calculated at the dew point temperature and rw is the saturation mixing ratio calculated at the dry-bulb temperature.

Scotland, April 1977.

Cloud top temperature (C^{o})	Cloud top temperature index (CTT)	Rainfall Probability (%)	Number of cases
0 to -10	0.0	0.0	5
-11 to -20	2.0	20	4
-21 to -30	4.0	40	6
-31 to -40	6.0	60	4
-41 to -50	8.0	80	5
-51 to -60	10.0	100	6

Table 3.5 To show the relation between the cloud top temperature, rainfall probability and the suggested cloud top temperature index.

The author here has used equation (4) to calculate the relative humidity at 1000, 900, 800, 700, 600 and 500 mb. and then took the average of them. The average relative humidity of the 1000-500 layer ($\overline{RH}$%) has been used as one of the six criteria mentioned in equation (1). An example of the extraction of the average relative humidity ($\overline{RH}$%) from a TØ-gram is shown in figure 3.6a.

Younkin et al (1965) have discussed a precipitation and cloud forecasting model which makes use of an average relative humidity.

Smagorinsky (1960) developed a linear relationship between relative humidity and cloud cover, using spatially-averaged relative humidity. Essenwangen and Haggard (1960) suggested that cloud cover and relative humidity are related through some exponential function, and their relationship is dependent upon temperature. For this they used point average relative humidity.

McClain (1966) found a relationship between the type of cloud conditions pictured by satellites and the vertically integrated saturation deficit (ie. the difference between the actual vapour pressure of a moist air sample at a given temperature and the saturation vapour pressure corresponding to that temperature).

3.3 Calculation of the Indices in the Rainfall Equation

Several example values had to be selected for the six parameters involved in the model (equation one) before the rainfall prediction index could be deduced for a 24 hr estimation.

The selected time of study was April 1977, for a meso-scale area (2^{o} latitude x 3^{o} longitude) covering 12 Scottish raingauge stations as follows:

1. Leuchars
2. Loch Leven
3. Edinburgh Airport (Turnhouse)
4. Bridge of Dyce
5. Dunbar
6. Haddington
7. Glasgow weather centre
8. Stronacluchar
9. Blackburn
10. Carnwath
11. Eskdalemuir
12. Prestwick

The numeration of these stations are distributed according to their distance from Shanwell radiosonde station (*) as shown in figure 3.2. Shanwell radiosonde station is the only station near them which is representative of the upper air information in the area.

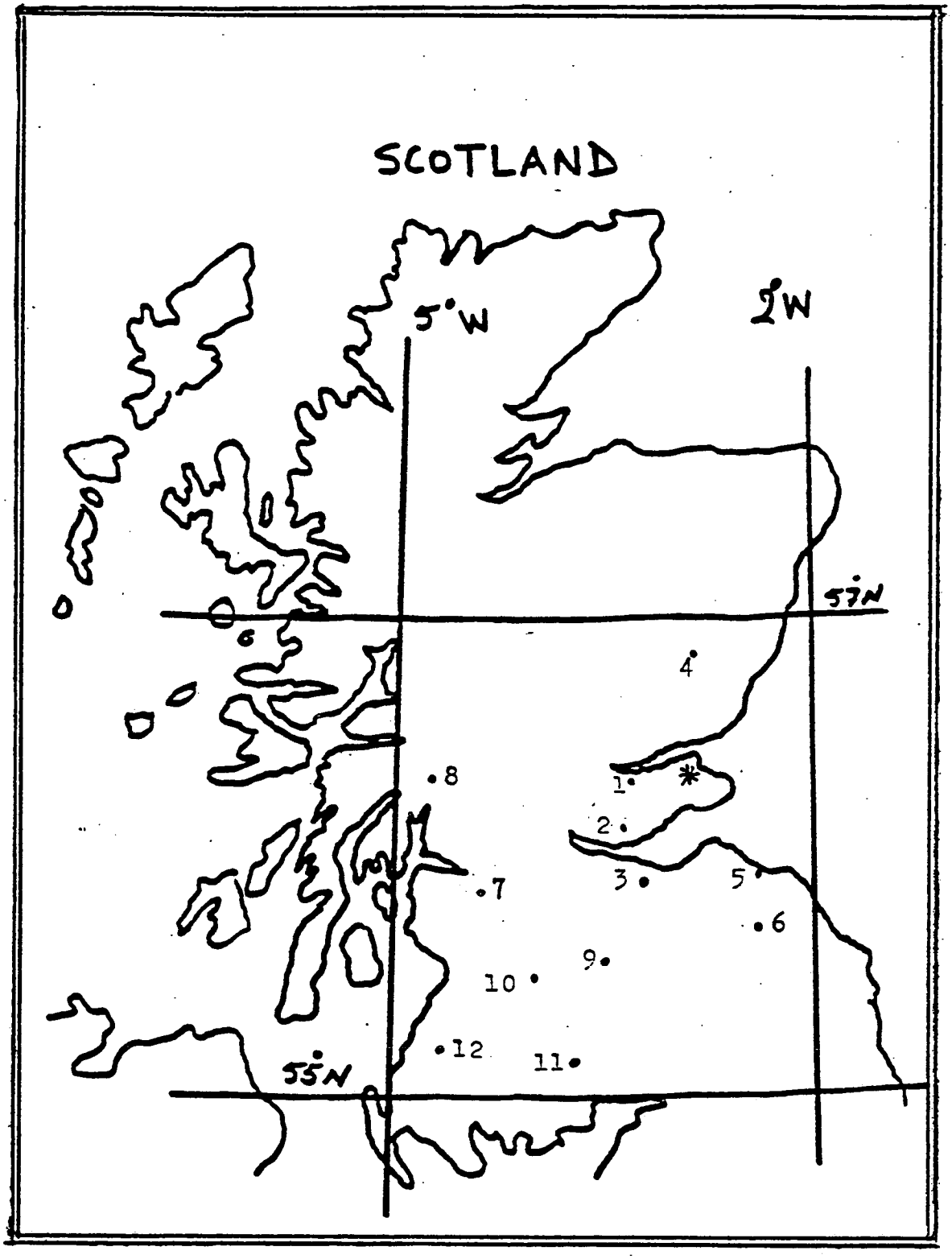

Figure 3.2 The 12 Scottish raingauge stations used in the analysis. Shanwell (*) is the representative radiosonde station being the nearest station.

The six parameters (mentioned in the previous item) are used to calculate the rainfall prediction index for estimating the average daily rainfall 24 hours ahead in the area shown.

The averaged daily rain (0900-0900 hrs) of these Scottish stations for April 1977 are shown in figure 3.3, used as initial data. Five days only had no rain, the fifth, seventh, eighth, fourteenth and eighteenth.

These six parameters (indices) were evaluated daily for the meso-scale area for April 1977, using the appropriate surface chart (from the daily weather report of the British Meteorological Office).

The nearest representative upper air sounding was "Shanwell" (from the daily aerological records of the British Meteorological Office); satellite photographs used were enlarged NOAA-5 photographs.

Unfortunately, there is a difference in timing between the parameters mentioned above and the rainfall. Despite this discrepancy we tried to get the optimal regression equation in order to calculate the 24 hour rainfall.

Once these parameters/indices had been established, the important step in the daily rainfall forecast process is the identification of the cloud quadrant most likely to affect the area concerned during the forecast period, namely, the next 24 hours, then the next step is to evaluate all the six parameters

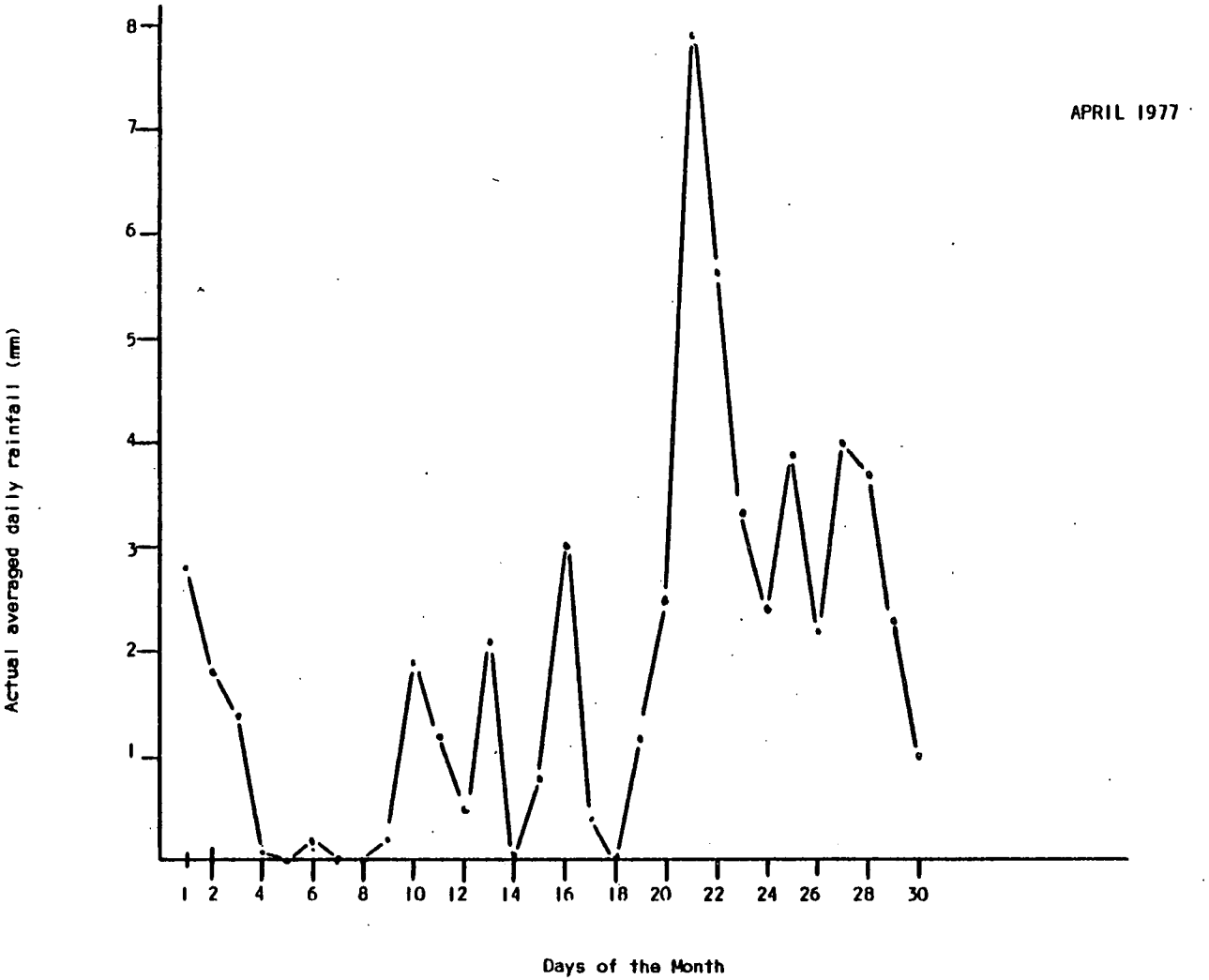

Figure 3.3 The distribution of averaged daily rainfall over Scotland in April 1977, used as initial data.

referred to above. It seems logical to assume that areas upwind of a station are more important in this context than those downwind. The area of the cloud quadrant on any individual day would seem to be dependent on the variability of the wind, and on its strength.

In practice, the area of the quadrant is determined by the 12 GMT radiosonde observation of the 800mb wind. It has been suggested that the 800mb wind is the advection (steering) wind of the rain-producing clouds over the British Isles (Barrett, 1973)

The equation calculating the quadrant area is:

$$Qa = \frac{(24 \times V_{800})^2 \times \pi}{4} \quad \ldots\ldots\ldots (5)$$

where Qa is the area of the cloud quadrant; π is constant; V_{800} is the observed wind speed at 12 GMT and $24 \times V_{800}$ is the radius of the circle (for detail see Barrett, 1973).

Example: The wind speed at 800mb of Shanwell on 17 April 1977 at approximately 12 GMT was 13 kts and the direction 330^{o}. The location of the cloud quadrant is shown in figure 3.4. After locating the orientation and the area of the quadrant for April 1977 and the six indices (synoptic weather pattern, cloud type, cloud cover, Rackliff index, cloud top temperature and relative humidity), we will have values of the rainfall prediction

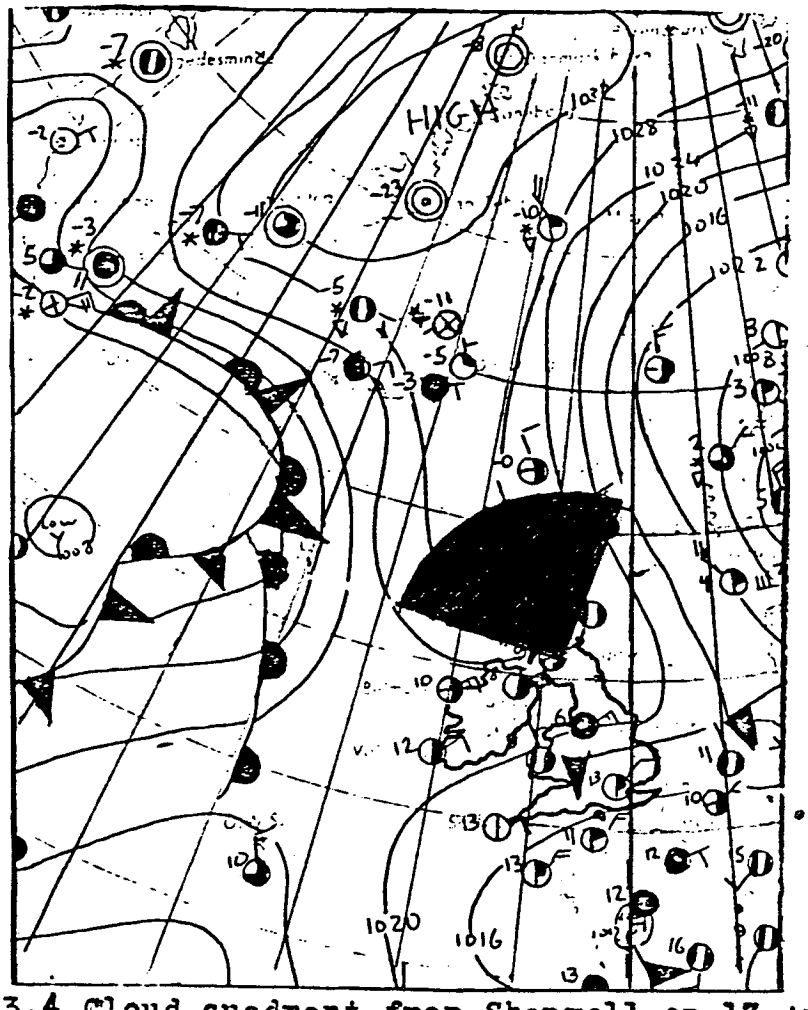

Figure 3.4 Cloud quadrant from Shanwell on 17 April 1977 based on 1200Z. 800mb wind speed 13Kt and direction 330°. Superimposed onto 1200Z surface chart(Daily Weather Report).

index of each day against daily rainfall, using the computer to facilitate the calculation and plotting. The output of the linear regression equation is:

$$Y = -0.071 + 0.012X \quad \ldots\ldots\ldots\ldots \quad (6)$$

The first degree polynomial line of the above equation is shown in figure 3.5.

By comparison Barrett's equation for the same month but with only three parameters (synoptic weather index, cloud type and cloud cover) yielded the following:

$$Y = -0.766 + 0.020X \quad \ldots\ldots\ldots\ldots \quad (6a)$$

Where Y represents the observed actual total averaged rainfall in millimetres and X represents the rainfall prediction index.

It was found that the correlation coefficient between the rainfall prediction index and the observed rainfall (mm) for April 1977, given by the new regression equation (equation 6) for the 24 hr rainfall, was 0.93, whereas in Barrett's equation (equation 6a) it was 0.90.

It seems that the independent variables (Rackliff index, average relative humidity and the cloud top temperature) improved Barrett's regression equation, of these independent variables were closely correlated with rainfall, for this particular data set.

The correlation coefficient (r) of equation (6) is significant at 99% using the sample size as equal to the number of independent values (N = 30). The significance of (r) was tested here using the t-test.

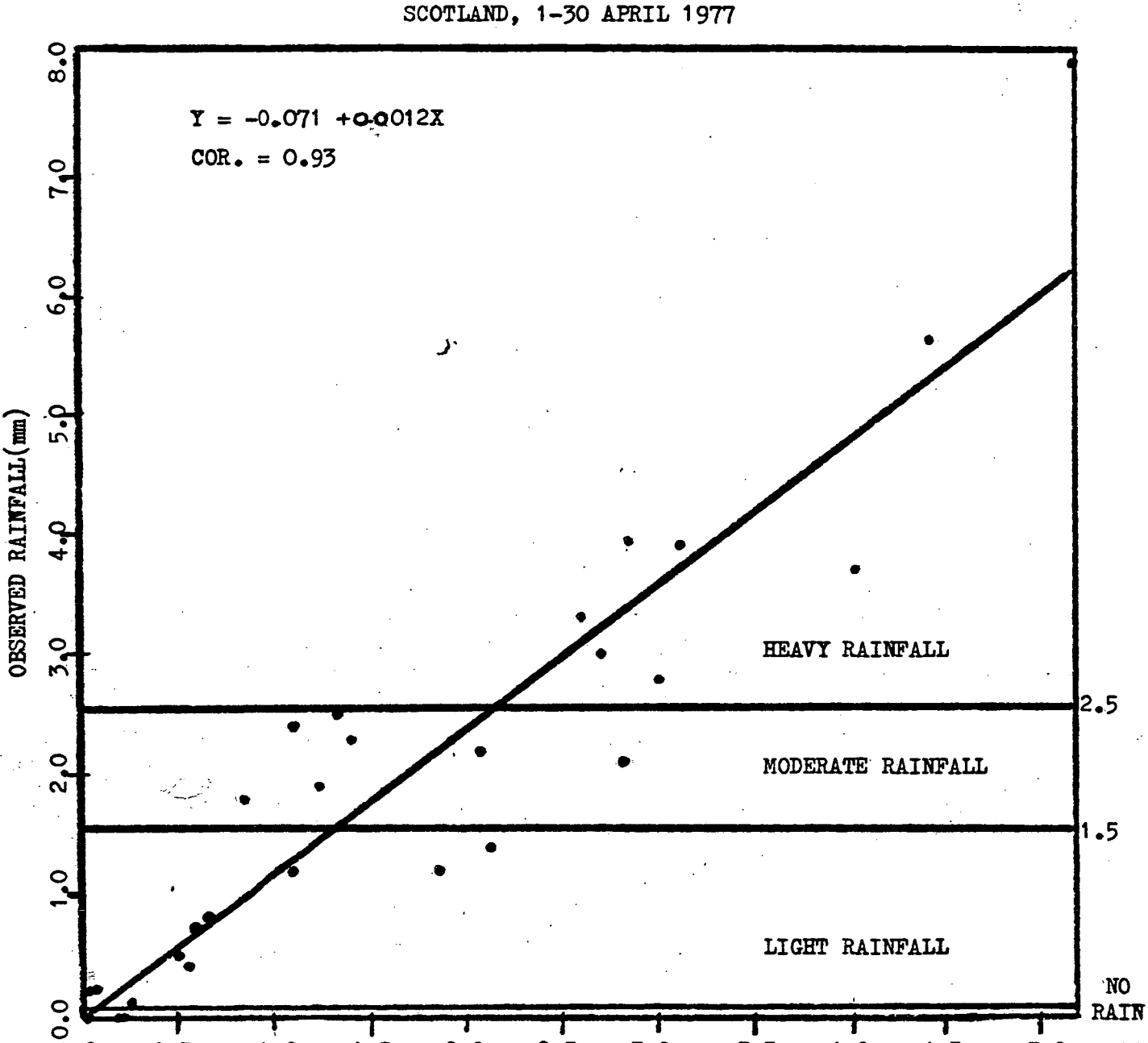

Figure 3.5 First degree polynomial regression line between the daily rainfall(mm) and the rainfall prediction index. Correlation coefficient(COR.) is 0.93.

N.B There are three values located at the origin.

3.4 Results and Verification

It appears that the results of the work are encouraging since the regression line for Scotland, 1-30 April 1977, has a correlation of 0.93. The regression line served to facilitate the choice of rainfall prediction index classes used later in the verification exercise. Observational data from Scotland for April 1977, were analysed to define appropriate categories of wet days (light, moderate and heavy rainfall) based on approximately equal groups (see table 3.6).

Table 3.7 is a complete statement for March 1977, listing the rainfall prediction index actual and estimated rainfall involved in the model.

For example, on March 13, 1977 the Rackliff index was 36 and the average relative humidity index of 1000-500 mb was 0.61 (see figure 3.6a); 800 mb wind speed 23 Kt and direction 170^{o} (see figure 3.6b) on the surface synoptic chart to show the synoptic pattern which was a non-frontal trough (ie. synoptic weather index = 6). Figure 3.6c of the NOAA-5 infrared has shown five cloud top temperature categories (index 2, 4, 6, 8, and 10) which have been mentioned in table 3.5 earlier. Each cloud top temperature category occupies approximately 15% of the total quadrant area, giving an average index (CTT) of the five cloud top temperatures of 6. The cloud cover per cent from NOAA-5 (figure 3.6d) shows approximately 75% of the

Scotland, 1 - 30 April 1977

Class	Rainfall(mm)		Number of days
	Lower limit	Upper limit	
None	0.0	0.0	5
Light	> 0.1	≤ 1.5	10
Moderate	> 1.5	≤ 2.5	7
Heavy	> 2.5	No limit	8

Table 3.6 Daily rainfall(mm) grouped to give approximately equal populations of wet days in the classes, "light", "moderate", and "heavy" rainfall.

SCOTLAND, 1-31 MARCH, 1977.

DATE	RAINFALL PREDICTION INDEX $(x10)^{-1}$	OBSD. RAINFALL (mm)	EST. RAINFALL (mm)	ACTUAL RANK	EST. RANK	SCORE	
						R	W
1	232.1	2.4	2.7	M	H		W
2	587.2	7.3	7.0	H	H	R	
3	137.6	4.0	1.6	H	M		W
4	211.9	1.7	2.5	M	M	R	
5	29.6	0.3	0.3	L	L	R	
6	65.8	0.0	0.7	NONE	L		W
7	211.7	1.8	2.5	M	M	R	
8	110.7	0.3	1.3	L	L	R	
9	309.6	4.3	3.6	H	H	R	
10	191.6	4.0	2.2	H	M		W
11	247.9	2.7	2.9	H	H	R	
12	204.3	1.4	2.4	L	M		W
13	266.8	3.7	3.2	H	H	R	
14	371.1	2.0	4.3	M	H		W
15	513.0	5.8	6.1	H	H	R	
16	301.6	3.0	3.5	H	H	R	
17	393.6	5.7	4.7	H	H	R	
18	494.3	6.2	5.9	H	H	R	
19	135.7	1.5	1.4	L	L	R	
20	190.6	1.9	2.2	M	M	R	
21	23.2	2.0	0.2	M	L		W
22	114.2	1.1	1.3	L	L	R	
23	172.9	2.4	2.0	M	M	R	
24	68.3	0.9	0.7	L	L	R	
25	58.4	0.4	0.6	L	L	R	
26	239.3	2.8	2.8	H	H	R	
27	214.5	1.1	2.5	L	M		W
28	85.4	0.0	0.9	NONE	L		W
29	4.5	0.0	0.0	NONE	NONE	R	
30	523.9	8.8	6.2	H	H	R	
31	687.0	8.0	8.2	H	H	R	

Table 3.7 Formation and verification of daily rainfall estimation for Scotland.

KEY:- EST. Estimated
OBSD. Observed
H Heavy rainfall
M Moderate rainfall
L Light rainfall
W Wrong estimation
R Right estimation

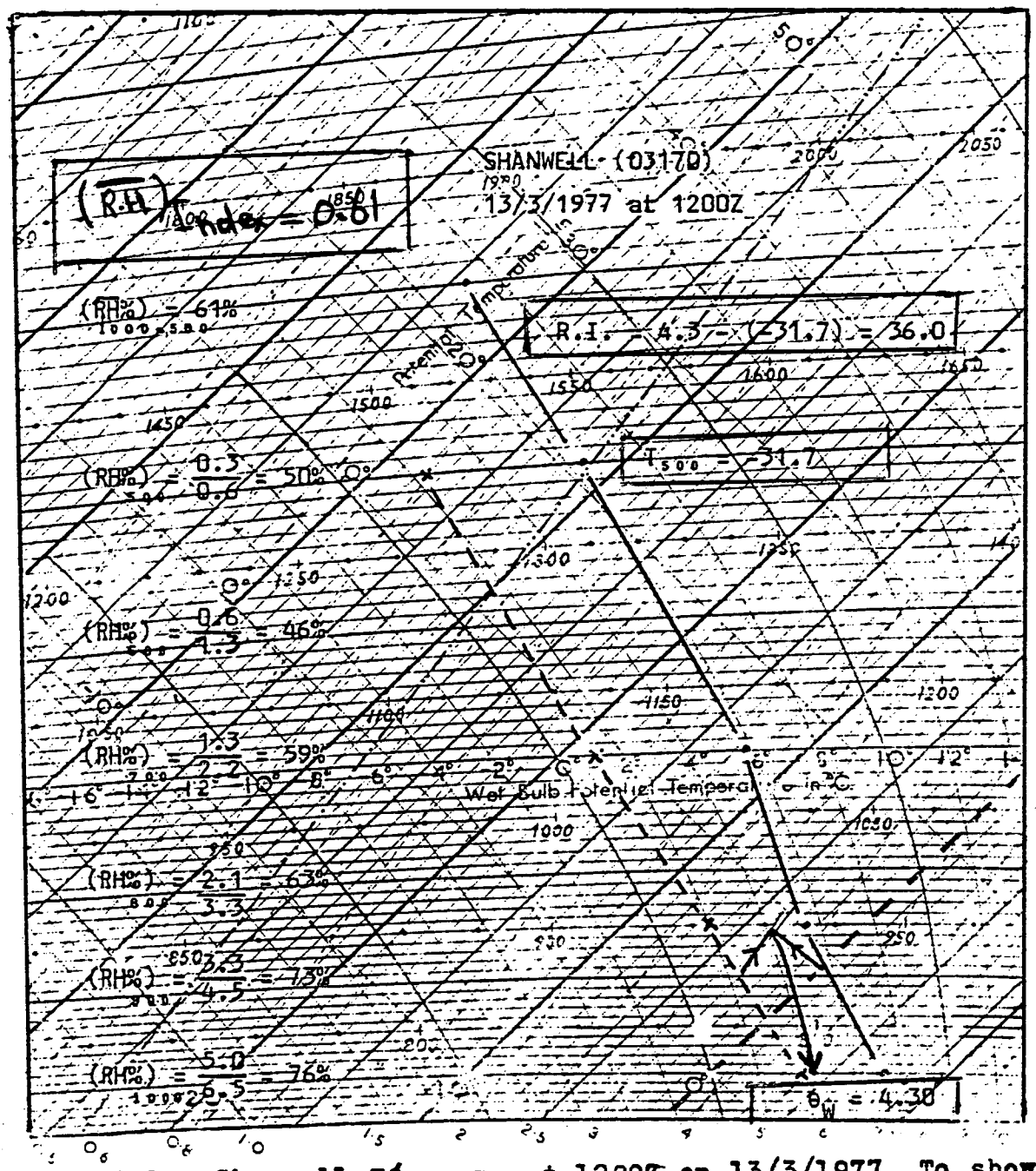

Figure 3.6a. Shanwell Tø-gram, at 1200Z on 13/3/1977. To show the extraction of the average relative humidity of 1000-500mb. layer($\overline{RH\%}$) and Rackliff Index(R.I).

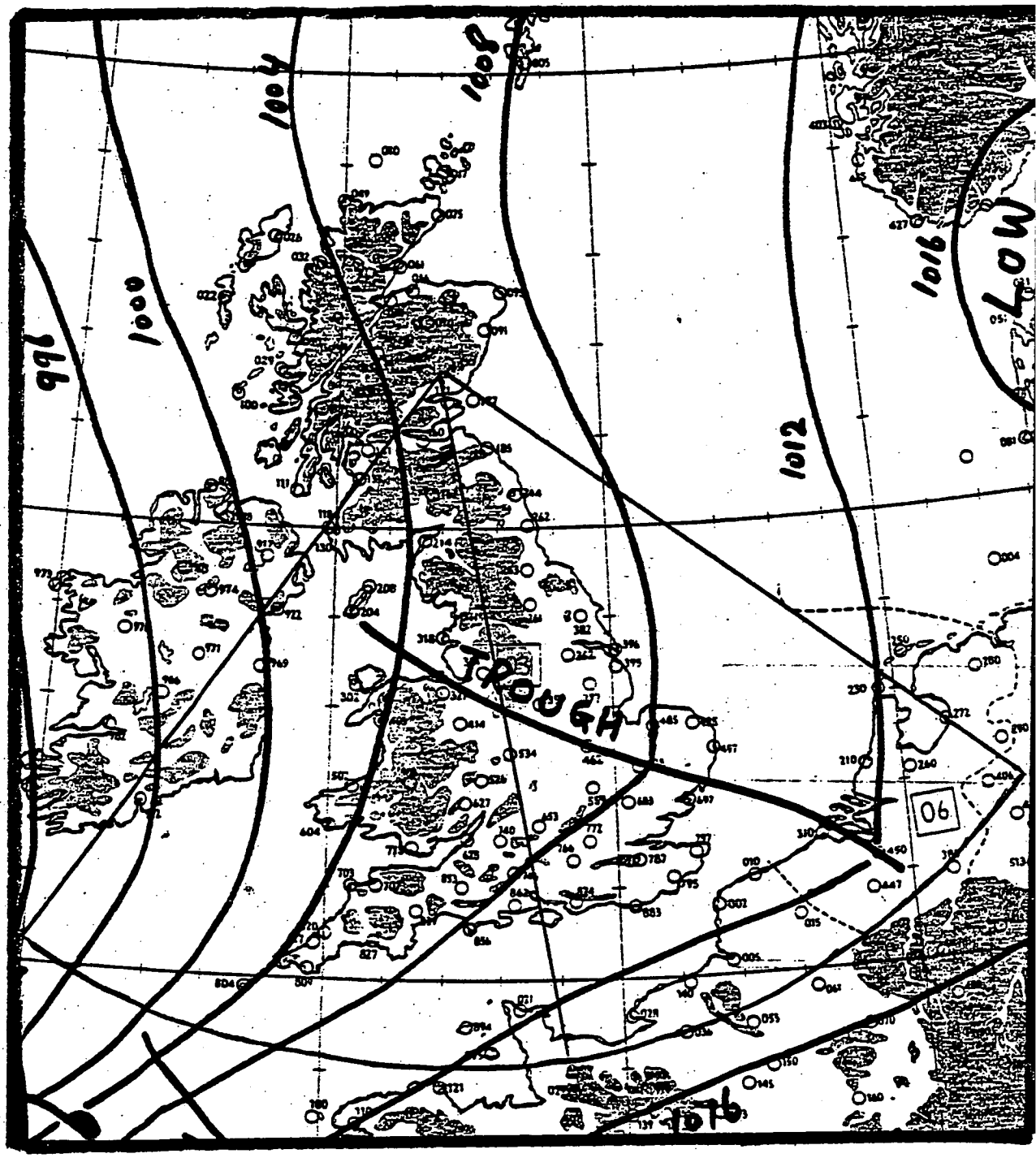

Figure 3.6b. Cloud quadrant at 800mb., wind speed 23Kt and direction 170°, superimposed onto the surface chart of 13 March 1977 at 1200Z to find the synoptic pattern(which is "Non-frontal trough").

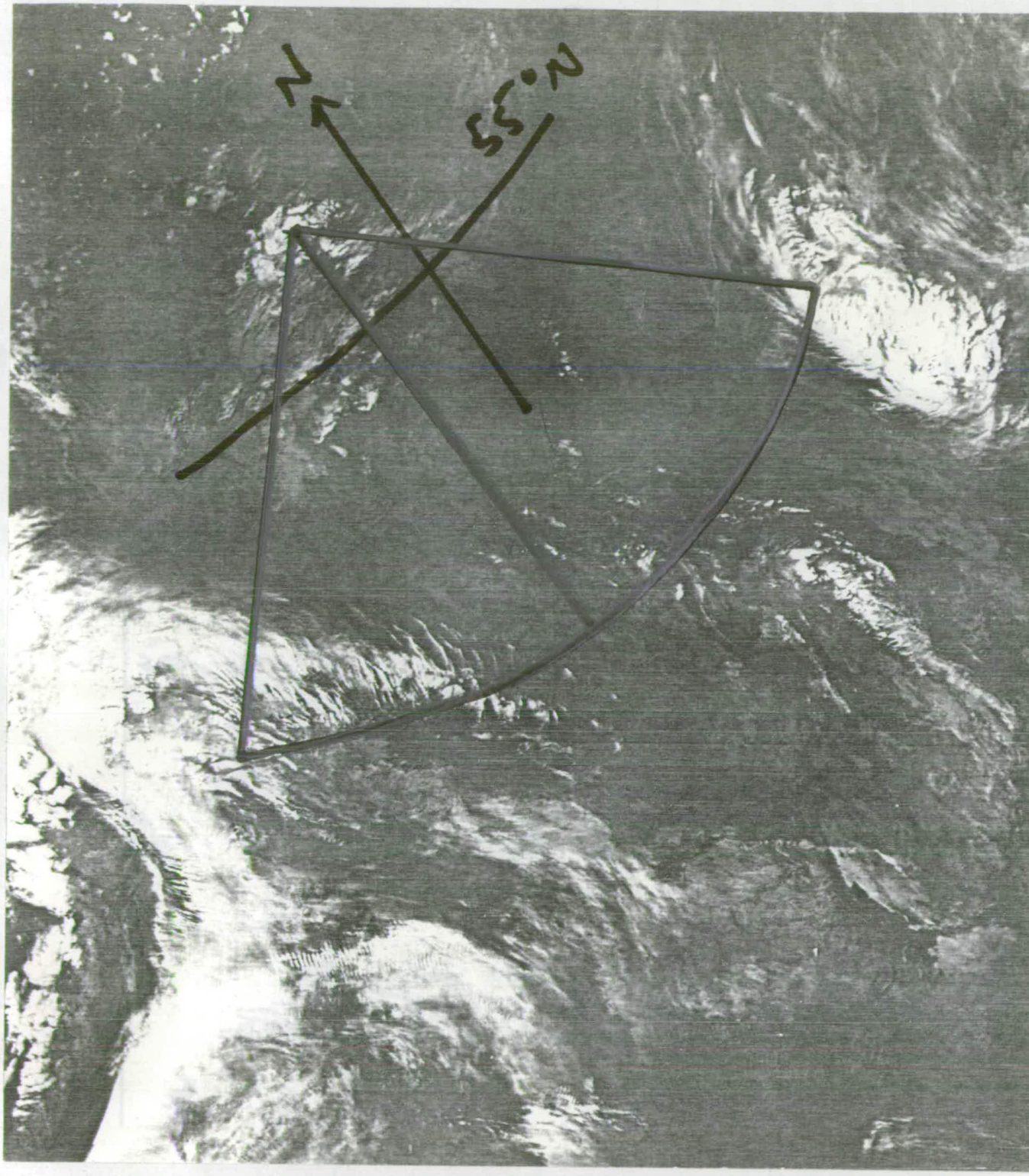

Figure 3.6c. The cloud quadrant superimposed onto the NOAA-5 photograph(IR) on 13 March 1977 at 0934Z. The quadrant shows approximately 75% of the area covered by five different cloud top temperatures. (see table 3.5).

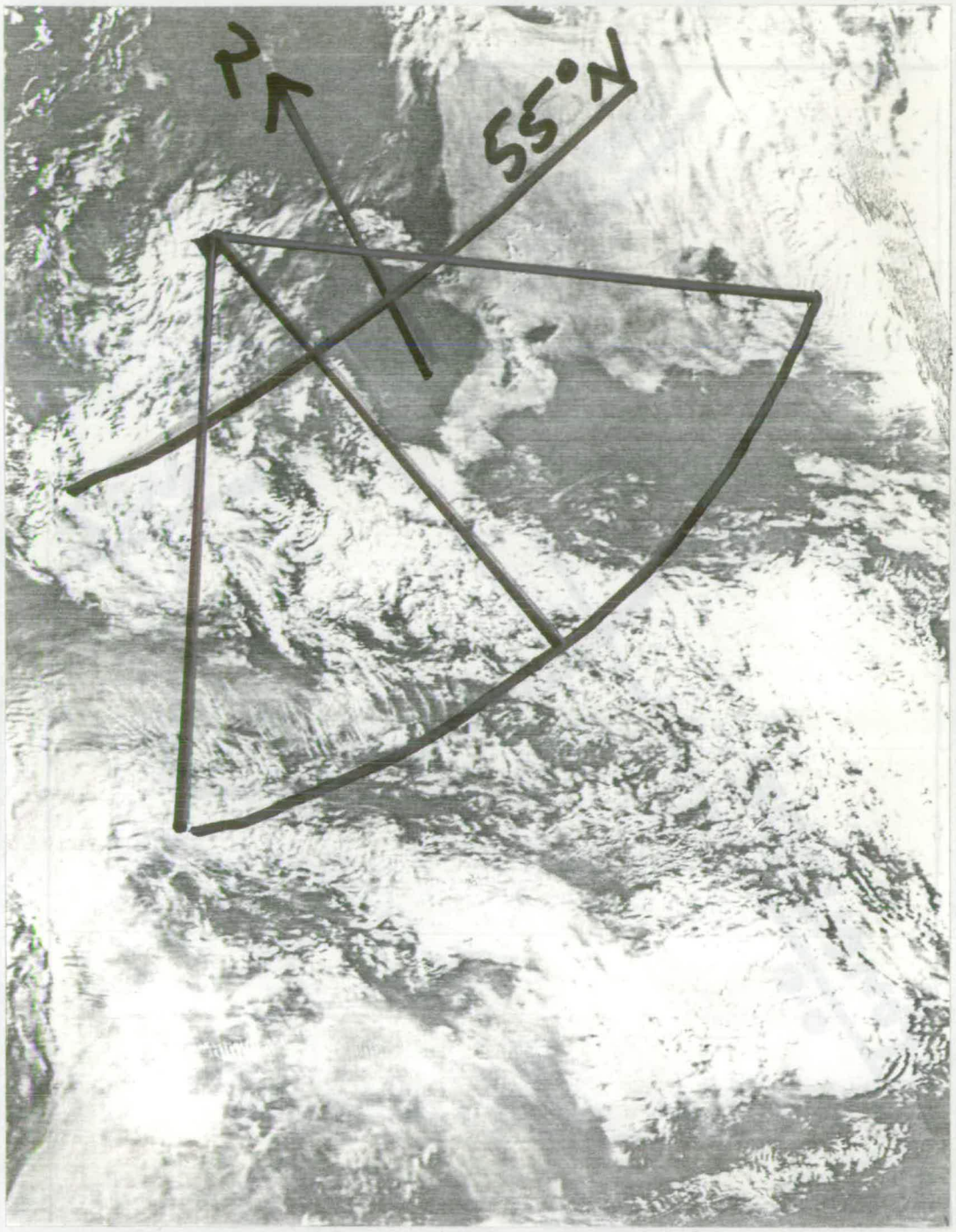

Figure 3.6d. The cloud quadrant superimposed onto the NOAA-5(visible)photograph on 13 March 1977. The NOAA-5 photograph shows approximately 75% of the quadrant area covered by "layered stratiform, stratiform with cirrus, stratiform with cumuliform and cirrus.(see table 3.3).

total area. The cloud type index (VIS and IR) shows (7.5/10) of mixed cloud "layered stratiform, stratiform with cirrus, stratiform with cumliform and cirrus" (ie. cloud type index = 0.75 x 6).

So

$$RR_{24} = Sw \times CTT \times C \times R.I. \times \overline{RH}\% \times Ct$$

$$RR_{24} = 6 \times 6 \times 0.75 \times 36 \times 0.61 \times (0.75 \times 6) = 2668.1$$

Figure 3.5 associates this with heavy rainfall. Table 3.7 indicates that the observed rainfall on 13 March 1977 was 3.7 mm and the estimated value 3.2 mm. Within the classification of rainfall both the actual and estimated values were in the heavy group, thus the forecast was correct.

In the case of no rain the correct forecast was made on 1 out of 3 occasions, for the light rain, 6 out of 8 occasions, for moderate rain, 4 out of 7 occasions and for heavy rain, 11 out of 13 occasions (see table 3.8).

Of the 31 estimates, 22 were in the correct category, which is 71% success rate. The number of correct forecasts exceeds the number of incorrect by the ratio 2:1. The method was therefore successful.

3.5 Discussion and Conclusion

The technique used to evaluate the rainfall prediction index from daily cloud pictures possesses important defects, arising from subjective analysis

Scotland, 1 - 31 March 1977

		Estimated value of rainfall				
		Heavy	Moderate	Light	None	Total
Observed value of rainfall	Heavy	11	2			13
	Moderate	2	4	1		7
	Light		2	6		8
	None			2	1	3
	Total	13	8	9	1	31

Table 3.8 Contingency table, showing the correct, over and under estimated values of rainfall.

which attempts to discriminate quantitively between essentially qualitative data. These defects are liable to produce errors in the identification of the cloud type, amount and height. In addition, some of these errors arise from the nature of satellite pictures themselves, for three main reasons, namely:

1. A lack of daily pictures with consistency: picture quality varied considerably from day-to-day introducing some amount of uncertainty. This problem was aggravated by unequal brightness response of the camera system on board NOAA-5 satellite and receiving land system providing pictures coverage during March and April 1977.
2. Inaccuracies, in the positioning of longitude and latitude grids and coast lines. These can be misplaced by distance by up to a few tens of kilometres. These inaccuracies could significantly affect estimates of cloud cover within the cloud quadrant.
3. Variation of terrestial brightness. These may be confused with small elements of clouds.

These problems have a strong influence upon assessment of cloud cover, amount, type and brightness, and also complicate the picture analysis. The most important source of error liable to occur in rainfall prediction index evaluation is associated with the

estimation of cloud features (cloud top temperature, cloud cover and cloud type), since the small scale cloud may not appear in the picture (smaller than the resolution of NOAA-5). These variables are used to determine the combined factor (cloud top temperature X cloud cover X cloud type).

Errors in the evaluation of the three parameters, relative humidity, synoptic weather pattern and Rackliff index, probably contribute less to the overall error.

However, in the worst cases all factors/parameters may contribute in combination to produce a large error.

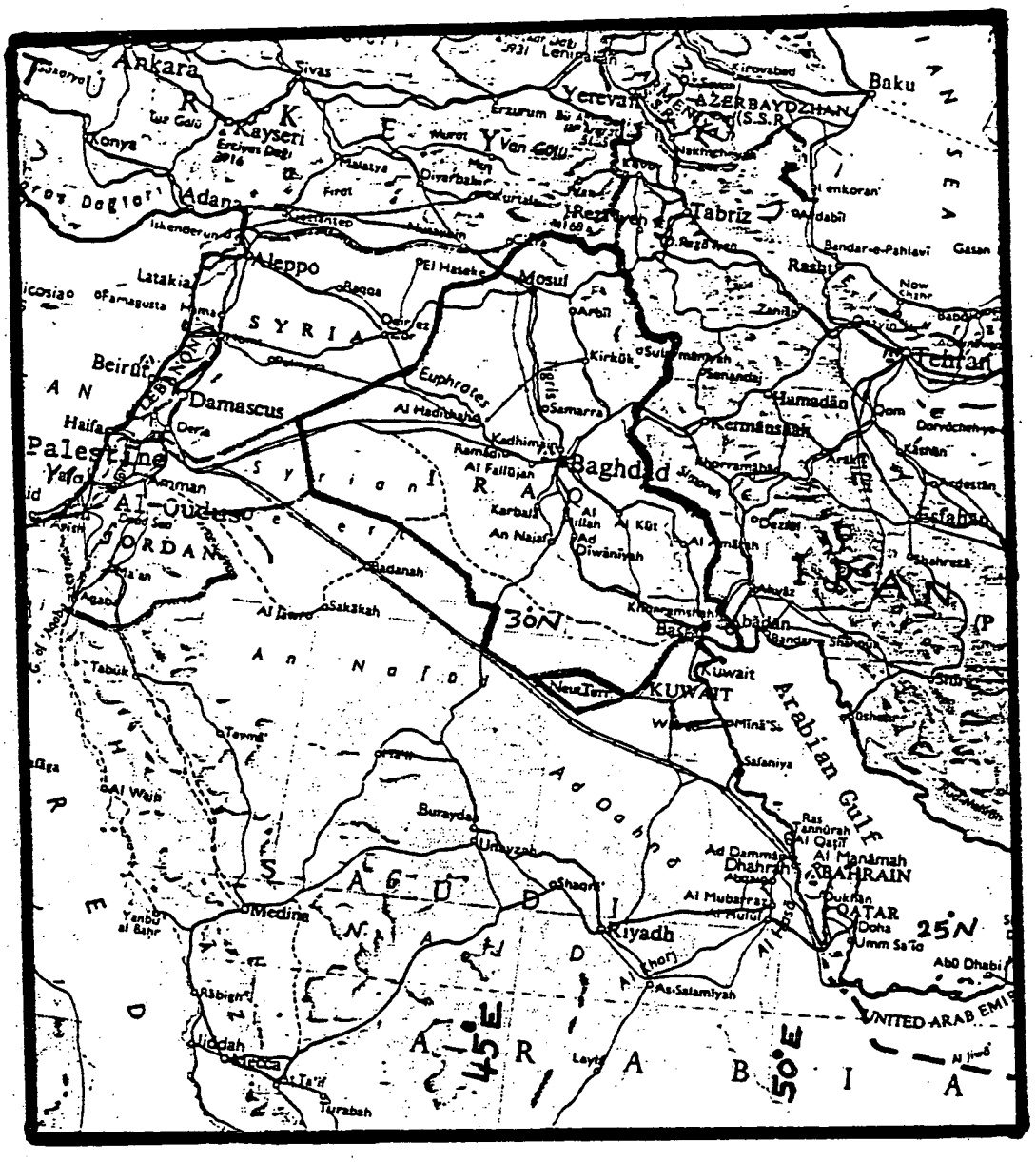

Figure 4.1 Map showing the geographical location of Iraq and its regional setting.

about 1,000 meters, and in the extreme northeast where some peaks rise to 2,500 meters above sea level; there is extensive marshland in the southeast.

4.3 General Climate

The Middle East/Iraq weather is influenced by the Mediterranean weather system as shown in figure 4.2a. It can be seen that 28% (16.5) of depression of the North West Mediterranean, and 61% (8.5) of those in the Atlas mountains influence the weather over the Middle East. Furthermore, a small percentage of depressions from the central and eastern Mediterranean and from adjacent areas also influence the Middle East weather (for details, see Air Ministry, M.O. 1962).

Iraq in general can be considered a semi-arid country. In winter it is mostly covered by an extension of the cold high pressure region of Central Asia while the Mediterranean is a region of low pressure, but without direct influence. Only the deep depressions, troughs and active fronts can affect the country (see, Taha, et al. 1981). They are fed by the warmth and humidity of the Arabian Gulf and are also influenced by the topographical features of Iraq and produced rain which is accompanied by cumulonimbus and thunderstorms for at least one day.

Based on Baghdad meteorological data for a 21 year period, it is estimated that about one third of the rain-producing clouds over Iraq are associated with thunderstorms. In the transitional seasons (Autumn and Spring),Mediterranean

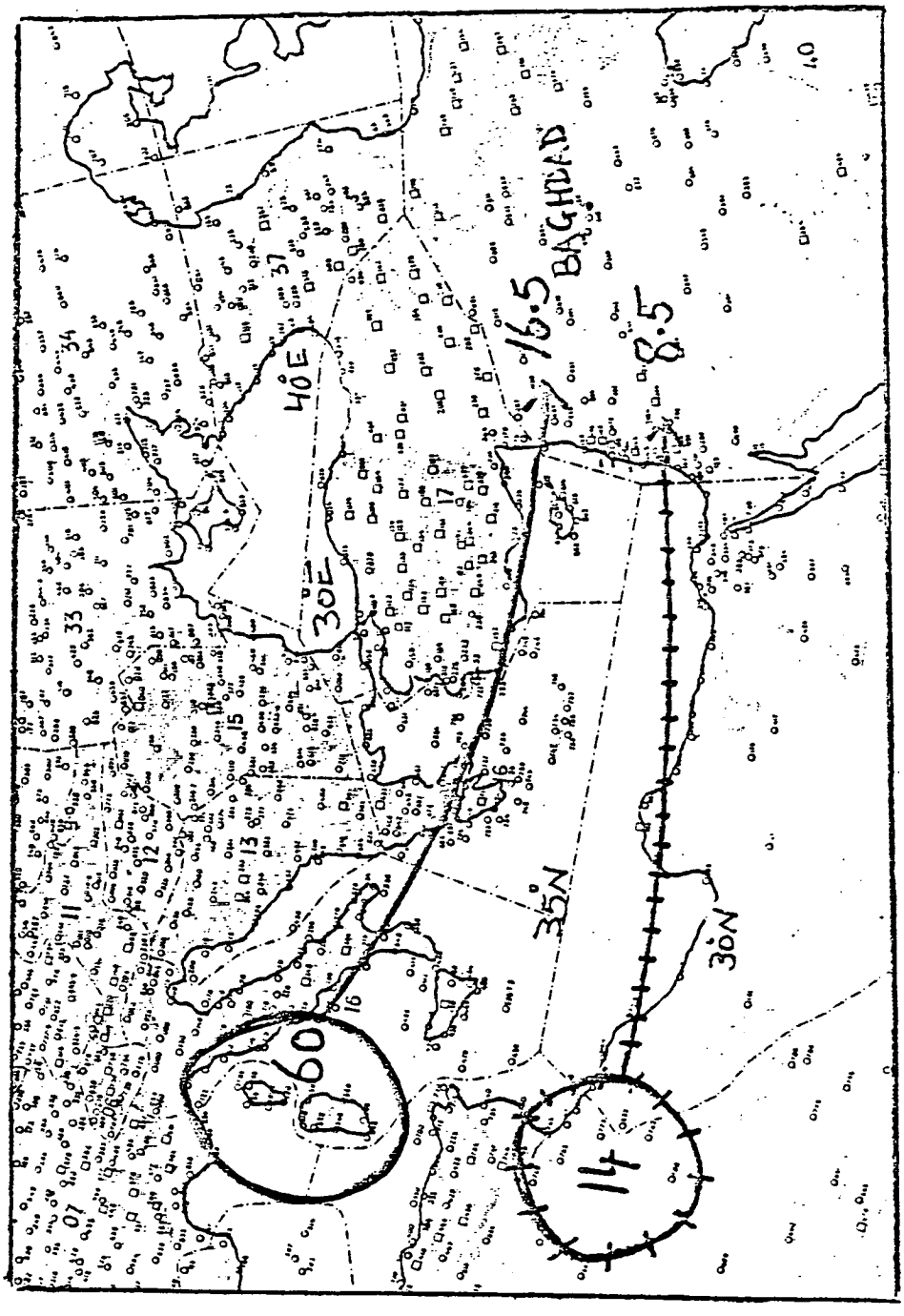

Figure 4.2a (Solid Lines) represent the annual frequencies of depressions in the North West of Mediterranean and the movement of them. On average 16.5 of them influence the Middle East every year.

(Dashed Lines) represent the annual frequencies of depressions in the Atlas mountains and the movement of them. On average 8.5 of them influence the Middle East every year.

depressions and fronts which pass eastwards are associated with thunderstorms but their frequency is less than those of the winter season.

For comparison, in general, Mediterranean (sub-tropical) depressions are smaller in size than those of higher latitude (Simmons and Hoskins, 1979, and Karein 1979), and the life time of the Mediterranean depression in general is shorter than the life time of those in the higher latitude.

Storms of very fine particles of sand and dust generally blow in advance of winter and transitional depressions. Particularly in Spring the air carrying these particles is generally very dry and hot. In Summer, due to the absence of travelling depressions,weather conditions are settled. However, the central and southern parts are subjected, during day-time hours, to heavy dust and sandstorms with dust rising to heights of over 3 kilometres; these have been observed by aircraft pilots flying over these regions.

4.4 Precipitation

4.4.1 Rainfall

The Mediterranean weather systems are the source of the rainfall of Middle Eastern areas. The distribution of the annual rainfall amount over the Middle Eastern area, including Iraq, is shown in figure 4.2b.

In Iraq, the rainy season begins in October and continues till May. The months from June to September can be considered rainless. Most of the precipitation

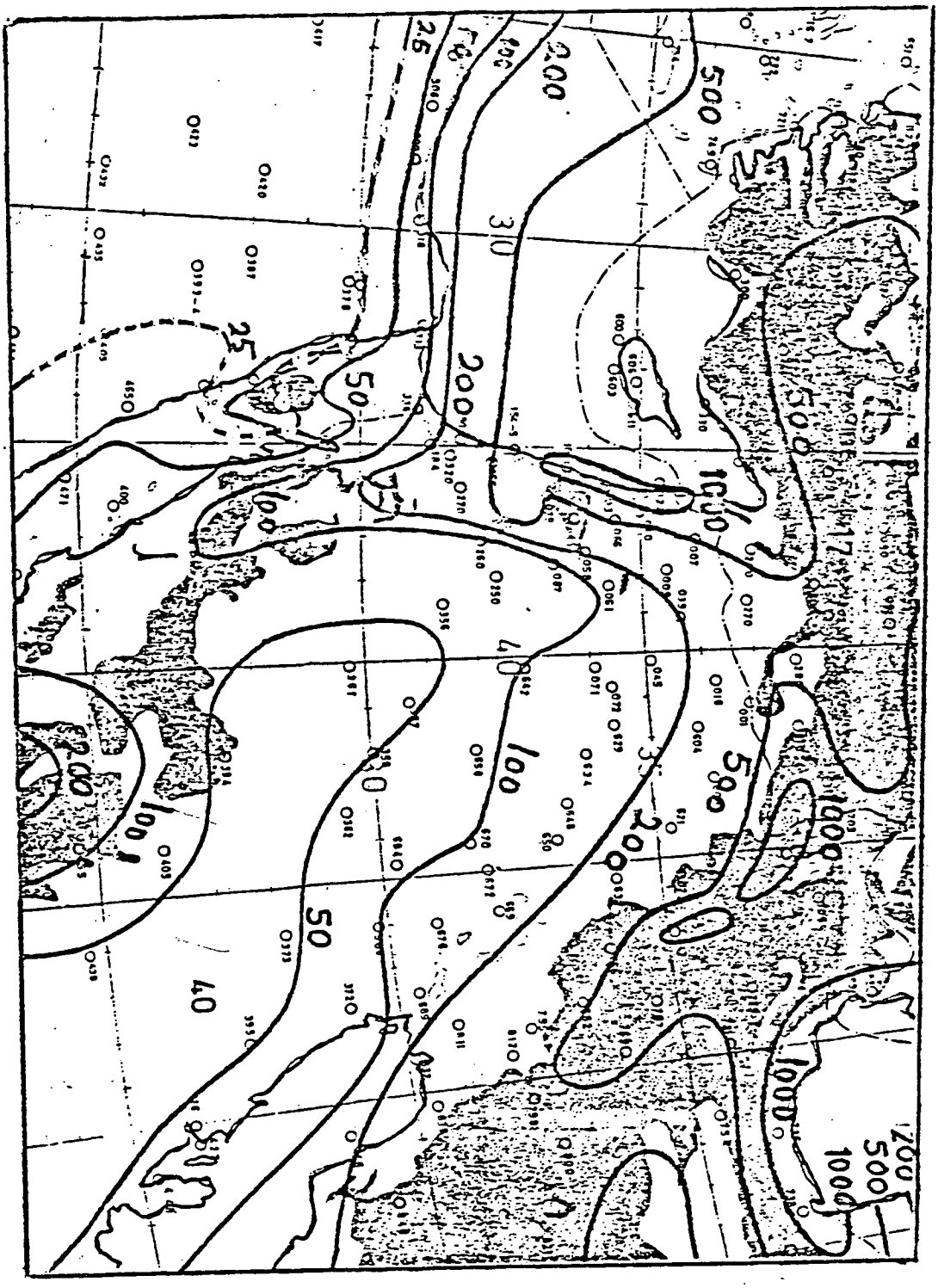

Figure 4.2b Showing the annual rainfall amount (mm) of the Middle East including Iraq (1935-1956).

(analysed by Baghdad M.O.)

occurs in the Winter season (December-February). The distribution of both the amount and the number of rainy days shows great variability with locality. Large amounts fall in a relatively small area in the extreme northeast of the country where the annual amount exceeds 1,000 mm in some localities. Southwestwards (south of 36°N and west of 45°E) the rainfall considerably decreases. The mean annual rainfall amount in the extreme southwest is less than 100 mm (see figure 4.3a). The mean annual number of rainy and thundery days is over 60 and 28 respectively in the extreme northeast and decreases to less than 10 and 8 days respectively in the extreme southwest (see figures 4.3b and c).

In the Spring season (March-May) convective activity is the source of most of the rain in Iraq. This convection results in violent thunderstorms, particularly in the north and is subject to diurnal variation unlike those of the winter season which are associated mainly with Mediterranean weather systems and have a relatively small diurnal variation.

4.4.2 Snow

Snow falls heavily in winter on the mountains in the north of Iraq. The Tigris and Enphrates reach their highest flood levels in the spring season, mainly from the melting snow. In the central region snow falls rarely and melts immediately. In the south and southwest, snow is absent. This aspect is not going to affect much the forecasting model of rainfall over a meso-scale area

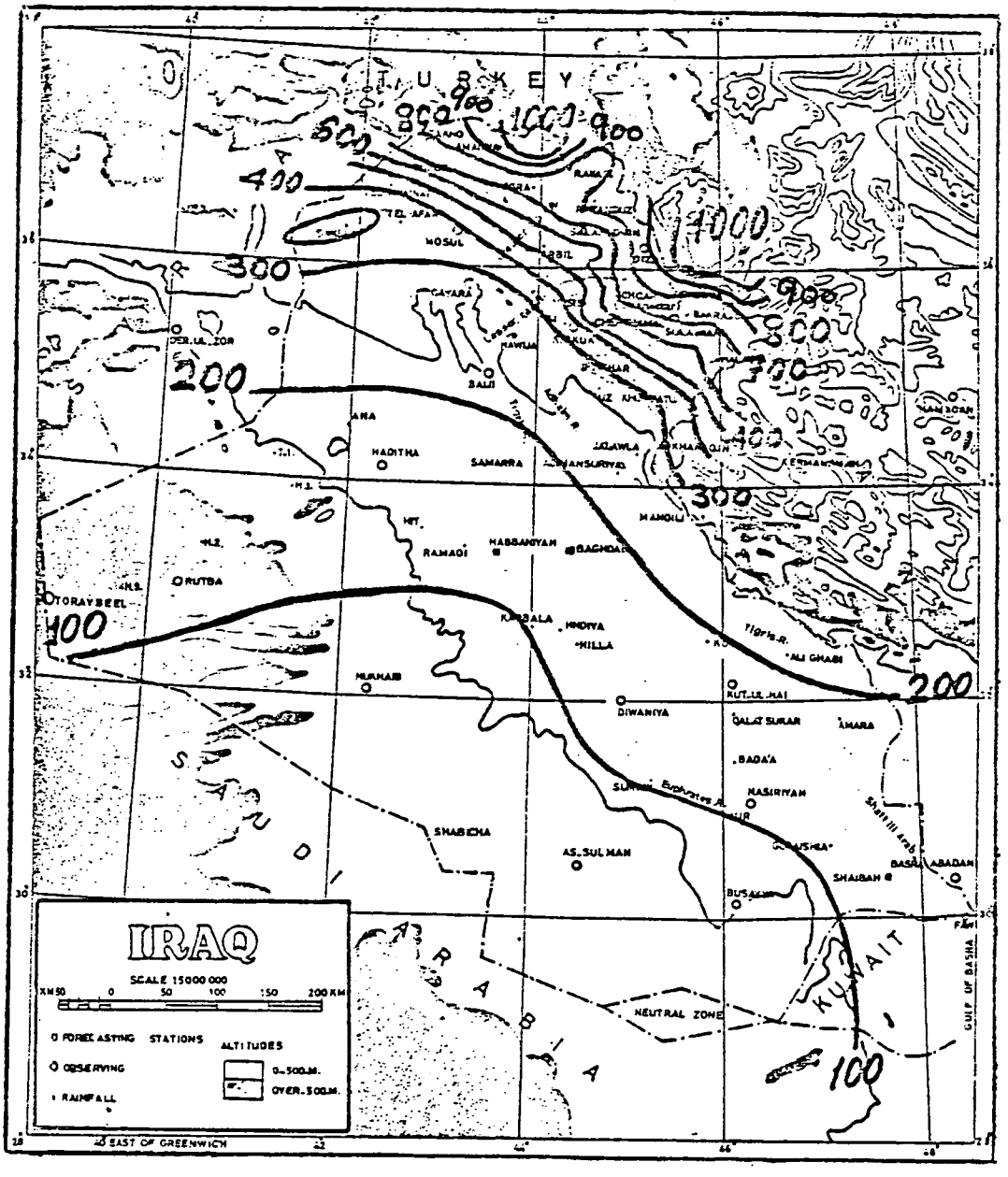

Figure 4.3a Showing the mean annual amount (mm) of precipitation (1935-1956).

Analysed by Baghdad M.O.

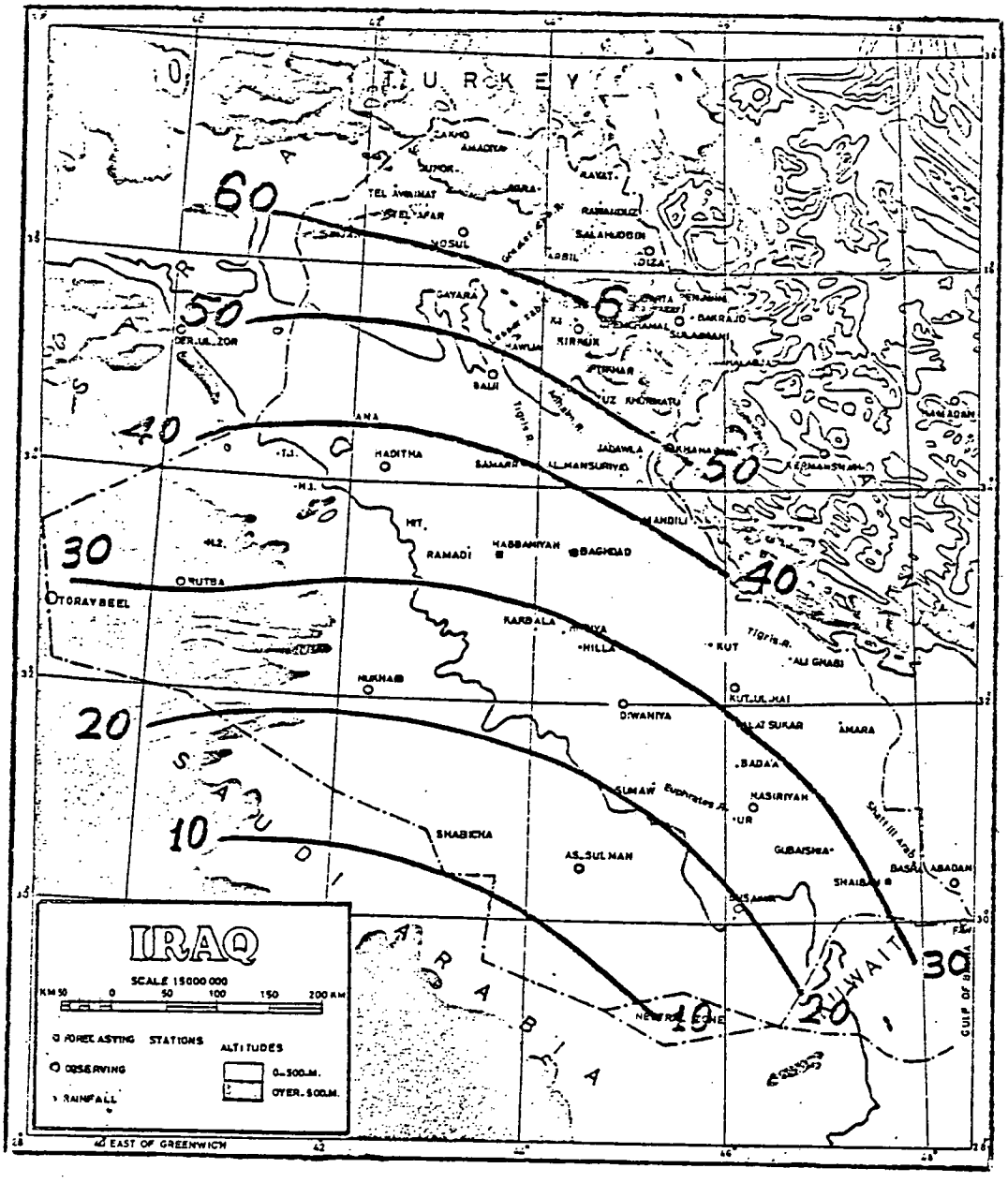

Figure 4.3b Showing the mean annual number of days with rain, period of records (1935-1956). Analysed by Baghdad M.O.

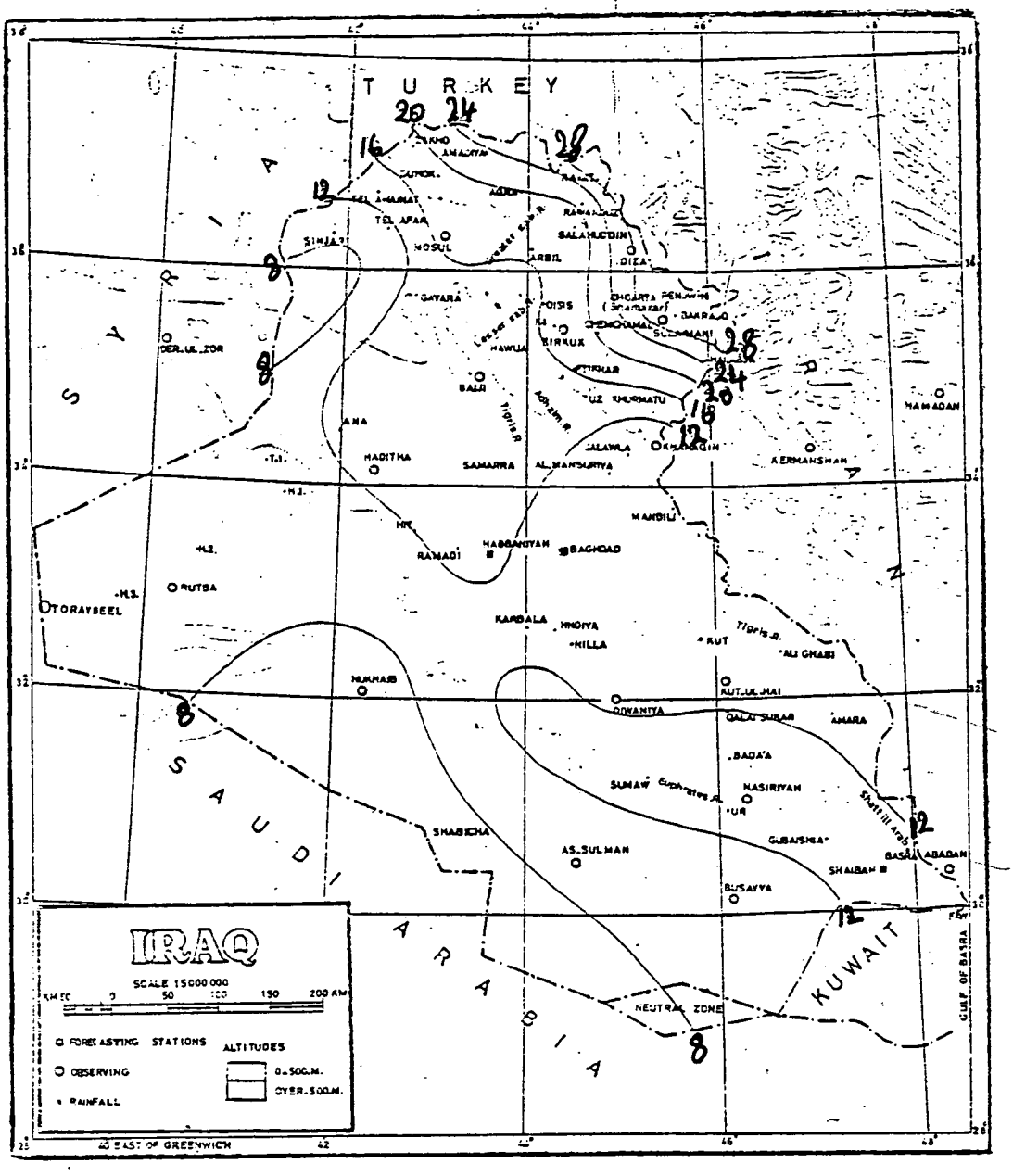

Figure 4.3c Showing the mean annual number of days with thunder (1935-1956).

Analysed by Baghdad Meteorological Office

(central region) over Iraq. The author will not therefore take this into consideration.

4.5 Rain-Producing Cloud System.

According to Baghdad climatological reports, a total of 25 cases of rainy systems (depressions, fronts and troughs) moved eastward from the Mediterranean basin to Iraq in the three winter months of 1978-79 (December - February). 10 systems were reported in December 1978, 8 in January 1979, and 7 in February 1979. Figures 4.4a and b show the average temperature (T)/ dew-point (Td) soundings for the 25 cases of the advected rainy systems for Baghdad at 0000 and 1200 GMT. The ascents (soundings) reflect the convective activity associated with those rainy systems over Iraq. It will be seen in both ascents that the air mass is relatively humid in the 1000-500mb layer. Potential instability is also apparent from the ascents referred to above. The above evidence suggested that rain over Iraq is associated with advection weather systems but that convections activity embedded in these systems makes a major contribution to rainfall.

Details of the convective and advective rain-producing cloud system over Iraq will be presented in Chapter 5, article 5.5.1.

4.6 Humidity

In January, the 24-hour spatially averaged surface relative humidity for a 25 year period is 90% in Britain, but 82% in Iraq. In July it was 86% in

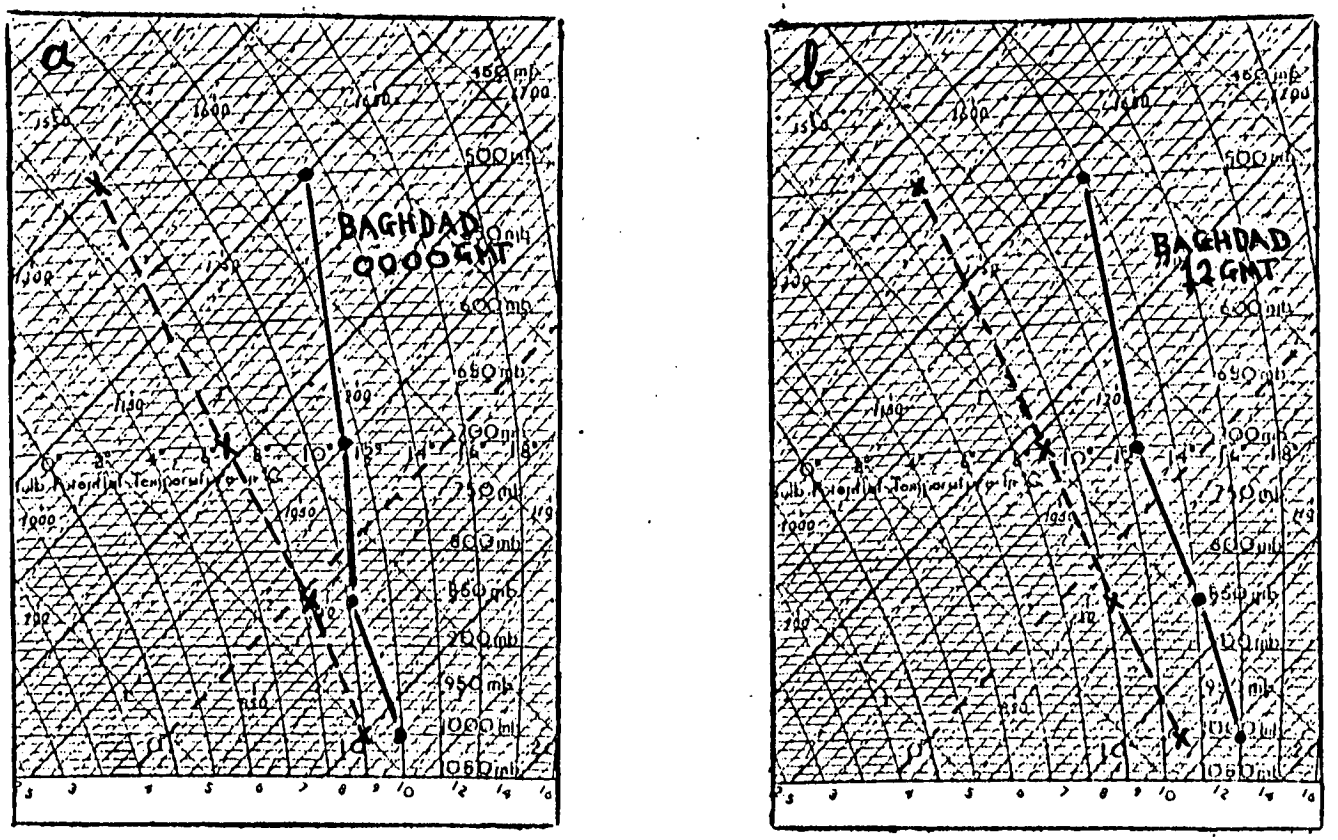

Figures 4.4a and b. Showing the average values of the temperature (T) dew point (Td) for the 25 cases of rainy systems at 0000 and 12 GMT for Baghdad in three months (December 1978, January 1979 and February 1979).

Britain and 30% in Iraq over the same 25 year period.

The Tephigrams of Baghdad (Iraq) and Shanwell (Scotland) have been analysed for 30 days of different classes (light, moderate and heavy) of rain. This analysis shows that the mean dew point depression (d.p.d) for 1000-850mb. layer for 30 wet days is $4^{o}C$ for Shanwell and $5.8^{o}C$ for Baghdad. Results of the average dew point depression of each rainfall class is listed in table 4.1. These results show that the air masses of Iraq on rainy days are drier in the 1000-850mb. layer than those over Britain suggesting that the heights of rain-producing cloud system over Iraq are higher than over Britain.

The 800mb. wind is the suggested wind for advecting the rain-producing cloud over Britain. Details of wind advection level over Iraq will be discussed in Chapter 5, article 5.4.

4.7 Conclusion

The discussion of weather systems and the different meteorological elements with the rainfall over Iraq bring out clearly that convective activity embedded in the advective system, is the major source of rainfall over Iraq. Therefore, Barrett's (1973) method with the modification suggested by the author and presented in Chapter 3 should prove more successful when applied to predicting rainfall over Iraq than over Britain. One important modification that has to be introduced

Radiosonde station	Average dew-point depression (d.p.d.) in C° for 1000-850 mb. layer		
	Light Rain	Moderate Rain	Heavy Rain
Baghdad (40650)	7.5	6	4
Shanwell (03170)	5	4	3
Number of Occurrences	10	10	10

Table 4.1 Comparison of average dew-point depression (d.p.d.) between Baghdad (Iraq) and Shanwell (Scotland)

also is to define the appropriate level for the wind direction and speed for advecting the rain-producing cloud system over the area of interest. This important aspect will be discussed further in Chapter 5, article 5.4.

CHAPTER FIVE

ESTIMATION OF DAILY RAINFALL OVER IRAQ USING METEOSAT-1 IMAGES.

5.1 Introduction.

Having developed the six-parameter model (relative humidity, Rackliff index, synoptic pattern, cloud type, cloud top temperature and cloud amount) to estimate daily rainfall over Scotland, described in chapter three, and having understood the weather and climate of Iraq described in chapter four, it is now possible to apply this model to estimate daily rainfall over Iraq with some simple modification to these parameters since the Iraqi weather and climate differs from that of Britain. This modified model is applied to estimate daily rainfall over Iraq (central region). The verification shows encouraging results as we can see later on in this chapter.

5.2 Data Used.

The data used in this chapter were enlarged visible and infrared images for the months of December 1978 and February 1979 from the European geostationary satellite METEOSAT-1, and midday upper-air and surface data from Baghdad Meteorological Office. The METEOSAT system will be discussed in detail in the following item.

Winter months (December to February) on average have the highest frequency of occurrence of rain over Iraq as described in chapter four.

December 1978 and February 1979 have been chosen and used for the development of the modified model and January 1979 data have been used for testing and verification.

The area chosen is the central area of Iraq because the number of meteorological stations is large compared with other areas and the observations are more reliable.

5.3 METEOSAT-1

Following the successful launch of METEOSAT-1 in 1977 the author was able to obtain METEOSAT-1 photographs of the Middle East/Iraq. This was the first geostationary satellite to give coverage of the Middle East.

The METEOSAT-1 programme was started in 1972 by the European Space Agency (ESA) and its eight member states (Belgium, Denmark, France, Germany, Italy, Spain, Switzerland and the United Kingdom).

METEOSAT-1 and its communication links form part of a global network of five geostationary satellites distributed around the equator (Bizzarri, 1975).

The METEOSAT-1 telecommunication system comprised the satellite itself and the ground system, of which the main components are the Data Acquisition

Telemetery and Tracking Station (DATTS) and the METEOSAT Ground Computer System (MGCS). The MGCS is located in the European Space Operation Centre (ESOC) in Darmstadt/W.Germany, and DATTS is situated 50 km. from Darmstadt from where the author has obtained the negative satellite transparencies of the visible, infrared and water vapour channels through the Meteorology Department/Edinburgh University. These negatives have been printed and enlarged as required in photographic form in the optical laboratory in the Department. These photographs have been used to estimate the daily rainfall over a meso-scale area in Iraq.

5.3.1 Earth Imaging

The principal payload of the satellite is a multispectral radiometer. This provides the basic data of the METEOSAT system as visible and infra-red images of the earth's disc (Iraq included).

The three channel radiometers include

i) two identical adjacent visible channels in the 0.4-1. 1 μm spectral band,

ii) a thermal infra-red (atmospheric window) channel in the 10.5-12.5 μm band.

iii) an infra-red (water vapour) channel in the water vapour absorption band (5.7-7.1 μm), which can be operated in place of one of the two visible channels.

Each infra-red image is composed of 2500 lines and 2500 pixels (picture elements) with a spatial resolution of 5 km. at the sub-satellite point. In the visible, performance can be twice as good (5000 lines and pixels where the two adjacent channels are operated, ie. when the water vapour channel is switched off).

Radiation data from the earth's disc are acquired during a 25 minute period, followed by a 5 minute retrace and stabilization period, so one set of pictures is available each half hour. Because the water vapour image replaces one of the visible channels the possible sets of image in any one half hour period are:

a. either 2.5 km. resolution visible with 5 km. infra-red, or

b. 5 km. resolution visible, with 5 km. infra-red and 5 km. water vapour.

Each image is transmitted in quasi real-time on a line by line basis, after line stretching in an on-board memory, to the DATTS and hence to the MGCS for further processing, distribution and archiving (ESOC, 1978). The useful area for qualitative use of these images extends to about 65 degrees great circle arc, from the sub-satellite point; but for quantitative use, extraction of meteorological parameters, this area is restricted to about 55 degrees arc. Examples of images in the three spectral channels are shown in Figures 5.1a

Figure 5.1a. Image from the visible (0.4 - 1.1μm) channel of the METEOSAT-1 geostationary satellite at 1155Z on December 1978. Clouds appear white.

b and c. The main characteristics of these images and their transmission are given in Table 5.1. All transmissions pass along the route from the METEOSAT Ground Computer System (MGCS) via the Data Transmission and Routing System (DTRS) and DATTS to METEOSAT and hence to the user stations.

For METEOSAT Weather Facsimile Experiment-Satellite Broadcast (WEFAX) thermal infra-red data the disc viewed is divided into nine roughly equal areas, D1 to D9 (see, figure (5.2a)), D3 being the most important format for studying the Middle East/Iraq weather. For visible data the disc viewed is divided into 24 areas, C1 to C24 (see, figure (5.2b), format C9 being the most important for the Middle East/Iraq.

The grids of longitude, latitude and the coast lines are shown in figures 5.2a and b. and are superimposed onto these formats by ESA station at Darmstadt.

METEOSAT-1 also transmit image data in the water vapour absorption band on format E1 to E9 (E1 covering the same area of D1 ... etc; see figure 5.2a), which are representative of moisture content of the middle and upper atmosphere (7-11 km.).

Image data from the U.S. Geostationary Operational Environmental Satellite (GOES-E) at $70^{o}W$ and USA-ESA (GOES) Indian Ocean at $70^{o}E$ are relayed to Bracknell via METEOSAT-1.

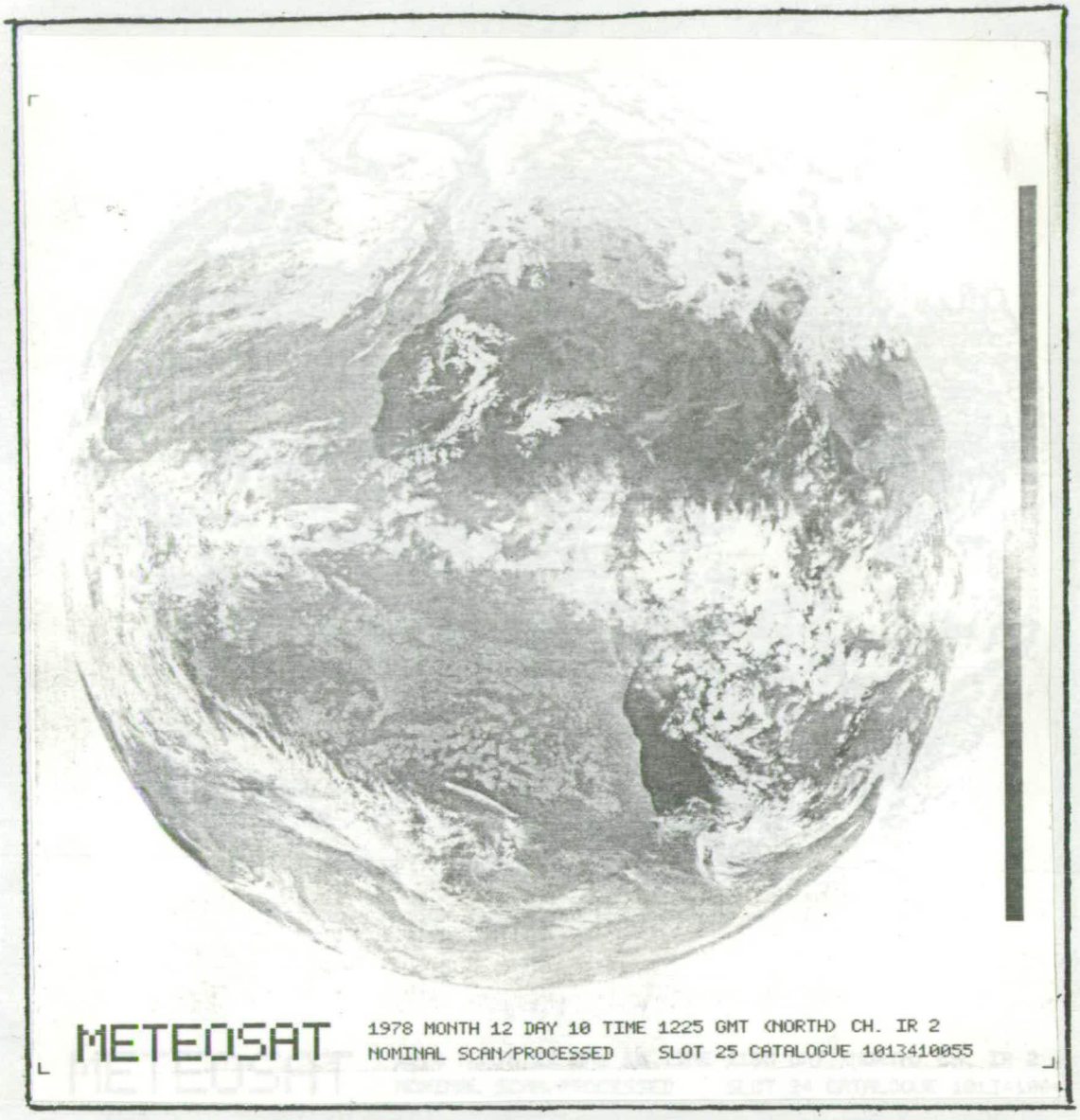

Figure 5.1b. Image from the infrared (10.5-12.5μm) channel of the METEOSAT-1 geostationary satellite at 1155Z on 10 December 1978. Cold high clouds appear white, warmer (low) cloud grey and hot lands as very dark areas.

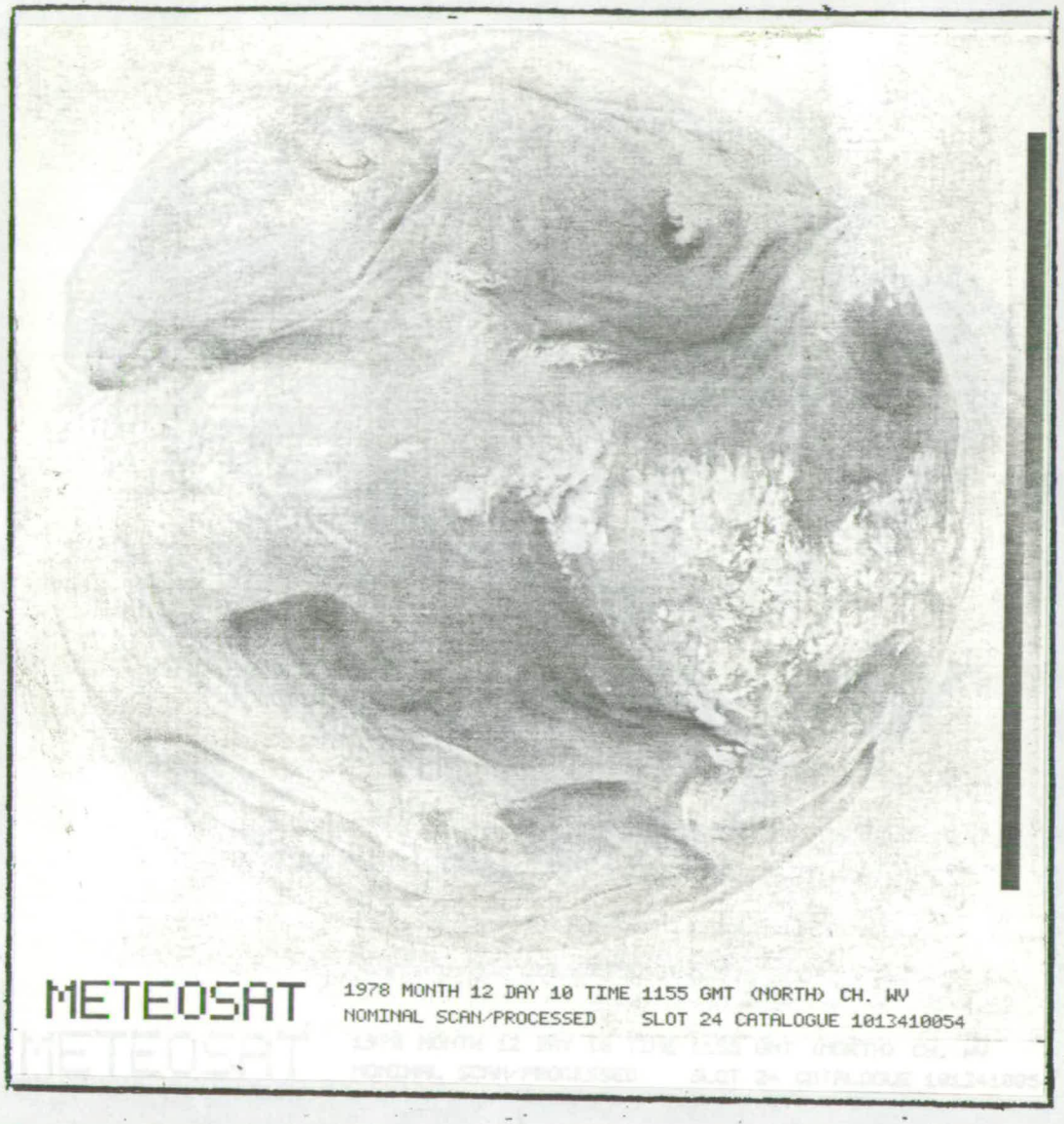

Figure 5.1c. Image from the water vapour (5.7-7.1μm) channel of the METEOSAT-1 at 1155Z on 10 December 1978. White areas represent low temperatures and can be equated with areas of high humidity. The darker shades indicate the lower level of tropospheric humidity. The image shows the (7-11Km.) tropospheric layer humidity.

Spectral bands	Visible (0.4-1.1μm)	Infrared (5.7-7.1μm)	Water vapour (10.5-12.5μm)
Number of channels	Two (simultaneous)	one (in time sharing with VIS.)	One plus one redundant
Number of lines per picture	5000 (2500)*	2500	2500
Number of samples per lines	5000	2500	2500
Resolution (satellite point)	2.5Km.	5Km.	5Km.
Line duration	30ms	30ms	30ms
Image - taking duration	25min.	25min.	25min.
Image recurrence	30min.	30min.	30min.
Transmission DATTS	Digital 2.7 Mbit/s.		

Table 5.1 To show the characteristic of the METEOSAT-1 images(visible,infrared and water vapour) and transmissions.

(*) case in which water vapour channel is also transmitted.

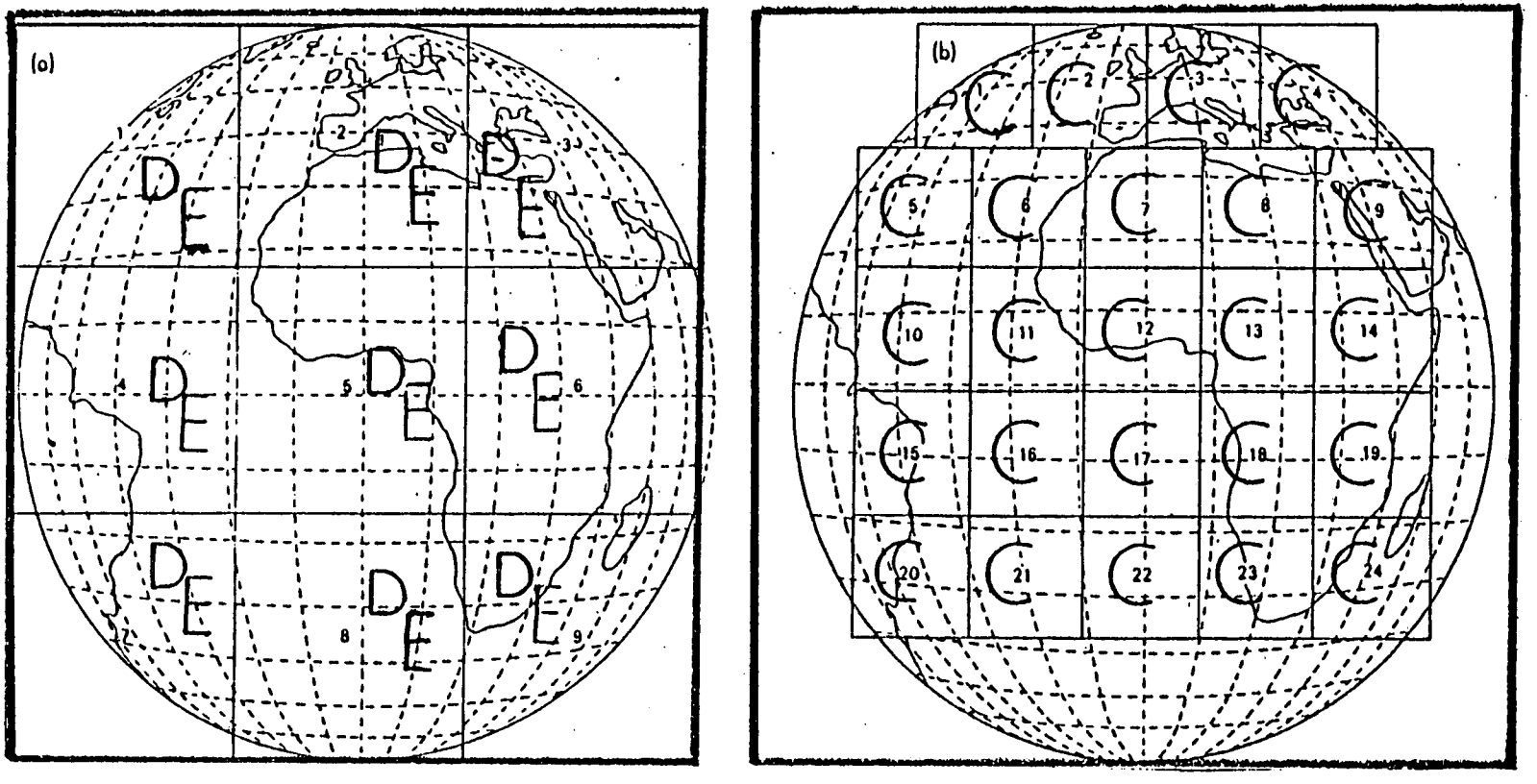

Figure 5.2 Area viewed by METEOSAT-1. Disseminated from European Space Operation Centre(ESOC).

a- WEFAX infrared'Format D' and water vapour'Format E'-9 subdivisions.

b- WEFAX visible'Format C'-24 subdivisions.

METEOSAT-1 images, enlarged format D3 and C9 (figures 5.3a and b.) without longitudes, latitudes and coast lines have been used to estimate the average daily rainfall in Iraq.

5.4 Extraction of the Indices

Subjective (analysis and nephanalysis of satellite images) and objective (extraction and interpolation of the in situ observations from meteorological charts and TØ-grams) approaches to this work have been adopted, producing the following parameters/indices on statistical and physical bases.

5.4.1 Synoptic Weather Pattern

There is a relationship between precipitation forms and intensities with various features of synoptic charts. Bjerknes and Solberg (1921) paid close attention to precipitation patterns in developing their frontal cyclone model. Some striking composite radar photography of cyclones in the central United States have been prepared by Smith and Lidga (1957) which show close agreement with the large-scale pressure system, fronts and precipitation.

The synoptic weather index involved in the present model has been evaluated from the average daily rainfall of 26 raingauge stations in a meso-scale area (3^{o} latitude x 7^{o} longitude) in the central region of Iraq (see figure 5.4) and from synoptic charts.

Rainfall and non-rainfall occurrences for December 1978 and February 1979 were classified in terms

FORMAT"C9"

Figure 5.3a. METEOSAT-1 photograph(VIS),which covers the Middle East.Photograph taken on 31 December 1978 at 1225Z.

FORMAT"D3"

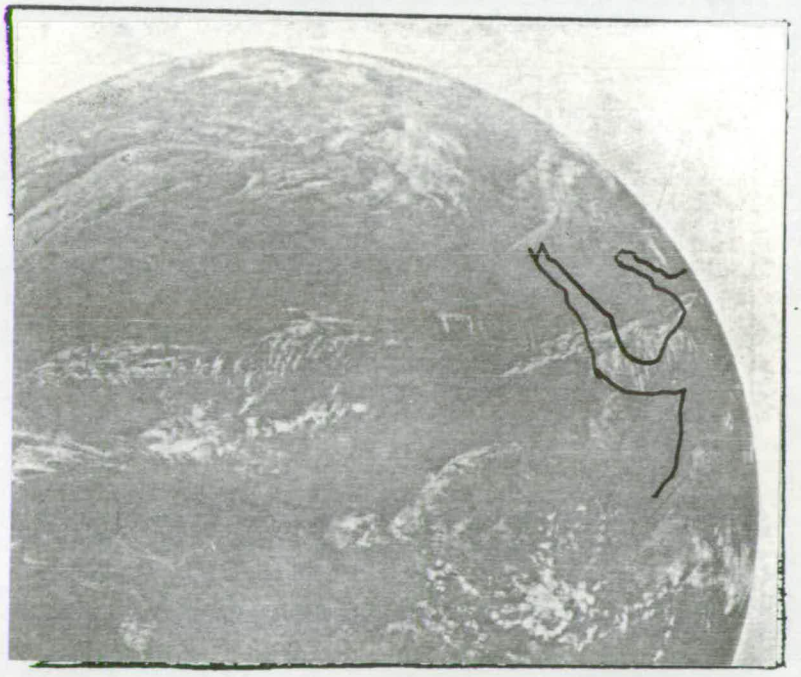

Figure 5.3b. METEOSAT-1 photograph(IR),which covers the Middle East.Photograph taken on 31 December 1978 at 1225Z.

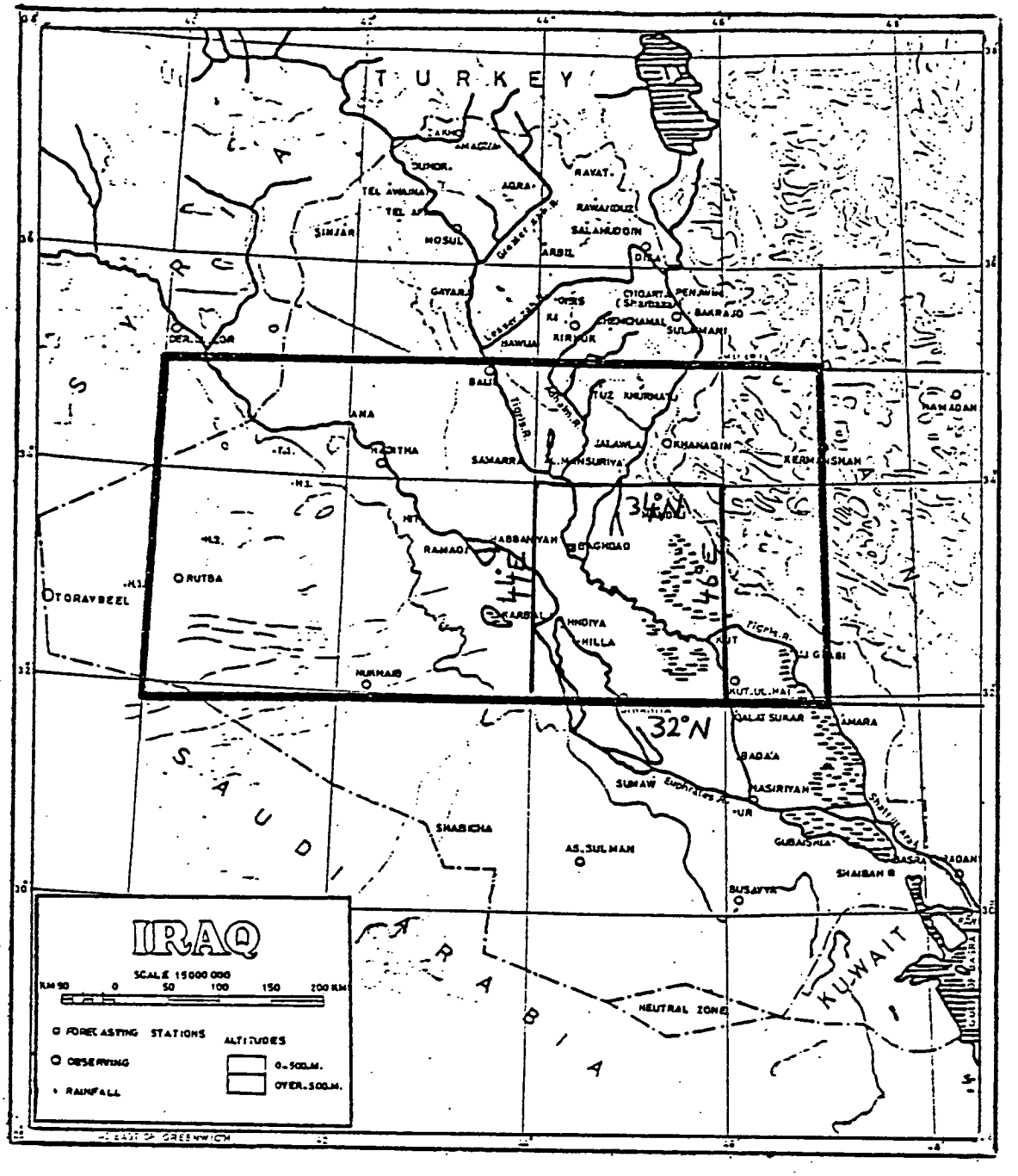

Figure 5.4 Map of Iraq, showing the central area of Iraq in the rectangle containing 26 raingauges.

of a single weather pattern ie occlusion, fronts, trough ..... etc. affecting the central region of Iraq on the day of each occurrence. Each day of December 1978 and February 1979 was accorded a rain or no-rain status in the rectangle shown in figure 5.4 The rain/no-rain observations for a number of specific weather patterns in the wind vector quadrant required were identified, and the weather patterns against the rainfall probabilities were listed and the results summarised in table 5.2.

For example, on 4 February 1979 when the passage of occlusion was indicated by synoptic charts (from Baghdad Meteorological Office) 22 stations out of 26 recorded rain and the probability

$$P = \left[\left(\frac{N-Nr}{N}\right)\right] x \ 100\% \qquad \ldots\ldots\ldots\ldots\ldots\ldots (5.1)$$

where P is the rainfall probability; N is the total number of the raingauge stations in the rectangle (N=26) and Nr is the number of raingauge stations recording no rain

$$P = \left[\left(\frac{26 - 4}{26}\right)_4\right] x \ 100\% = 85\%$$

The subscript 4 represents the date of the month for February 1979. The probability of rain for more than one case for the same synoptic weather pattern is averaged. For example, on 17 February 1979 a trailing cold sector (cold air behind the cold front) was indicated and two stations recorded rain, and on 22 February 1979

December 1978 and February 1979.

Synoptic weather pattern (Sw)	Rainfall probability (%)	Synoptic weather index	No. of cases
Occlusion	85	8.5	1
Frontal succession	74	7.4	1
Cold front	38	3.8	6
Warm front	33	3.3	5
Non-frontal trough	32	3.2	8
Warm sector	20	2.0	6
Trailing cold sector	12	1.2	2
Leading cold sector	3	0.3	2
Ridge of high pressure	1	0.1	8
Cell of high pressure	0.0	0.0	19
Col	0.0	0.0	1

Table 5.2 Rainfall probability index, based on the observation of rain versus no-rain days associated with specific synoptic weather patterns in the Middle East(Iraq), for December 1978 and February 1979.

another trailing cold sector was indicated and four stations recorded rain; the probability in this case is

$$P = \left[\left(\left(\frac{26 - 24}{26} \right)_{17} + \left(\frac{26 - 22}{26} \right)_{22} \right) / 2 \right] 100\% = 12\% \quad \ldots\ldots (5.2)$$

and the probabilities of the synoptice weather pattern were represented in terms of indices as listed in table 5.2

5.4.2 Cloud Type Categories

The synoptic weather features and their analyses are poorly documented over the Middle East/Iraq as a whole. This is particularly so over the deserts where very few surface observations exist. METEOSAT-1 cloud pictures would help to fill this gap and pursue the present research.

The data used to analyse the cloud type categories from satellite images are the actual daily rainfall reported from six Iraqi stations (Baghdad, Mandili, Hindiya, Hilla, Diwaniya and Kut) inside 2° latitude x 2° longitude (ie. inside 44°E 34°N, 46°E 34°N, 44°E 32°N, 46°E 32°N) as shown in figure 5.4 , actual cloud observations from the available synoptic chart of the Middle East/Iraq zone and enlarged METEOSAT-1 satellite image covering the same area. The area 2° longitude x 2° latitude area over Baghdad and other five stations mentioned above were chosen because the stations inside the area provide more reliable data of rainfall than those of the remote area of Iraq.

Since all the data required for the evaluation of the cloud type categories were for two months (December 1978 and February 1979) and METEOSAT-1 images involved were simple (i.e. without enhancement), the author then could distinguish only eight types of cloud categories for the Middle East/Iraqi zone.

The rain/no rain observations for a number of specific cloud types/categories against the rainfall probability are shown in table 5.3 (the rainfall probability has been calculated for each cloud type/ category index in the same way as for the synoptic weather index as was described in the previous item). For example, on 11 December 1978 and 9 February 1979 the dominant cloud type in 2^{o} longitude x 2^{o} latitude area, projected over Baghdad and the five stations, were cumulonimbus and cirrus and all six stations reported rain (irrespective of the amount of the rainfall) thus giving a probability of 100% for the cumulonimbus with cirrus category. Similarly, on 5 December 1978 and 8 and 10 February 1979 we had a probability of 100% when the area mentioned above was covered by cumulonimbus with a cumulus on the days mentioned and the six stations in the area reported rain on each day.

In contrast, no cloud was reported on 15, 18, 20, 22 and 29 December 1978 and also on 5, 12 and 13 February 1979, and none of the six stations in the area mentioned above reported rain on the days listed.

IRAQ

Cloud category	Rainfall probability (%)	Cloud type index	No. of cases
Cumulonimbus with cirrus	100	10	2
Cumulonimbus with cumulus	100	10	3
* Mixed cumuliform with stratiform	70	7	8
* Stratiform	60	6	10
* Stratocumuliform	40	4	10
* Isolated cumulus	10	1	14
Cirriform	0.0	0.0	4
Clear skies	0.0	0.0	8

Table 5.3 To show, cloud category, rainfall probability and cloud type index based on 2 months(December 1978 and February 1979) data of actual daily rainfall and actual cloud observations.

N.B. The rainfall probabilities of the above cloud categories indicated by(*) have been amended to the nearest 5%.

Similarly, on 28 December 1978 and 16, 25 and 28 February 1979 a cirrus cloud cover dominated the area projected over Baghdad and other five stations and none of the six reported rain on the above mentioned days. Therefore the probability of the clear skies category is zero, as is the cirrus cloud category.

On ten occasions when the stratocumuliform dominated the 2^{o} longitude x 2^{o} latitude area, it is shown that on 2 December 1978 and 4 February 1979 only four out of the six stations in the area concerned reported rain in each day; this yields a probability of 66.6% for each day for the above category. (i.e. stratocumuliform). On 9 and 25 December 1978, five out of the six stations reported rain in each day, so the probability is 83.3% for each day mentioned above. On 16 December 1978 and 6 February 1979, three out of the six stations reported rain in each day and this gives a 50% probability of rainfall for each day. No rain was reported at each of the six stations when the stratocumuliform clouds dominate the area projected over the six stations concerned on 23 and 27 December 1978 and 21 and 24 February 1979. This gives 0% probability for rainfall for each of the four days mentioned above. So, the probability of rainfall for the stratocumuliform category from the above calculations is equal to 39.9%. (The author has amended the probability to the nearest five per cent). So, the stratocumuliform probability of 39.9% could be written 40%.

For the isolated cumulus clouds, we have 14 occasions (days) in December 1978 and February 1979. For example, on 17, 19, 21, 24, 30 and 31 December 1978 and 20, 21, 26 and 27 February 1979, none of the six stations recorded rain on each of these days; this gives a probability of 0%. On 10 and 13 December 1978, only two out of six stations recorded rain and this gives 33.3% probability of rainfall for each day mentioned above. On 18 February 1979 only one out of six stations recorded rain and this gives 16.6% probability, and on 23 February 1979 three out of six stations recorded rain, this gives 50% probability. Therefore the probability of the isolated cumulus cloud category is 9.5% (9.5% amended to 10%). The eight cloud type categories and their probabilities are listed in table 5.3

5.4.3 Cloud Top Temperature

As has been mentioned in chapter 3, section 3.2.2. cloud top temperatures can be estimated from infrared images and TØ-grams. It can be estimated also from maps in Weather Facsimile (WEFAX) format designed for dissemination via METEOSAT-1 images. Such data are not available to the author at this stage. One of the objectives of WEFAX is to provide information on the height (temperature) of the cloud top determined from the infrared images with horizontal resolution of about 20 km. The height (temperature) of the top of

the cloud is presented by one of eight grey scales on the map. This product would be disseminated every six hours. Five categories of grey shade were used: black, dark grey, moderate grey, light grey and white, determined subjectively from METEOSAT-1 infrared images (for December 1978 and February 1979).

For each day a rainfall probability was determined and ascribed to the appropriate grey shade and temperature (from Baghdad midday radiosonde) as shown in table 5.4.

For example, on 11 December 1978 and on 9 February 1979, the dominant grey shades were white in the 2^{o} longitude x 2^{o} latitude area and all the six stations mentioned in the previous section (i.e. section 5.4.2.) recorded rain; the probability of rainfall produced by the white shade then is 100%.

In contrast the grey shades were black in the 2^{o} longitude x 2^{o} latitude area on 14 days in both months December 1978 and February 1979, and all six stations recorded no rain; the probability of rainfall of the black shade then is 0%.

Intermediate grey shades probabilities were calculated in the same way (see article 5.4.1. equation (5.2) for the probability calculation). It was not possible to extract eight grey shade scales, only five, because the METEOSAT-1 images were of different exposures and without enhancement and the human eyes are able to resolve far less than satellite radiometers.

Iraq (central region), December 1978 and February 1979.

Shade	Probability (%)	Number of cases	Probability index	Cloud top temperature (C^{o})
White	100	2	10	< -35
Light grey	90	10	9	-25 to -35
Moderate grey	58	12	5.8	-10 to -25
Dark grey	33	21	3.3	0 to -10
Black	0.0	14	0.0	> 0

Table 5.4 Rainfall probability index, based on 26 raingauge observations of rain versus no-rain associated with a specific shade of the infrared of the METEOSAT-1.

5.5 Cloud Motion.

TV and IR images received from meteorological satellites do not as yet provide us with direct information on wind. However, cloud data, certain optical phenomena and ice movement observed from satellites can be used to indirectly determine the wind velocity of the atmosphere. The accuracy of deduced data is, of course, much lower than that obtained by instrumental measurements. Television, infrared and water vapour pictures are best combined with other available data. Satellite data are especially useful in areas with a sparse network of meteorological stations.

In pre-satellite days it was recognized by Kuettner (1959) that, in the organisation of clouds in rows down to the mesoscale, from the tropics as far north as the Arctic, most cloud bands line up in the direction of flow. Similarly, Malkus and Riehl (1964) affirmed that, at least in the tropics, the common mode of "cumulus" organisation is parallel to the flow. Satellite evidence confirms that, under appropriate conditions there are cloud elongations through the cloudy layer of the atmosphere, especially where that layer is shallow.

Gaby (1967), for example, concludes from careful comparisons between satellite and conventional wind direction in the tropics that the larger cloud lines, constituting the locally 'dominant' mode of arrangement vis-a-vis the observed wind, appeared to lie parallel

to the surface wind direction more often than not. But Gaby did strike a cautionary note. He showed that relationships between cloud lines and observed wind speed cover the entire range of possibilities from the "parallel" mode to the 'normal' and support the now well-substantiated fact that, especially where deep cloudiness is concerned, other factors may be more critical in determining the alignment of cumulus and cumulonimbus with which Gaby was occupied primarily.

A pioneer study was undertaken by Lyons and Fujita (1968). They examined the alignments of mesoscale striations in oceanic stratus sheets across part of the north Pacific. On account of their scale, similar straitions have only been identified infrequently from conventional observations while often appearing as patterns in otherwise rather amorphous stratiform cloud fields photographed by satellite.

Anekeeva (1968) analysed cloudiness photographs obtained by meteorological satellites and determined the wind velocity at different levels associated with cloud spirals. Since cloud pictures have been available from geostationary satellites, considerable attention has been given to deducing wind velocity from cloud motion. Suomi (1969) and Fujita et al (1969) describe some of the first of such investigations which are of special value in the equatorial zone where atmospheric motion cannot be

deduced from a knowledge of distribution of pressure. Clouds at two levels are generally available for observation, cumulus cloud typically at 900 mb. levels and cirrus cloud typically around the 200 mb. level. When cloud images from a satellite are being tracked, however, clouds are not observed singly but in groups, so that possible errors arising from individual cloud not moving with the wind is much reduced.

Suchman and Martin (1976) studied the accuracy, representativeness and reproducibility of a cloud tracer wind in the area of the GARP Atlantic Tropical Experiment (GATE). They found that different scientists using the same image data deduced winds differing by less than 2 m/s at cirrus level and 1.3 m/s at cumulus level. They also compared winds derived from satellite data with those derived from radiosondes launched from ships and found differences of less than 3 m/s, which is close to the "noise" level of the radiosonde determinations. They concluded that the derivation of wind from cloud tracer is as good as, if not better than, those derived from GATE network of radiosondes. Suchman and Martin admitted that determination of cloud height with sufficient accuracy remains a significant problem.

Hubert (1976) also reported studies comparing winds derived from satellite images with conventional wind data. He found somewhat larger differences than those reported by Suchman and Martin and also emphasized

particularly the problem of height determination, especially for cirrus clouds. Heights are determined by observing the cloud in the infrared, thereby determining a radiometric temperature. If an emissivity of cloud is then assumed, and also a profile of temperature against height, a height can be assigned to cloud tops. The largest uncertainty here, especially with cirrus cloud, is estimating the cloud emissivity which may vary over a wide range. The experience of the satellite image analyst can be an important factor in assigning a value for cloud top temperature from considerations such as cloud type and synoptic pattern.

The usefulness of satellite-derived wind is clear from the many studies in the literature which make use of them. For example, a climatology of low-level wind from satellite images has been published by Gaby and Potent (1973) and the use of satellite pictures for weather analysis and forecasting by WMO (1973). Work has been done by Leese et al (1971) to estimate the cloud motion from ATS-1 geostationary satellite images using a cross correlation method. From this method they could calculate the cross correlation coefficient which represent the cloud motion of two different times (24 minutes apart). They have used the fast Fourier Transform (fFT) which the author will not go into details of. Studies of the flow around a particular convection cell have been carried out by

Skidar and Suomi (1972) and by Suchman et al (1977) and the role of satellites in the tropical observing system by Houghton (1979a). The five above mentioned studies demonstrate that realistic divergence fields can be produced from satellite-derived winds from which calculations of vertical velocities can be made, giving values in reasonable agreement with estimates from other considerations.

Morgan (1979) described the roles of the METEOSAT-1 system in the calculation of wind vectors routinely from highly automated procedures. The basis of the wind vectors calculation by METEOSAT-1 system is very simple. Identifiable cloud features are tracked from one image to the next and, on the assumption that they move with the wind, their displacements can be converted to wind speed and direction. Unfortunately, this assumption is not always true. For instance, development or decay of clouds may give the illusion of motion, or clouds associated with mountains may remain more or less stationary while a strong wind blows through them. The best method in deriving wind from cloud motion must exclude, as far as possible any cloud not moving with the wind,and select clouds not changing its systematic shape significantly in a short time period.

Despite the varieties of methods mentioned above the author has used a simple technique to derive wind from METEOSAT-1 images as we can see in article 5.5.1

5.5.1 Image Referencing.

In the present study, the basic principle used to determine the motion of rain-bearing cloud from METEOSAT-1 data is simple. The starting point is a sequence of METEOSAT-1 infrared images, all covering the same area of the earth. These images must be carefully aligned so that all the coastlines and the earth horizon coincide from image to image. The movement of cloud across the sequence is then apparent from the superimposed images and can be measured. The height of the clouds is then determined from their grey shades scale as described in items 5.4.3

The first step was to choose a sequence of two images so that they can be superimposed on each other. This enables the location of specific rainy cloud to be given in earth co-ordinates. This is known as "image referencing", and was achieved manually using transparent METEOSAT-1 images and a light table. The accuracy of the cloud motion determination is extremely sensitive to the precision of this step, since mislocation of coastline and land features of images 12 hours apart by as little as one millimetre causes an error of several metres per second in the results.

Before any attempt was made to compute the cloud motion, it was necessary to know if suitable rainy clouds were present over the Middle East area.

The days 2 and 6 of December 1978 were chosen for three reasons, firstly, there is a very extensive area of clouds producing rain as shown in Fig. 5.5 a and b, which is not significantly changed in systematic shape within 12 hours, hence in this case we avoid the tracking of small bands of clouds which typically dissipate and grow within a few hours, so causing some error as occurred with Fujita et al (1975), who found about ± 40% difference between wind wind motion and cumulus cloud motion. Secondly, on those days the atmosphere was baroclinic and the wind direction and speed distinctly changed with height, as mentioned below, because this leads to a more realistic choice of the level of advected rain-producing cloud. Thirdly, rain was reported at Beirut meteorological station (31° 49'N, 35° 29'E) and other neighbouring stations on the days mentioned above. At Beirut on 2 December 1978, the wind velocities were 290° of 6 kts at 800 mb at 12GMT, 270° of 23 kts at 700 mb and 240° of 50 kts at 500 mb, whereas in an area of 5° latitude x 5° latitude over Beirut a distinguishable mass of rain-bearing cloud was advected with direction of 260° and speed of approximately 25 kts as shown in figure 5.5c.

It appears that the whole cloud mass inside the square (on average) at time 0555 GMT had been advected a distance of approximately 300NM after 12 hours (i.e.

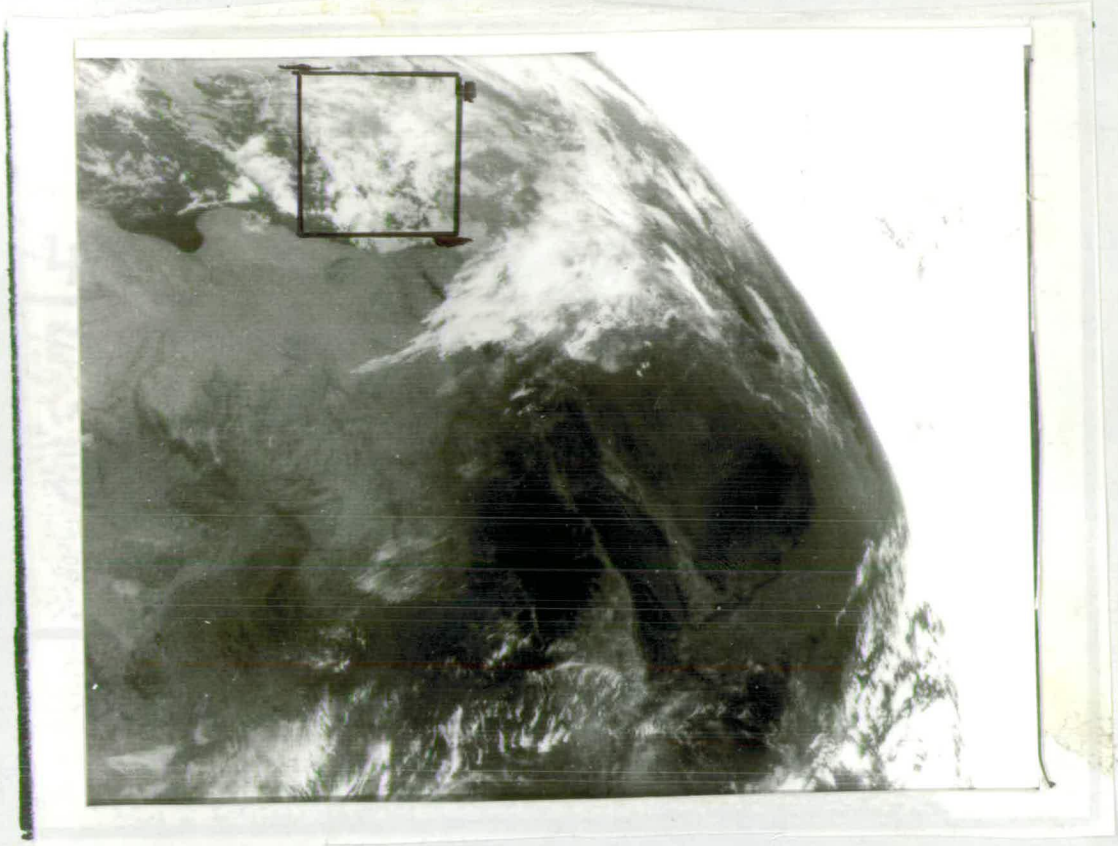

Figure 5.5a. Image from the 10.5-12.5μm channel of the METEOSAT-1 at 0555Z on 2 December 1978.

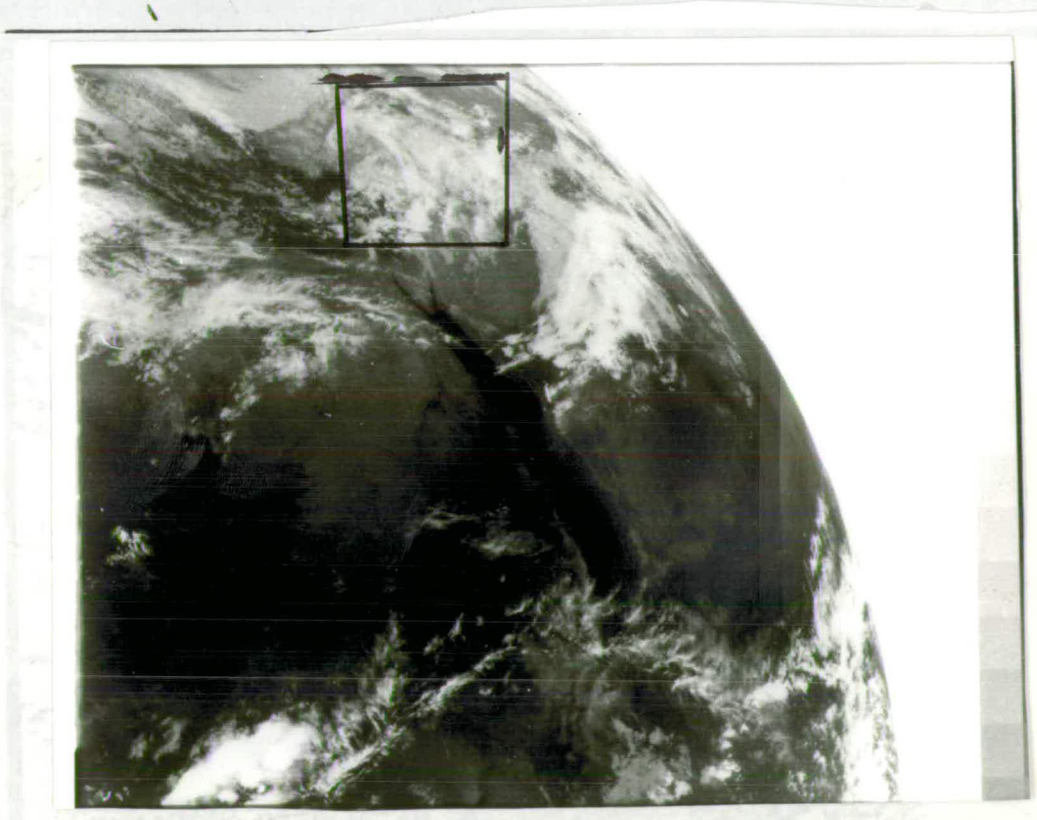

Figure 5.5b. Image from the 10.5-12.5μm channel of the METEOSAT-1 at 1755Zon 2 December 1978.

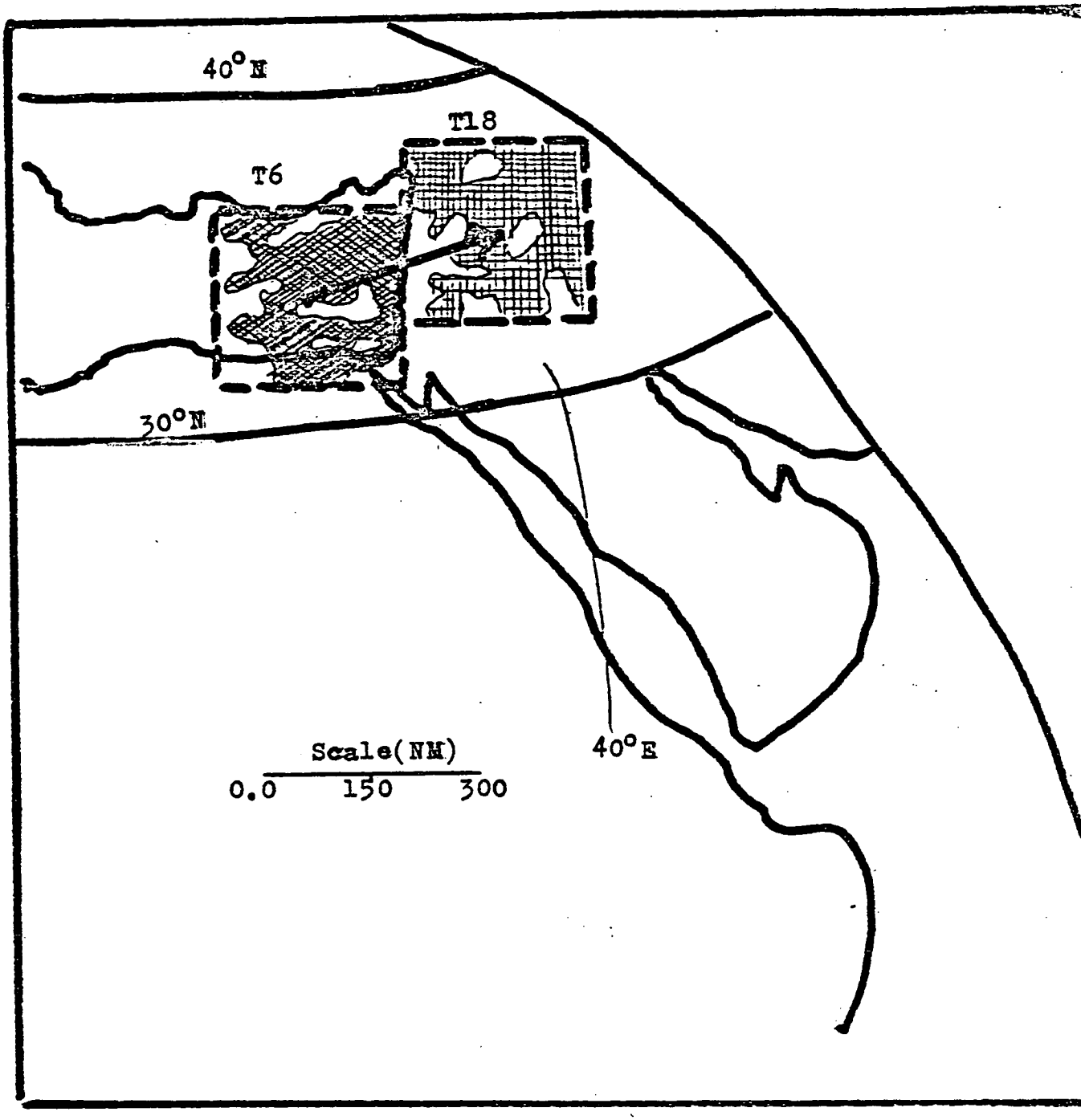

Figure 5.5c. To show the cloud motion on the 2 December 1978 over the Middle East area.

Key:-

➡ cloud velocity
T6 cloud band at 0555Z
T18 cloud band at 1755Z

at 1755 GMT) on 2 December 1978.

Another example is that for 6 December 1978, when the wind velocities at Beirut were 350° of 18 kts at 850mb at 12 GMT, 220° of 27 kts at 700mb and 250° of 64 kts at 500mb, but the rain-bearing cloud velocity was approximately 230° of 23 kts.

For the above reasons 700mb wind velocity is chosen in this model to advect the rain-bearing cloud over the Middle East and Iraqi zone to estimate the daily rainfall.

5.6 Results and Verification.

The correlation coefficient between the precipitation prediction index and the observed average daily rainfall of 26 raingauge stations in central Iraq for December 1978 and February 1979 is 0.90 and the linear regression equation is

$$Y = -0.014 + 0.001\,X \quad \ldots\ldots\ldots\ldots\ldots\ldots\ldots\ldots (5.3)$$

where Y is the estimated value of averaged daily rainfall in millimetres and X is the rainfall prediction index. The correlation coefficient of the above equation, which was tested using the "t" statistic, is significant at 99% using the sample size as equal to the number of independent values (N = 59).

The regression line of the above equation for 59 observations (December 1978 and February 1979) 32 of them at or very near the origin, is shown in figure 5.6.

In the regression equation, theoretically it has been found that the rainfall value is zero, when the rainfall prediction index is 104.

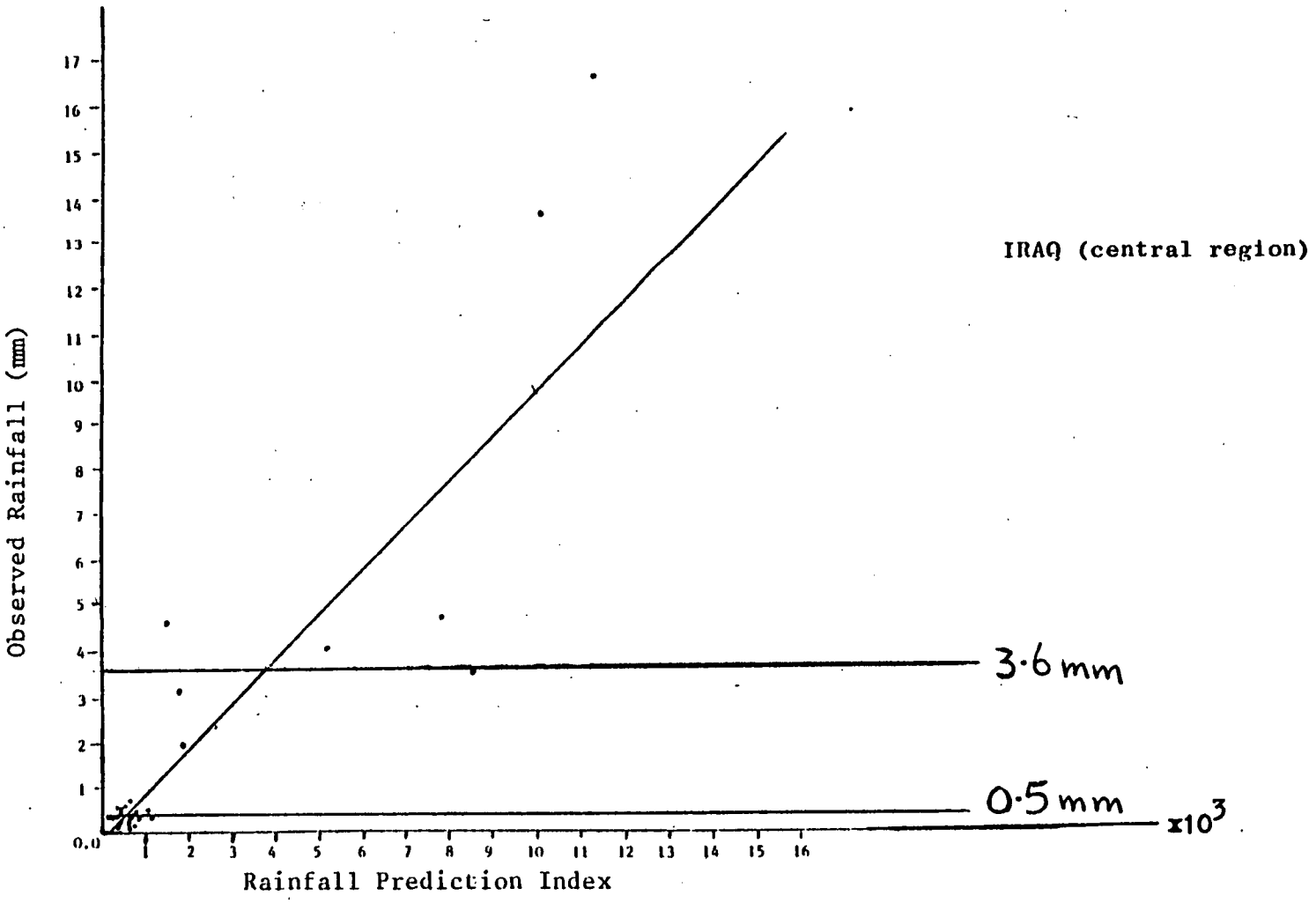

Figure 5.6 Rainfall against rainfall prediction index for December 1978 and February 1979.

N.B. 32 Observations at or very near the origin are not shown.

In practice when the rainfall prediction is less than or equal to 104 the estimation is considered to be dry (no rain).

Figure 5.6 facilitated the choice of rainfall prediction index values used later in the verification example defining rainfall class limits for forecasting purposes. These limits were established for local classes by grouping its wet days into three groups of approximately equal likelihood (see table 5.5).

The 1-31 January data for 1979 were used to test the method of calculation of the rainfall prediction index; it is shown that the results were encouraging.

Table 5.6 for January 1979, lists the rainfall prediction indices, forecast rainfall classes, actual/observed rainfall and their accuracies of forecasts involved in the method.

For example, on January 9, 1979,the Rackliff Index (R.I.) was 34.7 and the average relative humidity of 1000-500 mb layer ($\overline{RH}$%) was 79% (see figure 5.7a), the 700 mb wind speed was 32 kts at direction of 190°; synoptic weather pattern was an occlusion as shown in figure 5.7b (i.e. synoptic weather index = 8.5). Figure 5.7c of the METEOSAT-1 nephanalysis shows that the cloud amount was mostly covered (approximately 70% of the total area of the quadrant) and cloud type was

Iraq, December 1978 and February 1979.

Class	Rainfall(mm)		Number of observations
None	0.0	0.0	32
Light	> 0.0	$\leqslant 0.5$	11
Moderate	> 0.5	$\leqslant 3.6$	11
Heavy	> 3.6	No limit	5

Table 5.5 Daily rainfall(mm) grouped to give approximately equal populations of wet days in the classes "light", "moderate" and "heavy" rainfall.

January 1979.

Date	Rainfall Prediction Index	Rainfall Prediction (Class)	Actual Rainfall (mm)	Accuracy of Forecast
1	101.4	None	0.0	Right
2	57.2	None	0.0	Right
3	173.0	Light	0.0	Wrong
4	734.1	Moderate	0.2	Wrong
5	218.2	Light	0.0	Wrong
6	21.0	None	0.0	Right
7	533.7	Light	0.1	Right
8	3004.3	Moderate	2.1	Right
9	5914.3	Heavy	6.3	Right
10	4303.7	Heavy	3.0	Wrong
11	404.2	Light	0.4	Right
12	216.0	Light	0.0	Wrong
13	94.2	None	0.0	Right
14	27.6	None	0.0	Right
15	2734.3	Moderate	0.8	Right
16	1004.3	Moderate	1.3	Right
17	415.2	Light	1.0	Wrong
18	3203.1	Moderate	4.0	Wrong
19	3652.9	Heavy	5.3	Right
20	1703.9	Moderate	3.1	Right
21	5303.8	Heavy	9.4	Right
22	4120.8	Heavy	7.7	Right
23	2002.9	Moderate	0.7	Right
24	602.9	Light	0.2	Right
25	14.7	None	0.0	Right
26	83.5	None	0.0	Right
27	28.5	None	0.0	Right
28	74.3	None	0.0	Right
29	18.1	None	0.0	Right
30	29.4	None	0.0	Right
31	31.5	None	0.0	Right

Table 5.6 Formation and verification of daily rainfall estimation for Iraq(central region).

Baghdad ,9/1/1979 AT 1200GMT

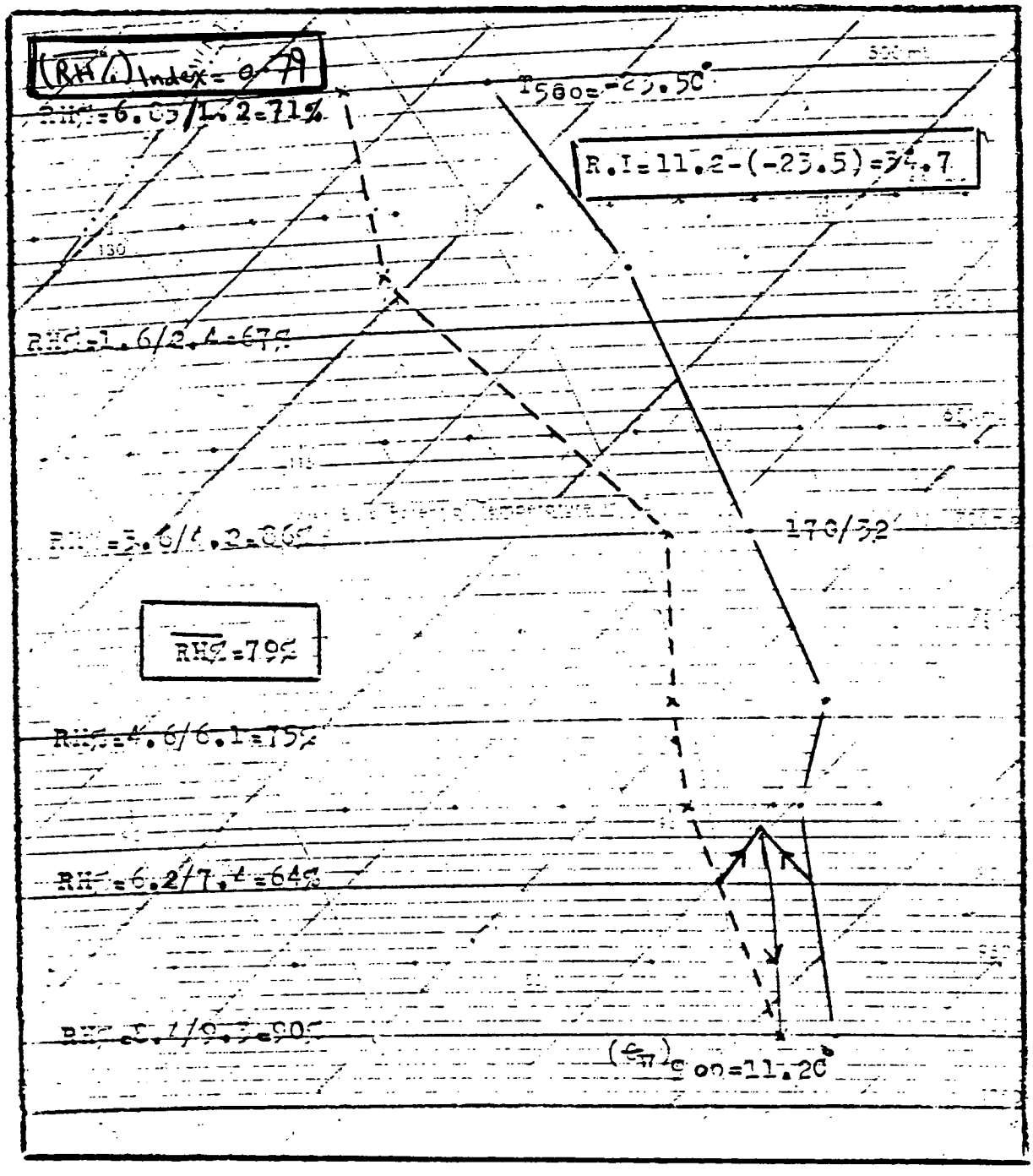

Figure 5.7a. Baghdad ascent for 9/1/1979 at 1200Z, showing the average relative humidity($\overline{RH\%}$) in the 1000-500mb. layer and Rackliff Index(R.I).

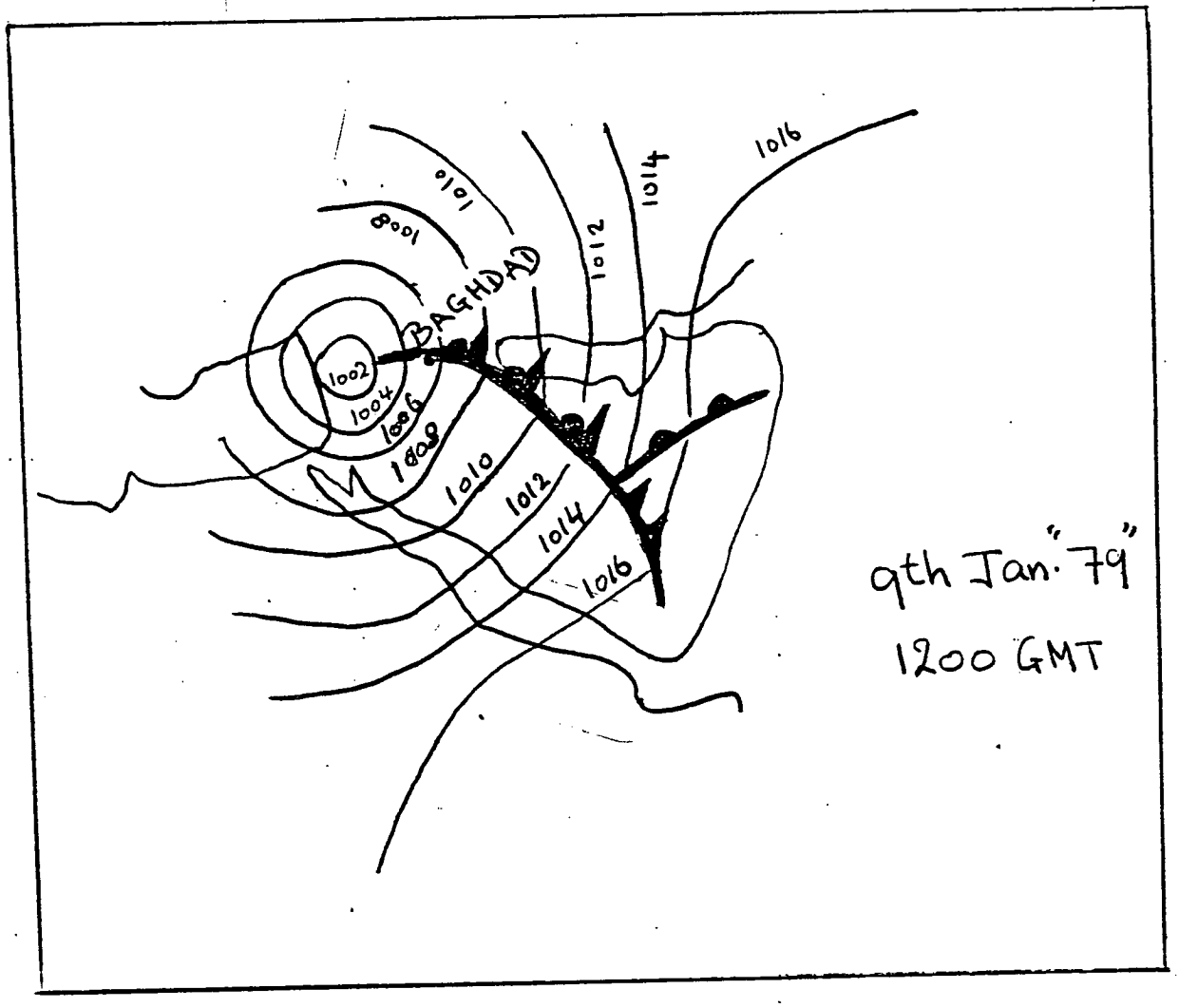

Figure 5.7b. Surface chart of the Middle East at 1200G.M.T. on January 1979 (from Baghdad Meteorological Office).

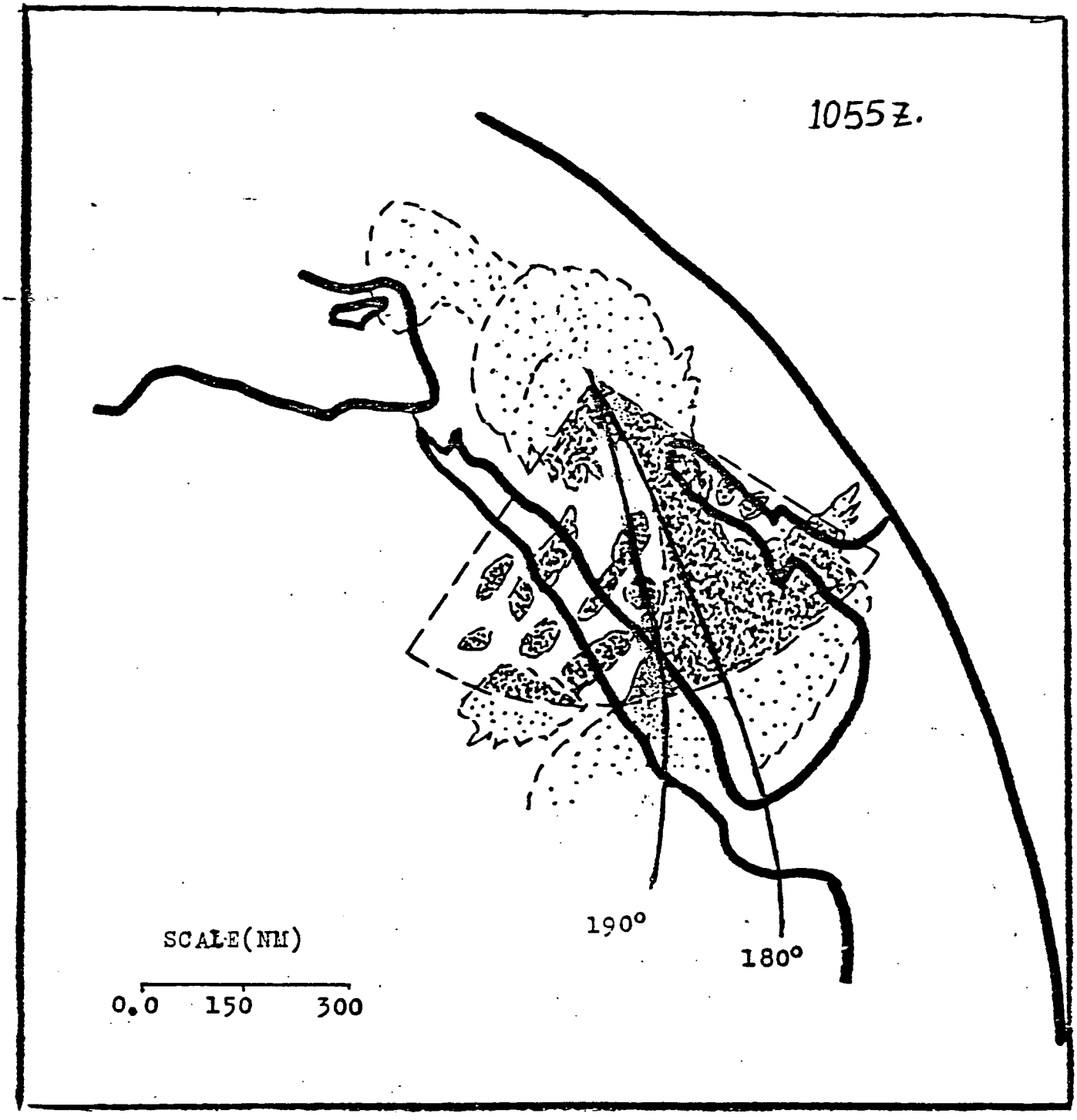

Figure 5.7c. Cloud quadrant for Baghdad, on 9 January 1977 superimposed on nephanalysis of the METEOSAT-1. (cloud amount ≑70% of the quadrant).

N.B. The distance scale is for the region around Iraq. Slight distortions of the quadrant due to the curvatures of latitude and longitude lines have been ignored.

7/10 of mixed cumuliform-stratiform cloud (i.e. cloud type/category index is (7/10) x 7 = 4.9). The cloud top temperature in the quadrant was a mixture of light grey and moderate grey shades (i.e. cloud top temperature index is (9 + 5.8)/2 = 7.4) So the rainfall prediction index is

$$RR_{24} = 34.7 \times 0.79 \times 8.5 \times 0.70 \times 4.9 \times 7.4$$

$$= 5914.3$$

Table 5.6 associated this prediction index with heavy rainfall. The actual rainfall of January 9 1979 was 6.3 mm (heavy) and the estimated was 5.8 mm (heavy), therefore the estimation was correct.

In the case of no rain the correct score was 80% (12 out of 15 occasions) for the light rain, 75% (3 out of 4 occasions) for moderate rain, 71.4% (5 out of 7 occasions) and for heavy rain 80% (4 out of 5 occasions), as shown in table 5.7.

Of the 31 estimates, 24 were in the correct category, which is 77.4% success rate. The number of correct forecast/estimation exceeds the number of incorrect by the ratio 3:1.

The observed rainfall values plotted against the estimated values for comparison is shown in figure 5.8.

Table 5.8 shows the observed rainfall values listed against the estimated values in order to calculate the (absolute) forecast errors and the average percentage

Iraq, 1 - 31 January 1979.

		Estimated values of rainfall				
		None	Light	Mode-rate	Heavy	Total
OBSERVED VALUES OF RAINFALL	None	12	3			15
	Light		3	1		4
	Mode-rate		1	5	1	7
	Heavy			1	4	5
	Total	12	7	7	5	31

Table 5.7 Contingency table, showing the correct, under and over estimated values of rainfall.

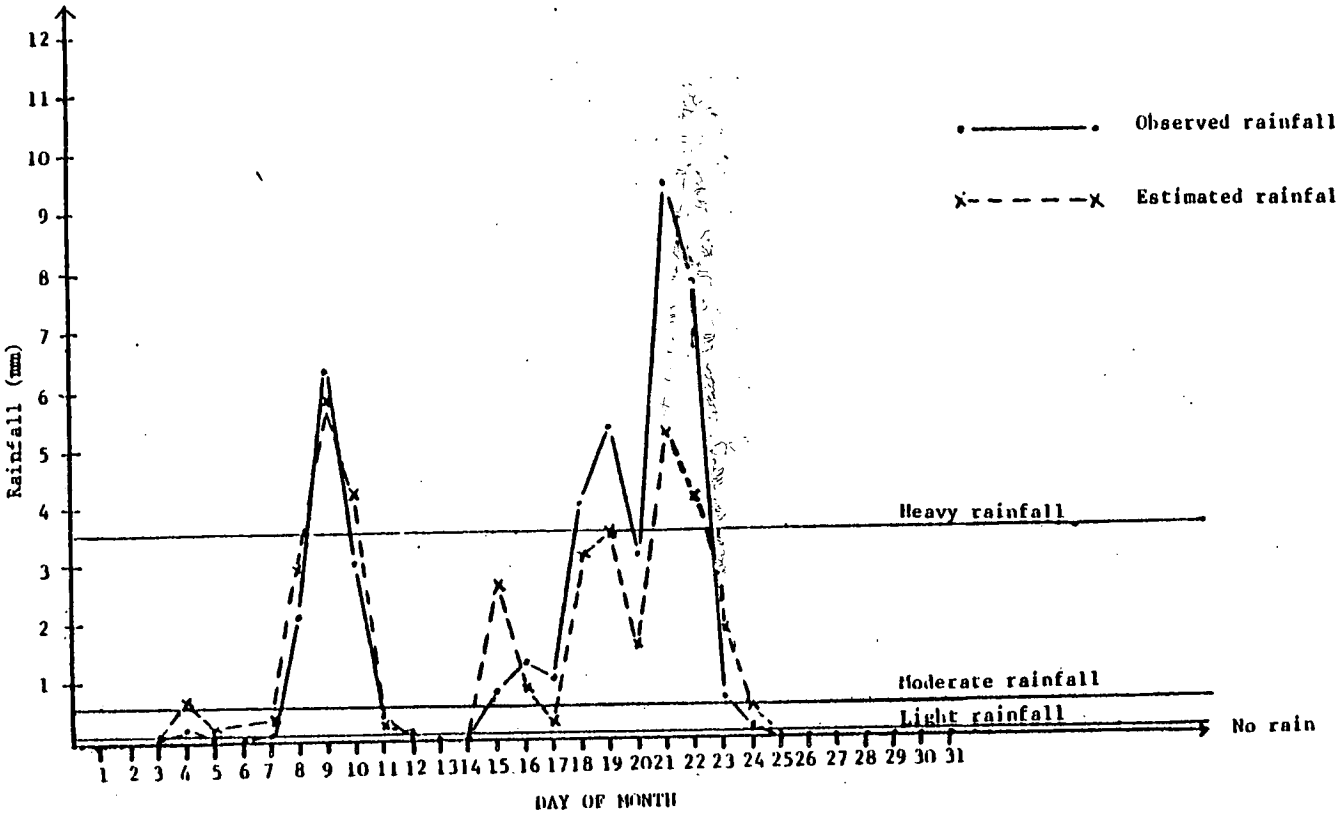

Figures 5.8 Estimated against observed daily average rainfall over Iraq (Central region) for January 1979.

IRAQ(CENTRAL REGION), JANUARY 1979.

DATE	ACTUAL RAINFALL (mm) ((A))	ESTIMATED RAINFALL (mm) ((B))	FORECAST ERRORS (FE) = ((A)) - ((B))	(FE) ABSOLUTE VALUE
1	0.0	0.0	0.0	0.0
2	0.0	0.0	0.0	0.0
3	0.0	0.1	-0.1	0.1
4	0.2	0.6	-0.4	0.4
5	0.0	0.1	-0.1	0.1
6	0.0	0.0	0.0	0.0
7	0.1	0.4	-0.3	0.3
8	2.1	2.9	-0.8	0.8
9	6.3	5.8	0.5	0.5
10	3.0	4.2	-1.2	1.2
11	0.4	0.3	0.1	0.1
12	0.0	0.1	-0.1	0.1
13	0.0	0.0	0.0	0.0
14	0.0	0.0	0.0	0.0
15	0.8	2.6	-1.8	1.8
16	1.3	0.9	0.4	0.4
17	1.0	0.3	0.7	0.7
18	4.0	3.0	1.0	1.0
19	5.3	3.5	1.8	1.8
20	3.1	1.6	1.5	1.5
21	9.4	5.2	4.2	4.2
22	7.7	4.0	3.7	3.7
23	0.7	1.8	-1.1	1.1
24	0.2	0.5	-0.3	0.3
25	0.0	0.0	0.0	0.0
26	0.0	0.0	0.0	0.0
27	0.0	0.0	0.0	0.0
28	0.0	0.0	0.0	0.0
29	0.0	0.0	0.0	0.0
30	0.0	0.0	0.0	0.0
31	0.0	0.0	0.0	0.0
TOTAL	45.6	37.9	7.7	20.1
Average	1.47	1.22	0.25	0.65

Table 5.8 Showing the values of the actual and estimated rainfall, forecast errors and their averages.

errors. It is noticed from the data in table 5.8 that the average forecast error is equal to 0.65, so this is the accuracy of the predicted/estimated rate in our model of rainfall estimate over central region of Iraq. It seems also from the data of table 5.8 that the average value of the actual rainfall is not significantly different from the average estimated value, when using the statistical test "Z-test for the difference of means".

5.7 Discussion and Conclusions

Despite the difficulties in obtaining quantitative results from the subjective analysis, one can use the method of estimating the daily rainfall over Scotland, Iraq and other countries simply by using the relevant parameters which suit that particular country.

It is difficult to say that this technique is the best in predicting/estimating rainfall even though the results were encouraging.

If we look at figure 5.6 we see scattered points along both sides of the regression line, and these may be due to the following reasons:

1. Lack of experience in obtaining quantitative results from cloud characteristics (height, amount and type).

from METEOSAT-1 satellite images because each image has different exposure.

2. Possible inaccuracies in obtaining initial data.
3. Time discrepancies between the rainfall data and other six parameters involved in the rainfall estimations.
4. Some of the indices are statistically not reliable as shown in table 5.2 and 5.3
5. Variations of cloudiness in time were not included.
6. Microscale isolated clouds in the METEOSAT-1 images were missing because they are smaller than the resolution of the satellites.
7. Only five grey shade scales of cloud top temperature cloud be differentiated from the satellite images, some of them not being statistically reliable as shown in table 5.4 whereas the METEOSAT-1 maps for cloud top temperature/height WEFAX format could recognise eight grey shade scales.

Improvements to this method could be made by the following:

a. Using intermediate times of satellite images in order to fill in the gaps to get more accurate estimation of cloud features and conventional observations.
b. Select the most appropriate of the five geostationary international satellites which are working for the

first GARP experiment to get a better resolution over a particular area (see figure 5.9 a and b).

c. It will be more appropriate if the 24 hr average forecast wind (rain-producing cloud advection wind) is used rather than the actual wind.

d. The METEOSAT-1 systems include provision for the routine extraction of meteorological parameters from basic image data. By using fully automated production of the parameters together with experience and skill one can improve this model.

This is accomplished in the Meteorological Information Extraction Centre (MIEC), which is part of the METEOSAT-1 ground system located at European Space Operations Centre (ESOC) in Darmstadt, West Germany. A fully automated approach to this task has been adopted, with a computer-based system known as the (MIEC) Automatic, producing the meteorological parameters on a regular basis, for example:

i) cloud motion

ii) cloud analysis

iii) upper and middle tropospheric humidity

iv) cloud top temperature (height)

In the recent future the parameters will be available and accessible to users in the developing countries with low cost, which then can be used for operational purposes.

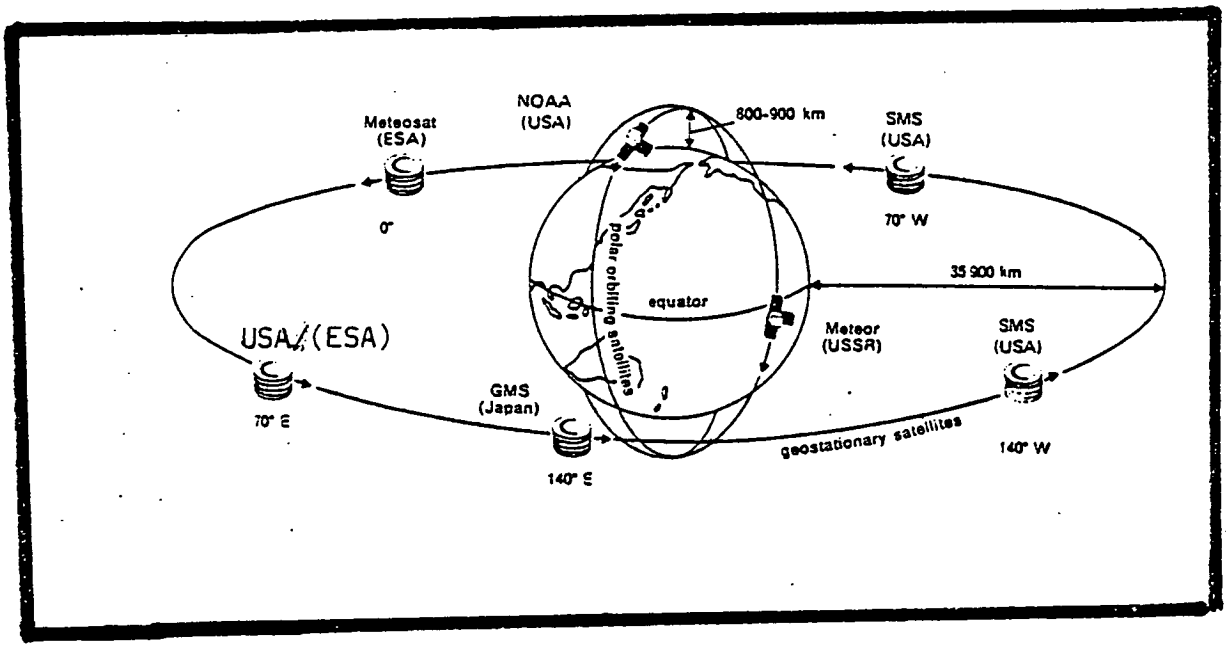

Figure 5.9a. The five geostationary satellites in operation for the FGGE, equally spaced around the earth.

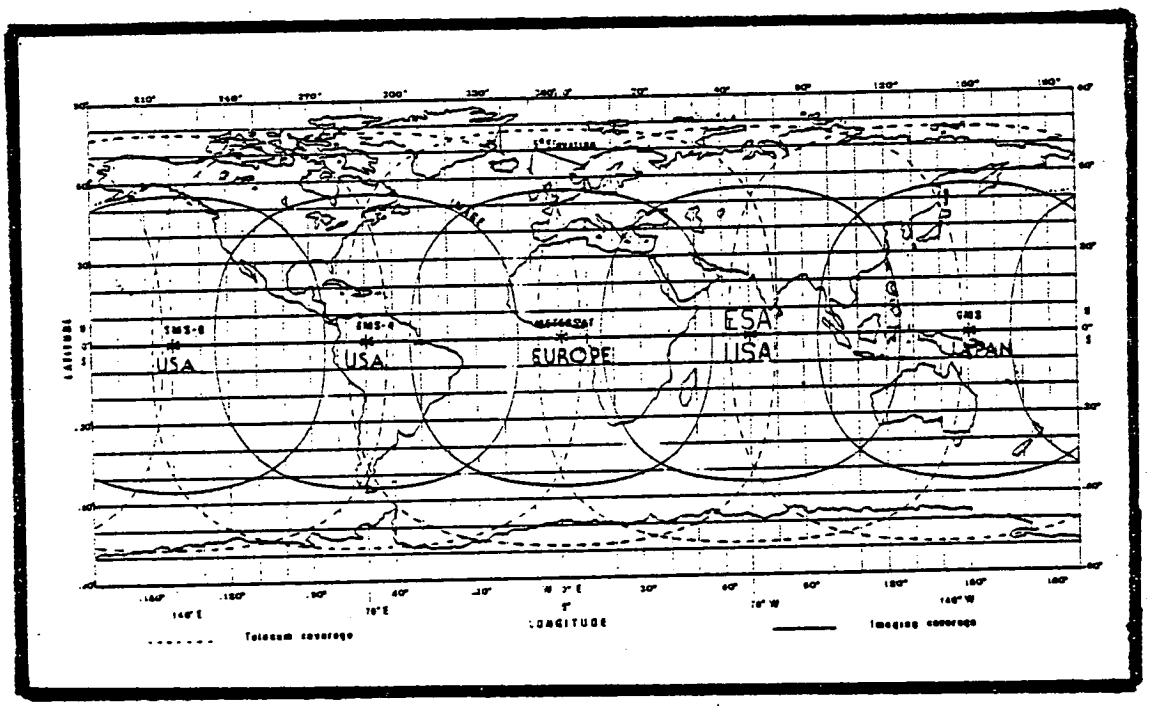

Figure 5.9b. Coverage and communication of the five geostationary satellites.

CHAPTER SIX

AN ANALYSIS OF METEOSAT-1 WATER VAPOUR IMAGES OVER THE MIDDLE EAST.

In this chapter the author analysed subjectively the water vapour images of METEOSAT-1 with radiosonde data over the Middle East to find guidelines for the vertical distribution of the moisture content in the troposphere and to find guidelines also for the spatial distribution of the moisture content and wind field at the 400mb level.

6.1 Introduction

Starr et al (1958) investigated the global scale distributions of the total water vapour mass, and Szava-Kovats (1938) investigated the global relative humidity of the troposphere.

The above analyses were based largely on radiosonde measurements. However, the extreme sparsity of stations over most of the earth's surface and the sizeable measurement errors cast doubt on the validity of these analyses.

Satellite measurements of thermal radiation in the atmospheric water vapour (6 μm) channel promise to yield better determinations once methods are developed to extract from such measurements information about the vertical water profile or the total water vapour content.

Radiometric observations from TIROS 2 were made in 1960 in the spectral region near the 6.3 μm water vapour absorption region. These observations have been

utilized to map relative humidity in the upper troposphere (Raschke and Bandeen, 1967).

It is known that the distribution of tropospheric water vapour and clouds are closely linked with the dynamics and circulation of the atmosphere. Martin and Salomonson (1970) inferred the location and extent of dynamic features in the upper troposphere. Steranka et al (1973) reported upper tropospheric circulation features under essentially clear sky conditions from the data of the 6.7μm channel of the Nimbus-4 THIR. They derived flow patterns under cloud-free conditions by following the changing orientation of the white and grey shade patterns in the image. Kastner and Fischer (1980) demonstrated the feasibility of using water vapour images from Nimbus-5 to determine winds. By tracking contours in the water vapour image, i.e., cloud edges and water vapour patterns, a large number of wind vectors were derived and compared with radiosonde observations. Kastner and Fischer's results showed that the water vapour tracking can complement cloud tracking, especially in regions where there are only low-level clouds or in regions without clouds.

Since 11 December 1972 the Nimbus-5 Satellite Microwave Spectrometer (NEMS) has been measuring the following:

1. the atmospheric temperature profile from 0-20Km
2. the atmospheric water vapour and liquid water abundances over open ocean
3. geophysical parameters such as snow and ice distribution and type.

Staelin et al (1976) have employed measurements from the NEMS on Nimbus-5 at wavelengths near 1.4 and 0.9cm to infer the total water vapour and total liquid water content of the atmosphere.

Eigenwillig and Fischer (1980) used time sequence METEOSAT-1 water vapour images enhanced by a high pass filter to remove the fuzziness and to bring out the sudden changes from cold or moist (white) to warm or drier (dark) regions, to extract upper wind vectors over cloud free areas.

Ward et al (1981) used the same type of images used by Eigenwillig and Fischer (1980). They followed the persistence of water vapour clusters on sequential images to determine more accurately the upper wind vectors.

Hunt et al (1981) demonstrated how quantitative atmospheric parameters can be obtained from satellite images using the Interactive Planetary Image Processing System (IPIPS) developed at the University College London (UCL). The IPIPS facilities are being expanded to produce a more interactive analysis of cloud tracking

to determine wind fields, using data from a variety of satellite measurements at visible, infrared and water vapour channels.

An extensive review of water vapour and liquid water content of the atmosphere has been made by Houghton (1979b).

In many of the efforts cited above, much of the data analysis involved the processing of rather large amounts of digital data on high-speed computers.

The objective of this chapter is to show that the relatively inexpensive and easily available imagery from METEOSAT-1 water vapour (5.7-7.1 μm) channel can be used with the aid of the visible, infrared images and quantitative conventional data to study the moisture and wind fields at about the 400mb level.

These satellite images permit one to refine and improve the spatial detail in analysing not only moisture and wind but also other atmospheric parameters and to extend the analyses into regions where conventional observations are sparse or non-existent.

An air mass can be considered to conserve its water vapour if there is no condensation and evaporation and if the air mass is above the turbulent mixing layer near the ground. Such conditions are realized in cloud-free areas of the middle and upper troposphere. Thus, by studying water vapour data, important details should be revealed about atmospheric features.

6.2 Data Description.

The first water vapour channel flown aboard the European geostationary satellite METEOSAT-1 provided equivalent blackbody temperature observations of cloud tops and the earth's surface with the 10.5-12.5μm window channel and also measurements of the moisture distribution in the middle and upper troposphere (250-500mb) with a 5.7-7.1μm water vapour channel. The window and the water vapour channels each have a spatial resolution of 5Km at the subsatellite point.

With respect to the water vapour channel, moisture rich or cloudy regions are indicated by the white or light grey shading on the pictures, and the drier areas are delineated by dark grey to black tones. It is in regions where the window shows no cloudiness that the potential utility of the water vapour channel begins to appear. Therefore with the water vapour channel considerable detail associated with the water vapour distribution is observed and outlined in the pictures. Figures 6.1a and b. illustrate the METEOSAT-1 photographs of the window and water vapour channels. In areas A1 and A2 on figure 6.1a and b cloud masses exist and they are visible in both channels. Areas B and C are clear, low cloud or thin cloud as shown in figure 6.1a and very noticeable detail delineating relatively dry and moderately moist

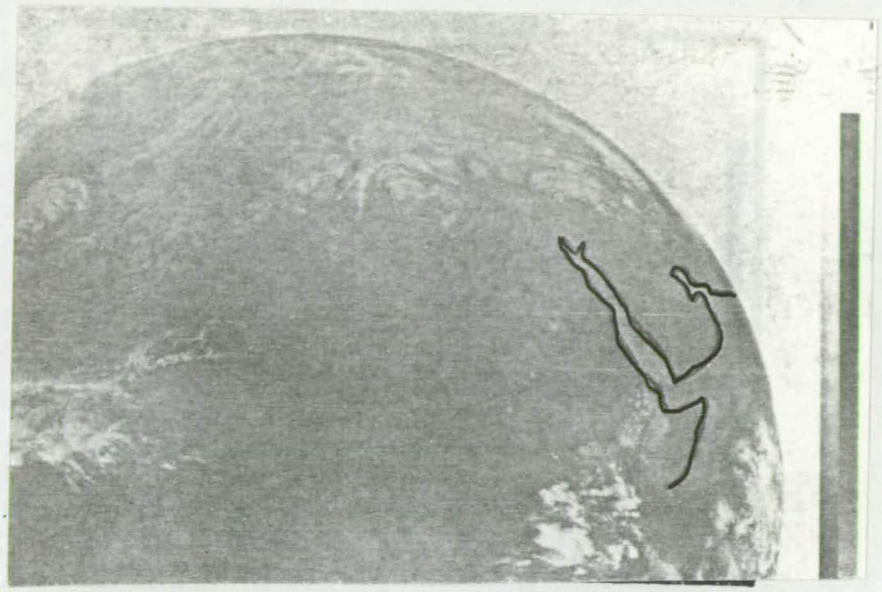

Figure 6.1a. METEOSAT-1 image in the 10.5-12.5μm spectral regions at 1155GMT on 18 December 1978. Areas A1 and A2 are shown as cloud masses and areas B and C are clear areas.

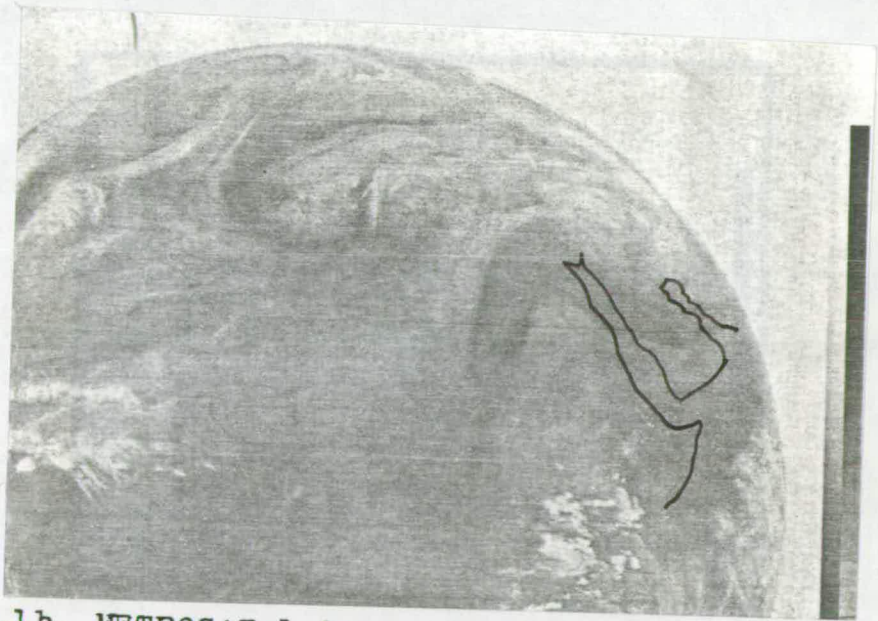

Figure 6.1b. METEOSAT-1 image in the 5.7-7.1μm spectral regions at 1155GMT on 18 December 1978. Areas A1 and A2 are shown as cloud masses and areas B and C are noticeably different than the above figure.

regions (according to their grey shades) can be seen in figure 6.1b.

6.3 Moisture Content Analysis.

Before one proceeds to apply the water vapour pictures for any purpose, it should be emphasized that the level or the vertical extent of the moisture producing the grey shades in the pictures is only very broadly defined as being commonly between the 600 and 250mb levels.

The spectral response of the water vapour channel of the METEOSAT-1 is similar to the 6.7μm THIR channels of Nimbus-4 and Nimbus-5 (Roulleau, 1978 and Kastner and Fischer, 1980).

The water vapour profile (height against contribution function) that applies to Nimbus-5 THIR 6.7μm channel as it would appear when applied to a standard atmosphere, is shown in figure 6.2a and the relative spectral response of the METEOSAT-1 water vapour channel in figure 6.2b. Furthermore, this contribution function will distort and/or move up and down as the amount and vertical distribution of the temperature and moisture in the middle and upper troposphere changes, as we will see later in our example.

Enlarged METEOSAT-1 images sub-divisions E3, D3 and C9 for the water vapour, infrared and visible images respectively were chosen (for E3, D3

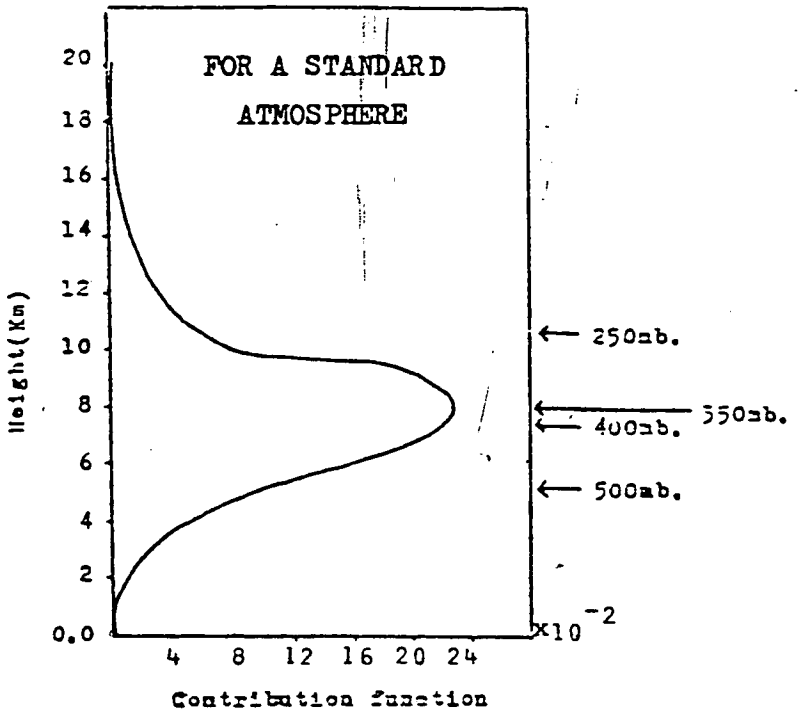

Figure 6.2a. Showing the atmospheric emission contribution at various altitudes to the radiance observed in the NIMBUS-5 THIR 6.7μm channel.

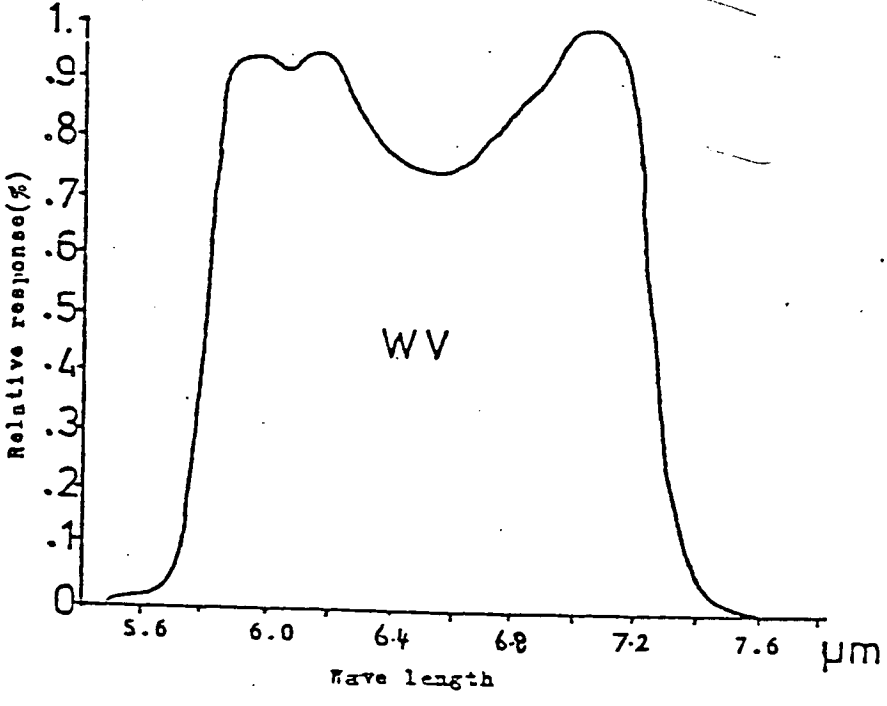

Figure 6.2b. METEOSAT-1 spectral response of the water vapour channel.

and C9 see chapter 5 figure 5.2).

The interesting region of study is centered over the Eastern part of the Mediterranean basin and the Middle East as shown in figure 6.3.

The available data for the water vapour study are for December 1978. It was difficult to locate many situations of clear sky in wintertime over a synoptic area covering the Middle East/Iraq and neighbouring countries, because this month on average is a cloudy and rainy month over the area concerned, though it was possible to locate some days where the sky was clear somewhere and cloudy elsewhere over the Middle East and neighbouring countries. These days (the days which show clear sky somewhere and cloudy sky elsewhere) are chosen because the spatial pattern of the water vapour images which show different grey shade, and the visible, infrared and synoptic charts whow less cloud amount over the area concerned than those of the other days of the month. From these we can make subjective judgements of the moisture distribution and the wind field in the middle and upper troposphere.

6.3.1 Spatial (Horizontal) Moisture Content Analysis

It is intended to demonstrate the possibility of utilizing the profile in the water vapour imagery and to compare it with conventional observations made at radiosonde stations. For this purpose the profile shown in figure 6.2a has been considered in order to

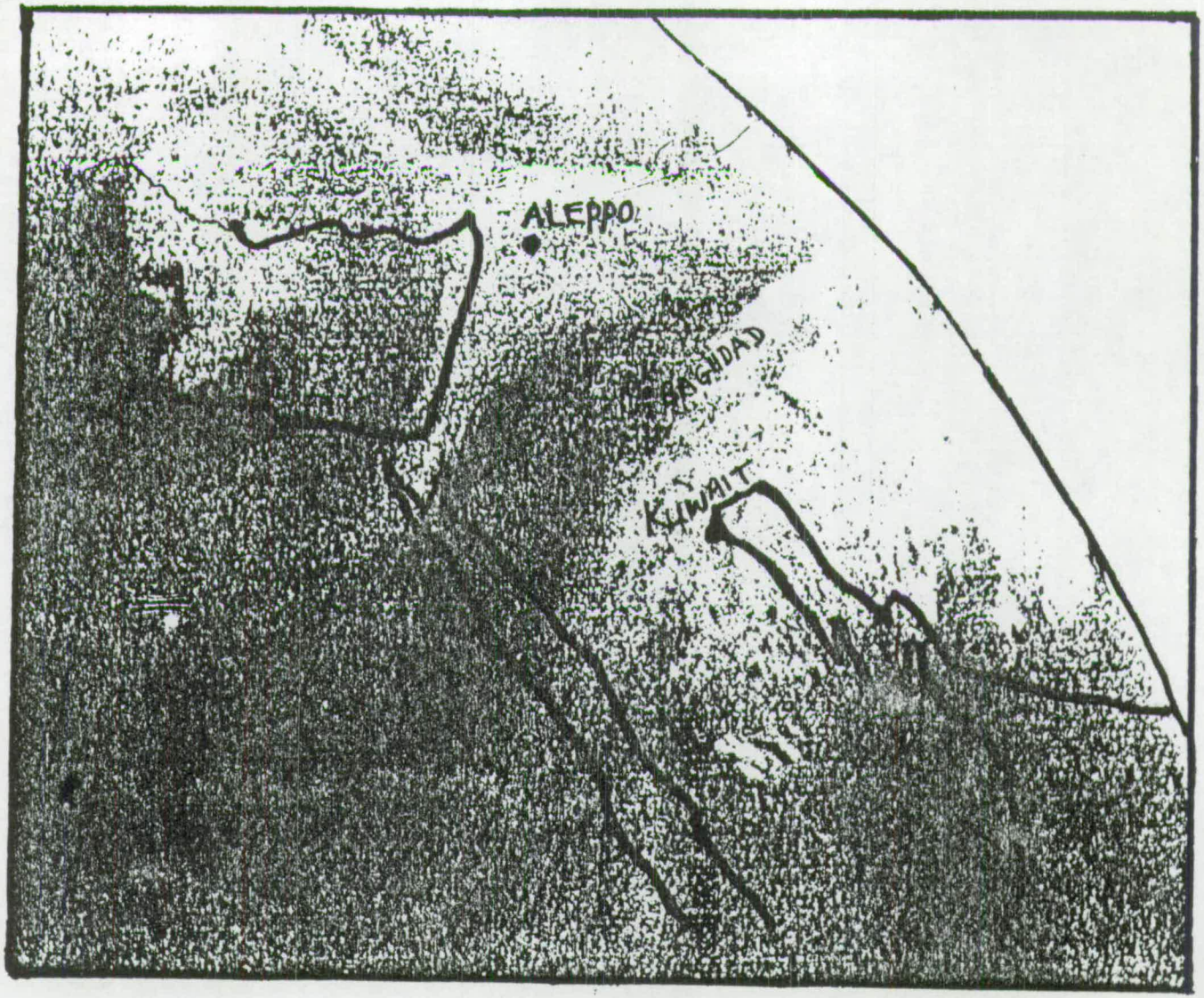

Figure 6.3 METEOSAT-1 image in the 5.7 - 7.1μm spectral regions at 1155Z on 10 December 1978. **The projections of the geography and coast lines of the Middle East onthe water vapour image are not in their exact positions, because of the slight curvature on the image itself.**

draw the 400mb mixing ratio for 1200 GMT on 10 December 1978. The 400mb level was selected because it is the closest standard pressure level to the 350-400mb layer where the maximum contribution to the emitted radiance observed by the water vapour channel sensor is believed by many authors to occur in middle latitudes and nearby.

The 400mb level data are the suitable data to be analysed in order to study the water vapour over the Middle East and Eastern Mediterranean, because the maximum level of the contribution function by the water vapour varies between 300-250mb in and near the tropics and between 600-500mb at and near the poles.

On most of the occasions in December 1978 the water vapour images show little spatial contrast over a large range of relative humidity of the 500-400mb layer. For example, on 10 December 1978 at 12 GMT the relative humidity of the 500-400mb layer at Kuwait (29° 13′N, 47° 59′E) and at Aleppo (36° 11′N, 37° 13′E) was 19% and 78% respectively and the relationship between them is not obvious because both stations are covered with white shade as shown in figure 6.3. Similarly, on 22 December Hefa (32° 00′N, 34° 39′E) and Dilizan (40° 45′N, 44° 52′E) were covered with white shade and the relative humidity of the 500-400mb layer at them is 18% and 59% respectively.

The relative humidity is a function of temperature difference between the dry bulb temperature (T) of an air mass at any pressure level and the dew point temperature (Td) of that air mass at the same pressure level. The higher the difference between T and Td the drier is the air (i.e., the lower the relative humidity will be). The relative humidity describes how close the air is to saturation. In order to be more precise about the study of water vapour, the author will introduce the mixing ratio.

The mixing ratio is the ratio of the mass of water vapour to the mass of dry air and is also equal to the saturation mixing ratio at Td. It depends on the vapour pressure and the total pressure. The mixing ratio is important because it is often conservative (no mixing, evaporation or condensation). A property of this mixing ratio is that its distribution near the surface is nonuniform from the equator to the poles in both hemisphere as a consequence of the latitudinal temperature gradient from the equator to the pole. In hot tropical coastal area it may reach a concentration of about 3% of the mass of the dry air. By contrast, in some localities it occurs in such small proportions that it is difficult to measure. Since the different grey shades on the water vapour image represent different radiative temperatures of different water vapour concentration at a certain tropospheric layer (in clear sky status or in the presence of low clouds), then the

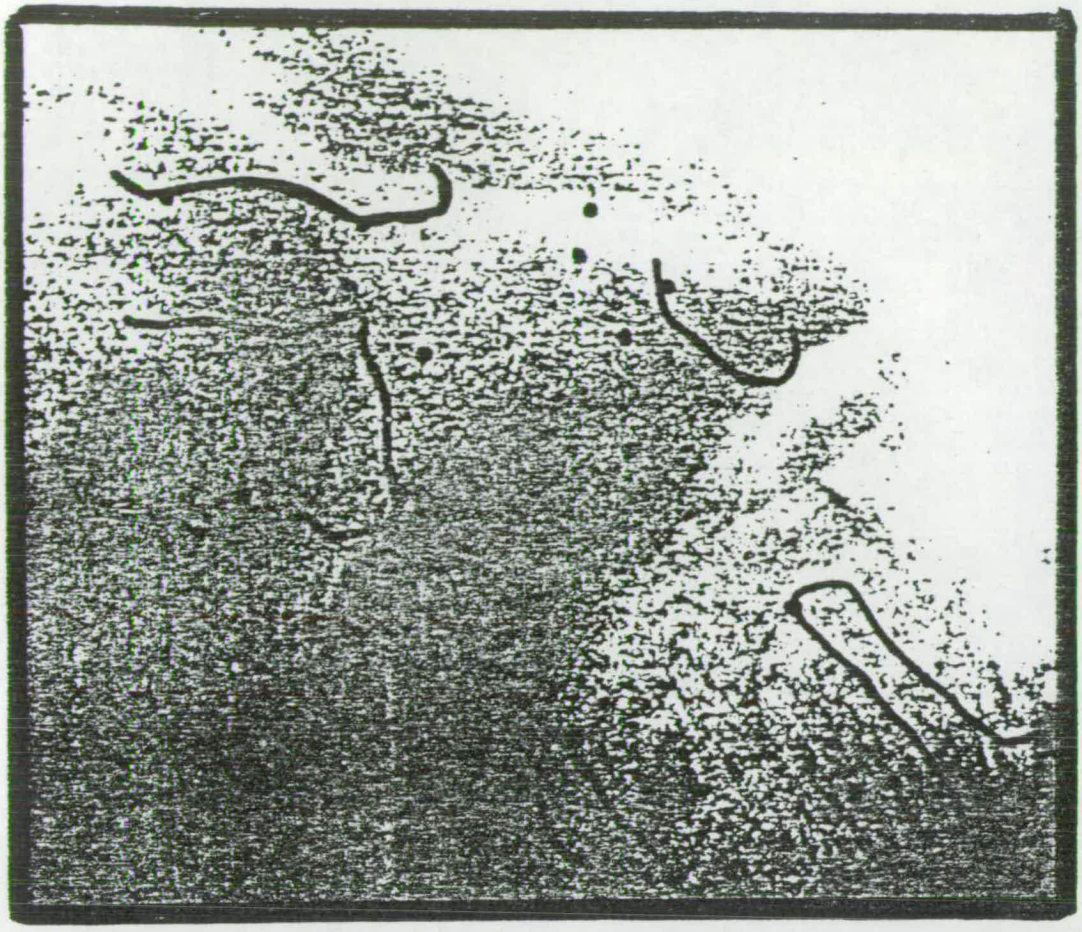

Figure 6.3 – For comparison with figures 6.4a and b below.

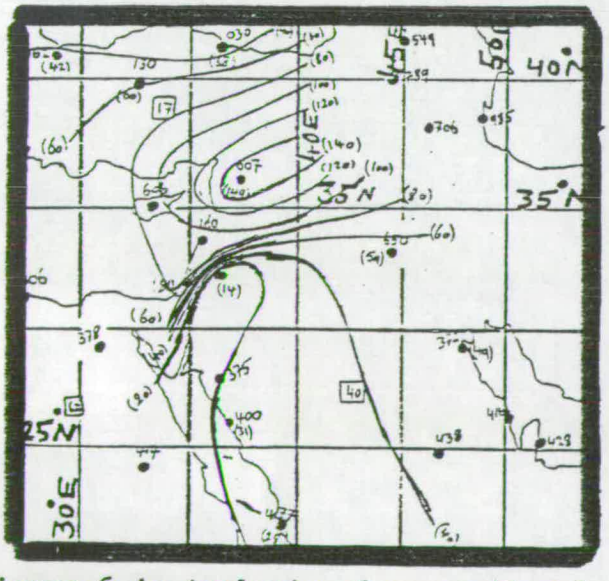

Figure 6.4a Analysis of conventional 500mb mixing ratios("g/Kg"x100) at 12GMT on 10 December 1978 over the Middle East. Analysis here shows weak agreement with the grey shades shown in figure 6.3 above.

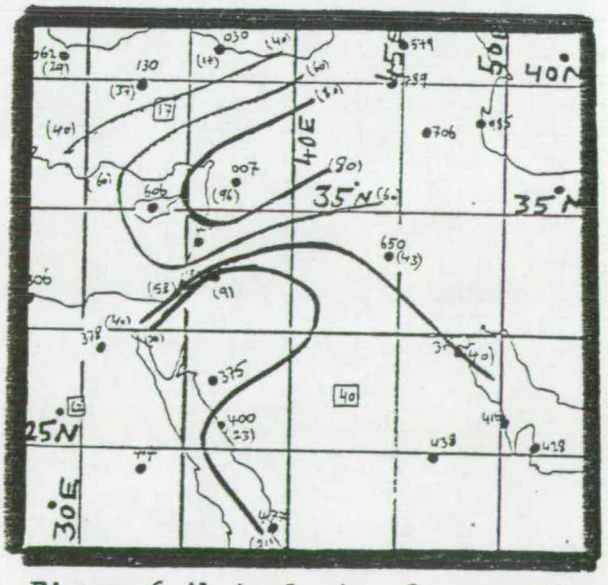

Figure 6.4b Analysis of conventional 500-400mb mixing ratios("g/Kg"x100) at 12GMT on 10 December 1978 over the Middle East. Analysis here also shows weak agreement with the grey shades shown in figure 6.3 above.

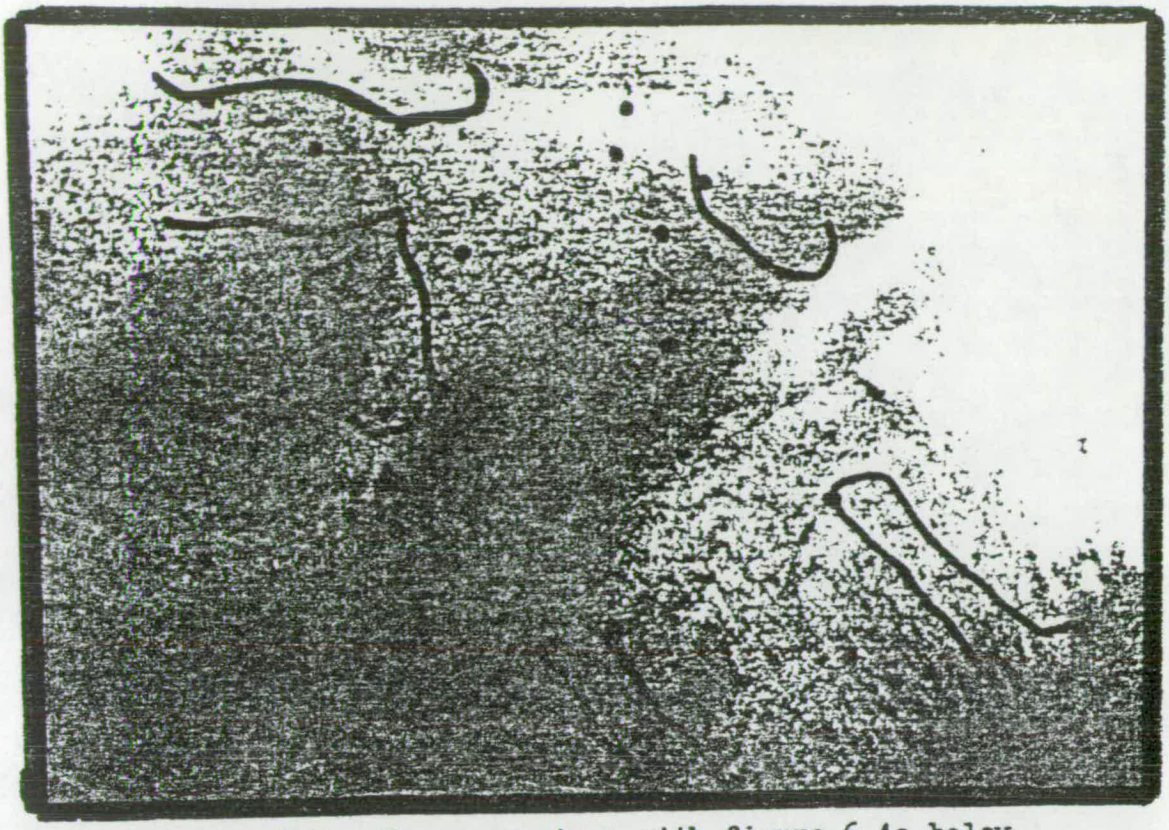

Figure 6.3 - For comparison with figure 6.4c below.

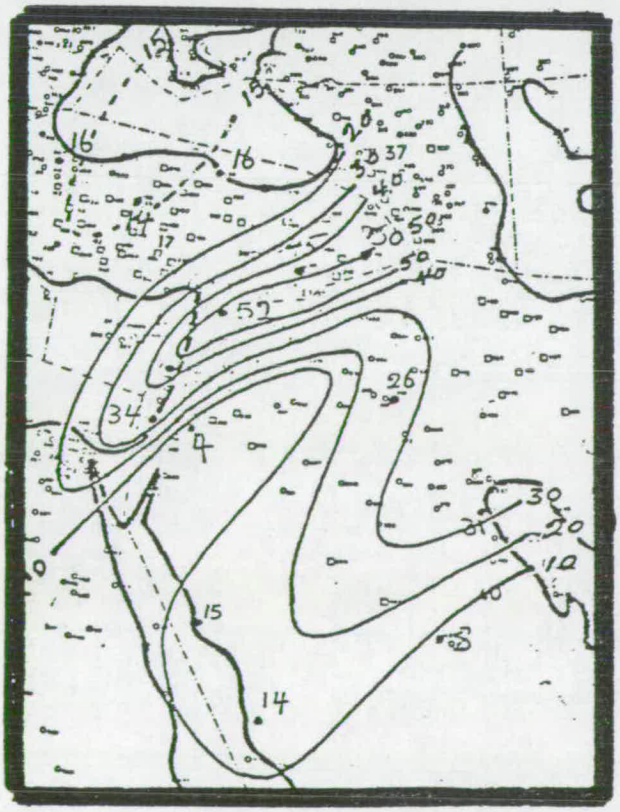

Figure 6.4c Analysis of conventional 400mb mixing ratios ("g/Kg"x100) at 12GMT on 10 December 1978 over the Middle East. analysis here shows good agreement with the grey shades shwon in figure 6.3 above.

above mentioned property of the mixing ratio will help in associating the grey shades with moisture content in the troposphere. A small amount of water vapour in the troposphere can absorb or emit a great deal of radiation in the water vapour wavelength (6.3 μm). The analyses of moisture content charts of December 1978 show acceptable agreement between the 400mb moisture content pattern deduced from radiosonde data and the grey shade of METEOSAT-1 water vapour images over the Middle East. The analysed moisture content charts over the Middle East for the 500mb, 400mb and 300mb levels and also for the 500-400mb layer for 10 December 1978 at 12 GMT using the limited available radiosonde data show that many of the grey shades in figure 6.3 correspond well with the moisture content at the 400mb level rather than the 500mb, 300mb level or 500-400mb layer as shown in figures 6.4a, b and c. (the 300mb moisture content chart on 10 December 1978 at 12 GMT has not been drawn here because it shows a very weak pattern of moisture content. The spatial variations of the mixing ratio over the Middle East area at 300mb level were small and range from 0.04 to 0.08 g/kg. The weak patterns of the moisture content were very dissimilar to that of the water vapour grey shade pattern of figure 6.3). For example, in general the three patterns of the moisture content

shown in figures 6.4a, b and c look nearly the same but the moisture pattern of the 400mb level (figure 6.4c) shows closest agreement with the grey shade pattern of the water vapour image shown in figure 6.3.

However, it is difficult to construct a pattern of moisture content on a 400mb chart that exactly agrees with the water vapour grey shade pattern even in clear sky condition because the reliability of the radiosonde measurements of moisture content in the middle and upper troposphere is poor, and the daily water vapour images are not consistent, because the grey shades vary considerably from day to day because of the satellite-ground receiving system.

A very noticeable spatial variation in grey shade appeared in the water vapour image (figure 6.4d) on 22 December 1978 at 1155 GMT covering the Middle East and neighbouring countries where extensive area of clear sky is reported. Unfortunately the actual data of the moisture content at 400mb level covering the area concerned were not enough to be analysed in order to draw the moisture content pattern. So, the author intends to separate the data and discuss them individually. For example, on 22 December 1978 at 1155 GMT the grey shades covering Aleppo (40007) and Riyadh (40438) were black and both stations reported at 400mb level moisture contents of 0.03 g/kg each (see figure 6.4d). Hefa (40180) and Al-Wejh (40400)

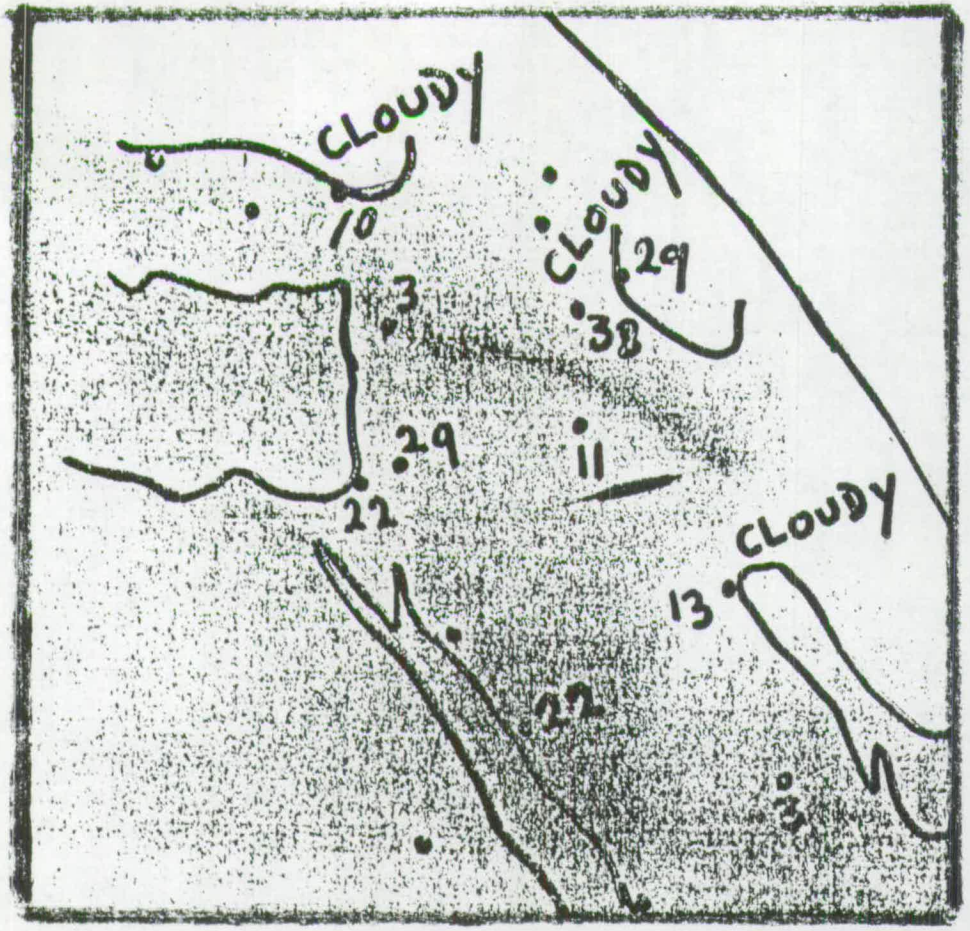

Figure 6.4d METEOSAT-1 water vapour image at 1155GMT on 22 December 1978. Middle East area is projected onthe image and the numbers represent the actual saturation mixing ratios("g/Kg"x100) of the 400mb of the same day at 12GMT.

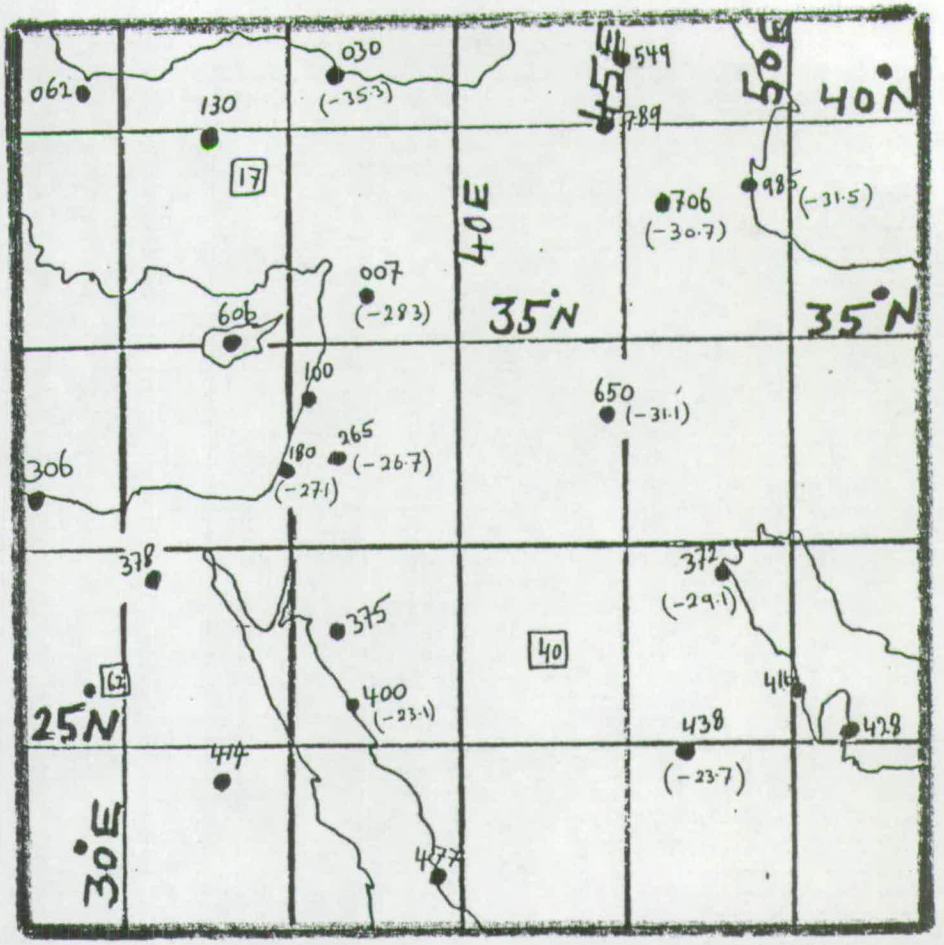

Figure 6.4e Showing the actual temperature in degrees centigrade(values in brackets) for the 400mb at 12GMT on 22 December 1978.

reported moisture contents of 0.22 g/kg each but Hefa appears whiter than Al-Wejh because the temperature at 400mb level over Hefa is colder by 4C^{o} than those over Al-Wejh (figure 6.4e). Baghdad (40650) reported a moisture content of 0.11 g/kg at 400mb level but it looked wheter than Al-Mafraq (40265) which had a moisture content of 0.29 g/kg. It was noticed that the temperature over Baghdad at 400mb is -31^{o}C which is 4.4^{o}C less than those of Al-Mafraq at the same level (see figures 6.4d and e for comparison).

However, it happens in this work that some of the grey shades of the water vapour images show some disagreement with moisture content at the 400mb level because of the existence of cirrus clouds. For example, over the area of 5^{o} latitude x 5^{o} longitude (30^{o}N, 40^{o}E. 30^{o}N, 45^{o}E. 25^{o}N, 40^{o}E. 25^{o}N, 45^{o}E.), the grey shade of the water vapour image (figure 6.3) seemed to be white whereas the moisture content of the 400mb level over the mentioned area was between 0.04 to 0.08 g/kg which is relatively dry. However, the visible image at 1155 GMT and infrared image at 1225 GMT showed cirrus cloud. Also surface synoptic stations in that area and immediately outside the 5^{o} latitude x 5^{o} longitude area reported cirrus clouds (see figures 6.5a, b and c.).

One must be careful in interpreting some

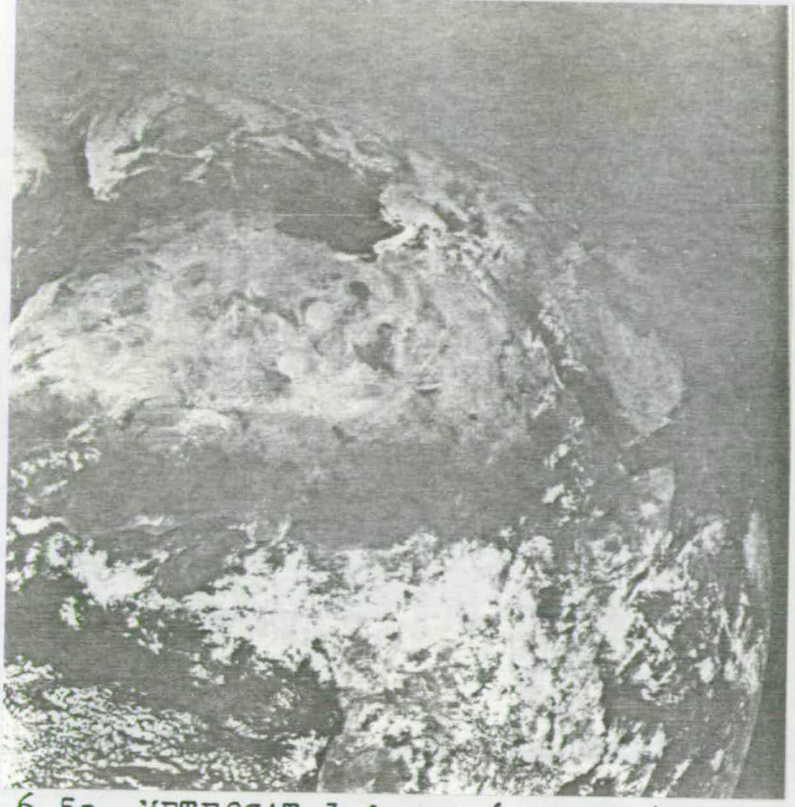

Figure 6.5a. METEOSAT-1 image (visible) at 1155Z on 10 December 1978, to show cirrus cloud over and around the Arabian Gulf.

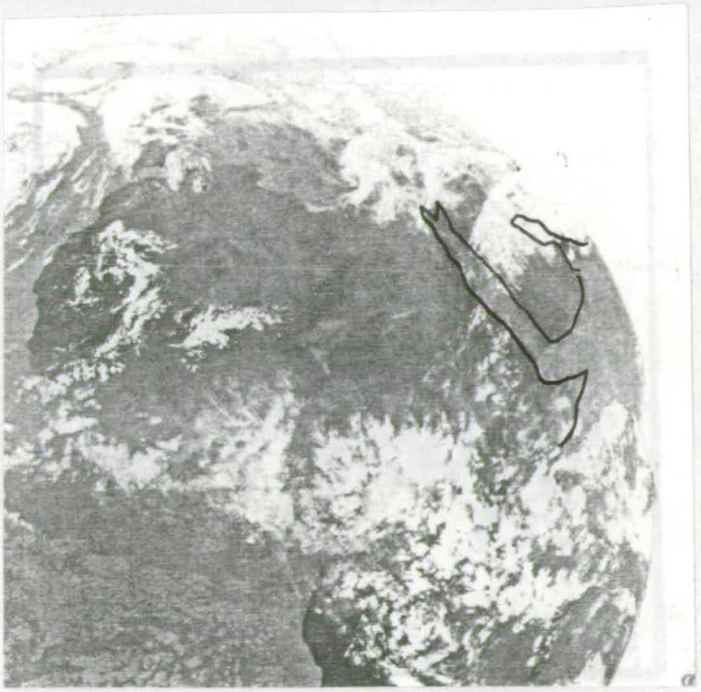

Figure 6.5b. METEOSAT-1 image (infrared) at 1225Z on 10 December 1978, to show cirrus cloud over and around the Arabian Gulf.

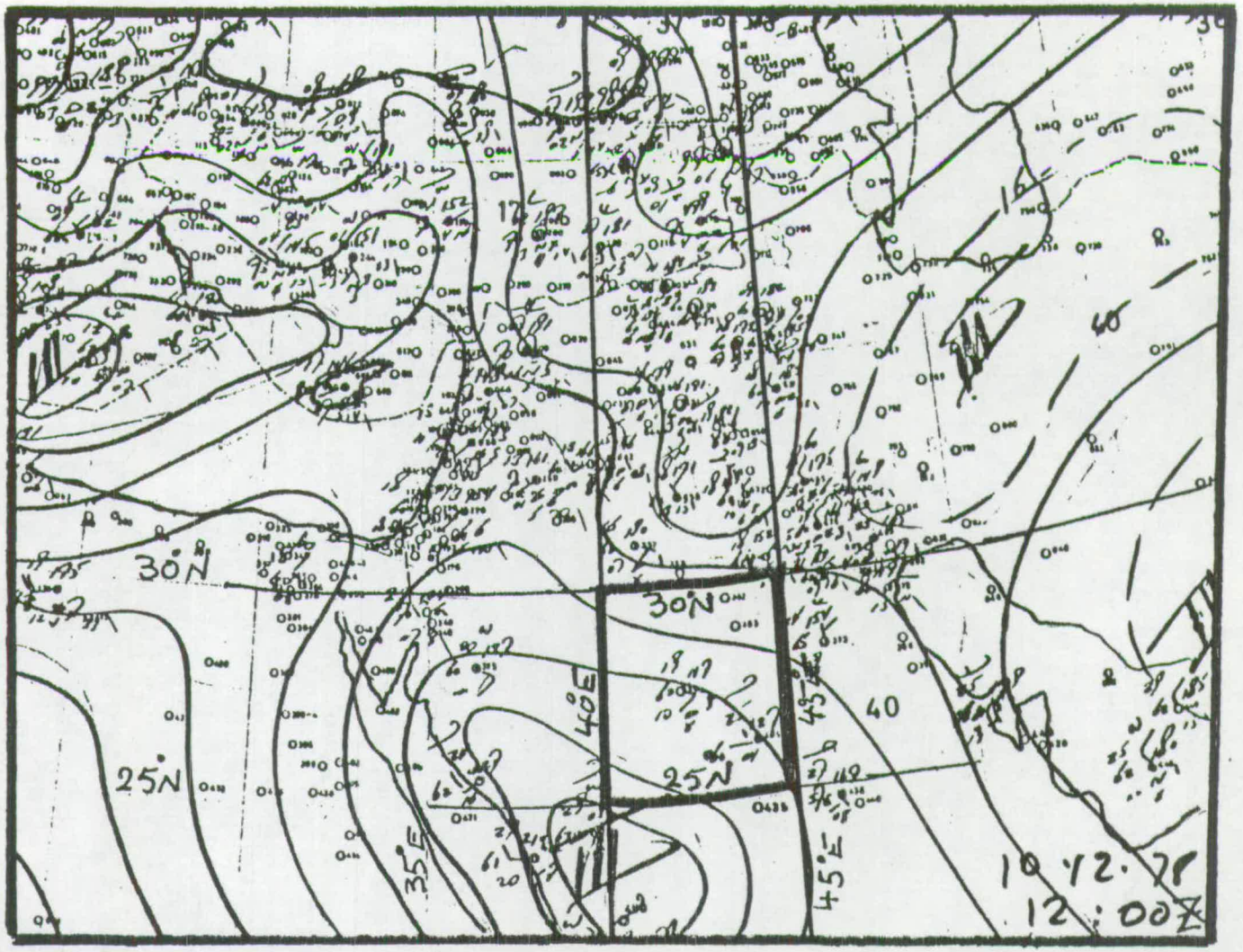

Fig. 6.5c To show the synoptic situation over the Middle East at 12Z on 10 December 1978. **Cirrus clouds are shown in and immediately outside the 5° latitude x 5° longitude area.**

parameters from the water vapour channel if there are some high or medium clouds above the maximum contribution function.

6.3.2 Vertical Moisture Content Analysis.

To associate the water vapour grey shades with the vertical moisture content values of the troposphere, radiosonde data are required. In doing this the grey shades are divided into only three grey shades - dark (black), moderate grey and bright (white) shade - since it is impossible for the author to discern more than these 3 scales from the available simple water vapour images. The available radiosonde data for December 1978 in the Middle East and neighbouring countries are sparse and include only six standard levels (i.e., 1000, 850, 700, 500, 400 and 300mb). Since the grey shade of the water vapour images represent the moisture content at the middle and upper troposphere but not at a specific level, the author has then decided to divide the six standard levels into three layers:

1. 1000 - 700mb (lower layer)
2. 700 - 500mb (middle layer)
3. 500 - 300mb (upper layer)

The division of the above layers was based on the choice of the author.

After a careful investigation of the December 1978 data for the Middle East and neighbouring countries, it is found that only 249 cases out of 1080 are suitable

for the association of the water vapour grey shade scales with vertical moisture content values. Considering all three grey shade scales, black, moderate and white, the median value of the moisture content at 12 GMT for the lower layer (1000-700mb) in December 1978 using 83 cases over the Middle East and neighbouring countries is 4.4 g/kg. This value is considered as a threshold value above which the lower layer is considered to be moist and below which the lower layer is dry. Similarly, the threshold values (medians) of the moisture content for the middle layer (700-500mb) using 83 cases is 1.5 g/kg and for the upper layer (500-300mb) is 0.31 g/kg for 83 cases (see table 6.1.) (The author has used the median rather than the mean value because the median is not affected by the extreme values which are in the data while the mean is affected by them).

Based on the above calculations one can relate the vertical moisture content in terms of grey shade. When the middle layer (700-500mb) and the upper layer (500-300mb) are dry over a certain area, then the water vapour grey shade images must show dark over that area whether the lower layer is dry or moist. The moisture contents of the lower layer does not relate well to the grey shade when the middle and upper layer were dry because the values of the moisture contents of the lower layer vary considerably above and below the threshold value (i.e., the threshold

DECEMBER 1978, MIDDLE EAST/IRAQ ZONE

Grey shade scale (WATER VAPOUR IMAGE)	Lower layer 1000 - 700mb			Middle layer 700 - 500mb			Upper layer 500 - 300mb		
	mixing ratio median = 4.4g/Kg			mixing ratio median = 1.5g/Kg			mixing ratio median = 0.31g/Kg		
	no. of obs.	<	>	no. of obs.	<	>	no. of obs.	<	>
Black	24	12	12	24	18	6	24	19	5
	50% dry 50% moist MOIST OR DRY			75% dry 25% moist MOSTLY DRY			79% dry 21% moist MOSTLY DRY		
Moderate	39	19	20	39	11	28	39	20	19
	49% dry 51% moist MOIST OR DRY			28% dry 72% moist MOSTLY MOIST			51% dry 49% moist MOIST OR DRY		
White	20	11	9	20	13	7	20	3	17
	55% dry 45% moist MOIST OR DRY			65% dry 35% moist MOSTLY DRY			15% dry 85% moist MOSTLY MOIST		

Table 6.1* Showing the relation between the grey shade scales and the vertical moisture content in the troposphere.

(*) since one month's data(December 1978) does not represent a large statistical sample, the numbers calculated in this table may change as more data are examined and good quality of water vapour images are used.

value of the lower layer is 4.4 g/kg) and all the moisture content values (i.e., above and below the threshold value) of the lower layer represent dark grey shade only. So, the total value of the radiation (i.e., the grey shade in our study) in the lower layer does not depend on the contribution from the concentration (above or below the threshold value) of the water vapour. The dark shade corresponds to higher temperature where radiation comes from the lower layer. So, when the middle and upper layer are dry the lower layer is seen dark (black) in the water vapour images whether the moisture content of the lower layer is higher or lower than its threshold value.

Sometimes this may not be true, especially where the troposphere is very dry and the surface is very cold or over regions of high surface altitude.

The grey shade in middle and upper layer depends on the concentration of the water vapour and temperature.

For example, on 1 December 1978 at 1155 GMT Baghdad (40650) and on 3 December 1978 at 1155 GMT Samsun (17030) both were covered with moderate grey shades. Baghdad recorded a moisture content of 2.5 g/kg in the middle layer (700-500mb) at 12 GMT on 1 December 1978 which is more than the threshold value by 1.0 g/kg and Samsun recorded 0.5 g/kg in the middle layer also at 12 GMT on 3 December 1978, which is less than the

threshold value of the middle layer by 1.0 g/kg. These stations (Baghdad and Samsun) have values of moisture content far more and far less than the threshold value respectively, but both of them were under moderate grey shades. The actual mean temperature of the middle layer for Baghdad at 12 GMT on 1 December 1978 was -7.5°C whereas in Samsun at 12 GMT on 3 December 1978, the same layer was -23.0°C. Hence Samsun is colder than Baghdad by 15.5°C in the middle layer.

Under white shade one expects intuitively that the upper layer (500-300mb) is always moist, but that was not the case, as 3 out of 20 occasions in December 1978 were dry (see table 6.1) because of the white shade could represent the middle layers. For example, on 17 December 1978 at 1155 GMT the grey shade of the water vapour covering Al-Mafraq (32° 22′N, 36° 16′E) was white and the moisture content at 12 GMT of the upper layer was 0.23 g/kg which is less than the threshold value (the threshold value of the upper layer is 0.31 g/kg). It has been noticed at that time and day, the moisture content over Al-Mafraq at 12 GMT of the middle layer is equal to 3.6 g/kg which is more than the threshold value of the middle layer (i.e., the threshold value of the middle layer is 1.5 g/kg).

A simplified guide to the interpretation of water vapour grey shades appears in table 6.1 and it is relevant to this study.

6.4 Wind Field Analysis

A qualitative comparison of the moisture patterns on the water vapour pictures of the METEOSAT-1 with the 400mb level conventionally measured wind field, also indicates that the grey shade pattern is generally aligned with the wind field. This suggests that the water vapour pictures could be used to infer the orientation of streamlines over data-sparse regions. Figures 6.6a and b show a streamline analysis derived from radiosonde observations. One can see that these streamlines indicate that the wind field at 400mb is aligned reasonably with the grey shade pattern of the water vapour images of METEOSAT-1 over the Middle East/Iraq.

For example, the streamline analysis from the conventional data (figure 6.6a) shows that the orientation of the streamlines over the north part of the Red Sea is southwest-northeast, as is the orientation of the grey shade in figure 6.3 where clear sky was reported over that part. Over the eastern coast of the Mediterranean area the streamline orientation correspond reasonably but not very well with the grey shade configuration, because high and medium clouds were reported at and near the area concerned. On 18 December the general orientation of the streamlines (figure 6.6b) agreed with the orientation of the water vapour shade patterns of the same day (see figure 6.6c), especially over Saudi

Figure 6.6a. 400mb conventional streamlines at 12Z on 10 December 1978. Streamline orientation agrees with the water vapour pattern shown in figure 6.3 below.

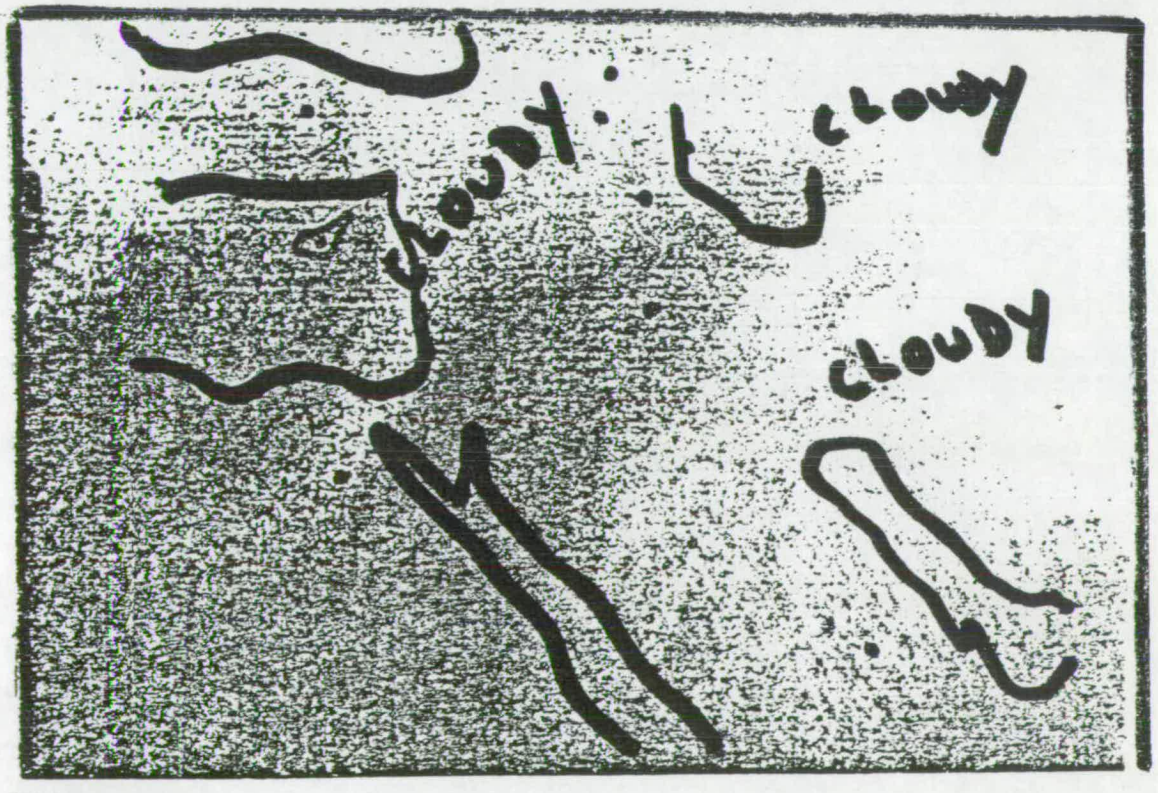

Figure 6.3 - For comparison with figure 6.6a above.

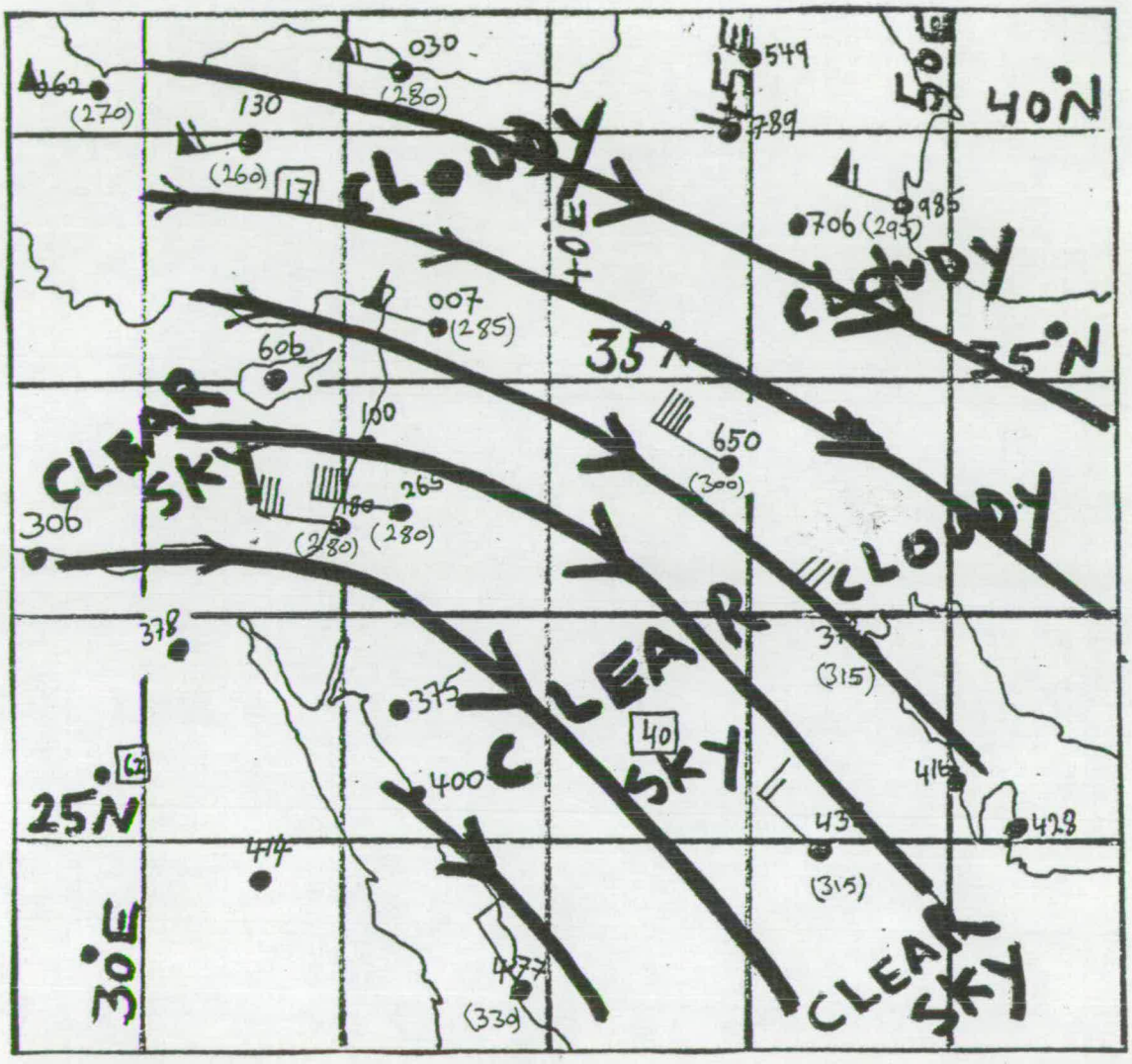

Figure 6.6b. 400mb conventional streamlines at 12Z on 18 December 1978. Streamlines orientation agree with the water vapour pattern shown in figure 6.6c(next page).

Figure 6.6c. METEOSAT-1 image(water vapour) at 1155z on 18 December 1978 to show the comparison between the grey shade pattern and the streamlines orientation of figure 6.6b(previous page).

Arabia, Iraq and the East coast of the Mediterranean Sea where clear sky was reported.

Analysis of simple water vapour images are inadequate and cannot possibly give detailed information and strong general conclusions about the wind field in the middle and upper troposphere. Detailed wind interpolation, further understanding and convincing conclusions can be achieved only if enough selected data of water vapour and reliable conventional observations are involved in the analysis.

From the above analyses, one can see at least that it is possible from simple water vapour images to interpret streamlines and this interpretation provides the general features of the synoptic scale circulations in the middle and upper troposphere. This will be of value in data-sparse regions especially over the Middle East, and this interpolation would, of course, be of benefit for forecasting purposes.

Particularly, in this section, it has been shown that the water vapour images (subjectively analysed) show acceptable agreement between the water vapour grey shade pattern and the actual wind field of the 400mb level over the Middle East and neighbouring countries.

It was difficult for the author to match exactly the actual wind field and the grey shade pattern

of the water vapour image on a broad scale because of the following reasons:

a. no longitudes and latitudes or coast lines are provided with the water vapour images of METEOSAT-1 and also a slight curvature near the Middle East area is ignored.

b. difficult to find a clear sky status or sky with low cloud reported over the whole zone of the Middle East area and neighbouring countries in December 1978 in order to draw all patterns (actual moisture content and actual wind field) on broad scales.

c. routine radiosonde stations are sparse over the Middle East and about half of the data required for this study are missing; this was misleading in the interpretation and drawing the streamlines despite moderate experience.

d. the patterns seen on the METEOSAT-1 images represent a layer ranging between 300-500mb and not only a specific level in the middle or upper troposphere.

6.5 Discussion and Conclusion

I have shown from simple analysis that there are some agreements between the water vapour pattern (subjectively analysed) and the conventional moisture content at 400mb level and agreements between the water vapour pattern also and the wind field at 400mb level. I have also shown a relationship between the

grey shades of the water vapour images and the vertical moisture content at different layers.

It is not feasible at this stage to deduce exact numerical values of the middle or upper tropospheric moisture content or to indicate the precise wind direction of the middle and upper troposphere from simple or even from enhanced satellite images. Water vapour images can be used to infer the wind direction (streamlines pattern) and moisture content field (i.e., moist, moderately moist or dry) over data-sparse regions on a synoptic scale. This procedure provides a definite and valuable guide for improving wind flow and moisture content analyses over the Middle East where data are sparse.

To show that there are objective agreements between the radiometrically observed water vapour pattern and conventionally observed moisture content and wind field in the middle and upper troposphere, this needs instruments and detectors for radiance measurements and computer analysis. This approach requires more sophisticated procedures and can be summarised as follows:

1. A special processing of METEOSAT-1 water vapour data (i.e., enhanced image and each grey shade or false hue representing a line of constant radiance) on a geographical basis.
2. The collection of reliable conventional data from the meteorological network and to derive interpolated fields.

3. To compare the results of the conventional and METEOSAT-1 data.

The above sophisticated procedures do give good but not precise agreements between the radiometrically observed water vapour grey values and either conventionally observed moisture content values or wind direction values in the middle and upper troposphere.

For example, Steranka et al (1973) found that the wind field and moisture content patterns over a synoptic scale of the 400mb level derived from radiance measurements (THIR) are generally in good agreement with actual wind field and moisture content pattern of the 400mb level.

Comparison of the THIR derived wind below or above the 400mb level does not show good agreement with conventional wind field below or above the 400mb level respectively.

Despite the good agreements of wind direction of the 400mb derived from the THIR data by Steranka et al (1973) and the conventional observed wind direction, they found that it was very difficult to indicate numerical values of wind directions from the radiance measurement derived wind. They used 143 samples and they found that the accuracy in the direction of the 400mb level wind derived measurement is about 23 degrees corresponding to the actual 400mb level wind direction.

Some of the samples show errors of less than ±10 degrees and some others show more than ±90 degrees. In general the two patterns (actual and radiance measurements) of wind direction at the 400mb level are in a good agreement on broad scales. It has been stated that despite the use of THIR data (radiance measurement in 6.3 μm) and some mathematical models, it is difficult to derive wind fields (see Kastner and Fischer, 1980).

Allison et al (1972) used THIR data of the NIMBUS-4 and they succeeded in improving the wind field analysis at the 400mb level over data sparse regions.

In conclusion, water vapour images provide more details about the tropospheric moisture content distribution and wind field over data-sparse regions and even over data-dense regions.

With the aid of the water vapour channel, it should be possible to use time series images of wet and dry regions as moisture and wind field tracers, because from the water vapour image over a synoptic scale the flow is more uniform and can more readily be seen than from visible or infrared images.

Furthermore, radiometric water vapour measurements can be used to determine the altitude of the weather phenomena observed on the pictures which depend on water vapour content, by considering the contribution function at different levels. This is

true in the case of clear sky status or if the clouds at middle and high altitudes are absent because the accurate altitudes associated with the weather phenomena depend on the water vapour profile, the temperature profile and the viewing angle of the satellite instrument (see Fischer et al 1981). The presence of clouds at high and medium levels affects the shape of the contribution function profile because it is dependent on the altitude and thickness of the cloud.

For the limited water vapour data used, the simple results of the moisture content and wind field analyses presented here must be considered as a provisional work and as a starting point for future water vapour work for the local and neighbouring meteorologists.

CHAPTER SEVEN

GENERAL CONCLUSION AND RECOMMENDATIONS

7.1 Concluding Remarks.

The present model for estimating daily rainfall over Iraq depends partially (50%) upon the quantitative analysis of essentially qualitative satellite data.

This model accomplishes good results of rainfall estimation with reasonable success. Hence its application to other areas seems worthwhile and possible.

Since there are no standard thresholds of visible or infrared radiance for isolating precipitating from non-precipitating clouds, or even differentiating between different types of precipitating clouds then the author has problems in relating the probability of rainfall to cloud type category using simple satellite images. This rainfall probability is relevant to the work in this thesis.

There is much scope for improvement and refinement of the present model. Method of picture analysis and rainfall prediction index construction should be scrutinised since there are many problems related to quantification of cloud features. For example, it would be rather difficult for two observers to assess cloud

features (type, amount, height, etc.) with sufficient consistency using simple satellite photographs to produce very similar results, since the photographs have poorly defined cloud boundaries and shades.

The development of the model requires the following guidelines:

1. To isolate areas of deep cloudiness from clouds less likely to precipitate using enhanced images, permitting more reliable estimates of cloud features (i.e., elaborate cloud categorisations, well-defined cloud boundaries and acceptable estimates of cloud top temperature).
2. Incorporation of planimetric and densitometric measurements of enhanced images might provide more accurate and consistent results. Such measurements might also provide better estimates of cloud features from unenhanced satellite images.
3. Vast amounts of data are generated by satellites and this calls for a high degree of automation in handling of the data; at the same time, however, the imperfections in the observational data and objective forecasting procedures, as well as the ill-defined nature of discrepancies between cloud imagery and surface precipitation are such that for the foreseeable future a combination of objective procedures and subjective judgement will be required in the analysis and forecasting.

4. The important requirement is to observe the mesoscale field on an almost continuous basis. Sequences of such a field can form the basis of a simple forecast by extrapolation in the 24 hour time frame, and can also be used to help initialize improved methods of prediction in the longer time.

5. The technology of interactive computer - satellite based systems can be exploited to enable the human forecaster to exercise his judgement effectively within the framework of an otherwise highly automated procedure; the degree of interaction required is far greater than that employed at the present.

6. The systematic archive of satellite data and the analytical experience gained by regular use of the above facilities will not only improve the rainfall estimation techniques but will contribute to further improvement in the weather forecasting techniques.

7. Simultaneous analysis of microwave, infra-red, and video data obtained from satellites might help to identify areas of particularly strong vertical motion from inference about cloud top temperature and cloud thickness. However, such studies will not become feasible until the problems of interpretation of microwave and infra-red data have been overcome.

So, since cheap, real-time estimates of daily rainfall are required, it should not be beyond the capability of modern technology to provide low cost methods of automatic analysis of satellite pictures using such techniques.

The future of rainfall estimation by simple methods at modest costs probably lies in enhanced infra-red analysis alone, partly because infra-red pictures can be taken during the day and night and are easily obtainable and accessible. These might permit reliable estimates of 12 hourly (or shorter time) rainfall to be made.

The present technique also possesses a degree of flexibility that might permit its development for use in hydrological as well as meteorological forecasting with relatively few adjustments.

Its special value is in subtropical regions where conventional data are sparse.

Such a model then has obvious advantages to life and property conservation schemes (in the case of extreme conditions), agriculturalists, hydrologists, energy suppliers, climatalogists, and other situations. The sociological and scientific importance of estimating and/or forecasting successfully shorter, daily and longer period rainfall from weather satellite pictures makes research into this topic fascinating.

Appropriate aims have been accomplished with some success. However, because data pertaining to only one month (April 1977) in case of Scottish rainfall studies and two months (December 1978 and Fabruary 1979) in the study of Iraqi rainfall have been used, the conclusion drawn from them must be regarded as tentative.

It is clear, however, that meteorological satellite data have a great potential in aiding the formulation and indexing of Middle East cloudiness and other remote areas useful to climatalogists, numerical modellers and synoptic forecasters alike. Hence, it is submitted that meteorological satellites are important tools for the description and comprehension of weather and climate in the Middle East regions (sparce data) at synoptic, meso - and microscales.

7.2 Recommendations.

Meteorological satellite data have an exciting future in studies of the atmosphere, especially since large data gaps remain over the oceans, developing and undeveloped continental regions:

Data types are continually changing. In fact, the future of meteorological satellites lies mainly in analysis of infra-red, visible and water vapour data.

Meteorologists would do well to keep abreast with the new scope of such data and new

methods of data processing will inevitably ensue. However, the future will require the application of more workers, money and conventional observations to maximise the use of remote sounding of the vertical structure of the atmosphere. International co-operation is essential.

Meanwhile, existing video data (and conventional observations) can help us to a better understanding of the atmosphere. They also have a useful operational role in meteorology. For instance, although manual methods of compiling summaries of video data may soon be rendered obsolete by automatic objective techniques, these could be used to compile short or medium term (say 3-10 days) summaries, (see for example Morgan 1978). These summaries, and individual pictures, could be used then to aid studies of the kinematics and dynamics of disturbances throughout the world, especially if planimetric and densitometric measurements are used.

The highly automated satellite-computer extraction of data would doubtlessly benefit studies of:

Firstly, the data obtained would be of help in the study of cloud (on a year-to-year basis) associated with abnormally high or abnormally low rainfall over an area, e.g., tropical areas. These might provide some useful statistical forecasting variables.

Secondly, the data would doubtless be of value in studying

a. Variation in cloudiness over the equatorial regions: and
b. The formation and dissipation of the intertropical convergence cloud bands around the equator in relation to their rainfall.

The above recommended points might benefit from the more prolific data coverage to be provided.

7.3 Suggestions for Iraq and the Middle East.

There are infinite uses of satellite data in the fields of meteorology, hydrology, oceanography and space environment.

Various countries have used satellite data to improve their work and research and to increase their skills in the fields concerned.

The Iraqi Meteorological Office has contributed to satellite use and has built a receiving station for orbital and geostationary meteorological satellite. It has been installed in Baghdad International Airport and this definitely will allow the improvement of the present model of rainfall estimation over Iraq by using the available satellite data in Baghdad. The training of recruits in receiving and using the satellite data will begin shortly.

Satellite data which are available at Baghdad Meteorological Office can be applied to a further test and verification to the present model and also be applied to the following:

a. Verification and correct placing of major synoptic features (fronts, vortices, tropical storms, etc.) over the Middle East and neighbouring countries on a geographical basis since the satellite images provide longitudes, latitudes and coast lines. These synoptic features are extremely difficult to locate over the area concerned without satellite photographs.

b. Depiction of the activity, intensification or weakening of synoptic processes affecting aviation, deepening or filling of Mediterranean depressions, evidence of the formation of new centres in the Middle East.

c. Understanding of the behaviour of air masses, e.g., in passing from land to sea or the reverse; the development of air mass thunderstorms or cumulonimbus clusters; fog formation ... etc.

d. Indications of geographical and orographical influences (mountain waves, dissipation of cloud on a lee side, forced convection).

e. Detection of climatic/synoptic factors affecting lives and properties such as the activation and displacement of ITCZ and the intensification of the monsoon.

f. Observational data from the data sparse area of the desert of North Africa and Saudi Arabia. Significant weather phenomena in those regions influence the Iraqi weather.

g. Subtropical jet streams are well defined by satellite observations especially in the extremely data-sparse desert areas of North Africa (see figure 7.1).

h. Extract quantitative analysis from qualitative data which are essential in numerical forecasting.

i. Instead of METEOSAT-1, GOES-I.O. (70°E) of the USA/ESA can be used and gives better resolution for the Middle East and neighbouring regions as shown in figure 7.2a and b.

j. Extract quantitative measures of moisture content and wind field from the water vapour channel (6.3 μm). This can be quite helpful in improving moisture and wind field analyses. The water vapour channel permits the extrapolation of conventional measurement into data-sparse regions so that much greater detail can be introduced into analyses of

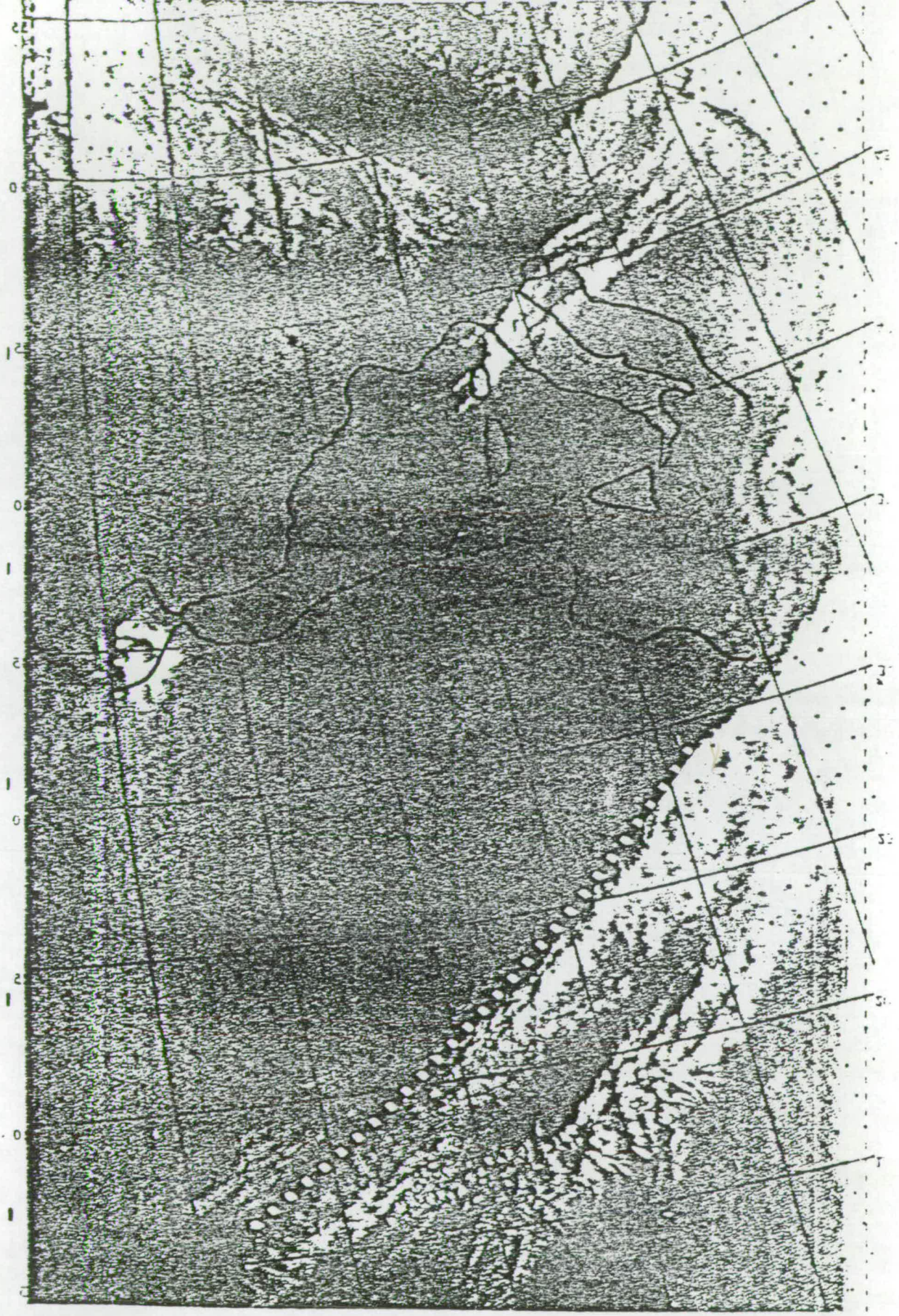

Figure 7 .1 DMSP - HR - IR for 0930 GMT, 7 December 1974, showing the subtropical jet stream (STJ) over North Africa (Dashed strip) and the associated cloud pattern.

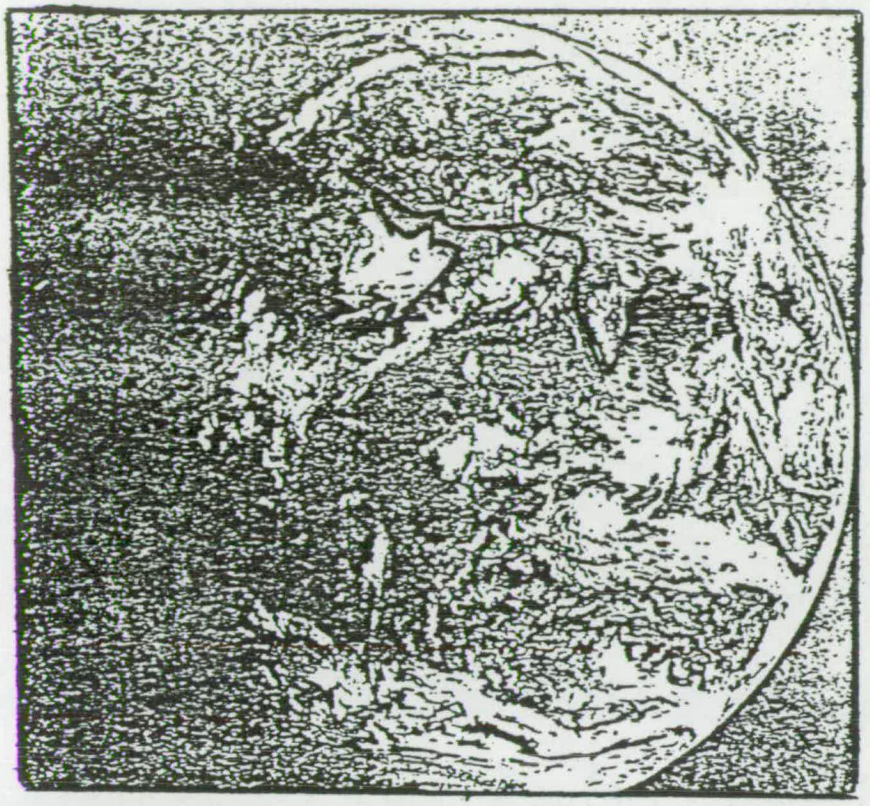

Figure 7.2a Image from the **visible** channel of the GOES - I.O. Satellite (70°E, 00°N) at 0620 Z on 31 August 1979.

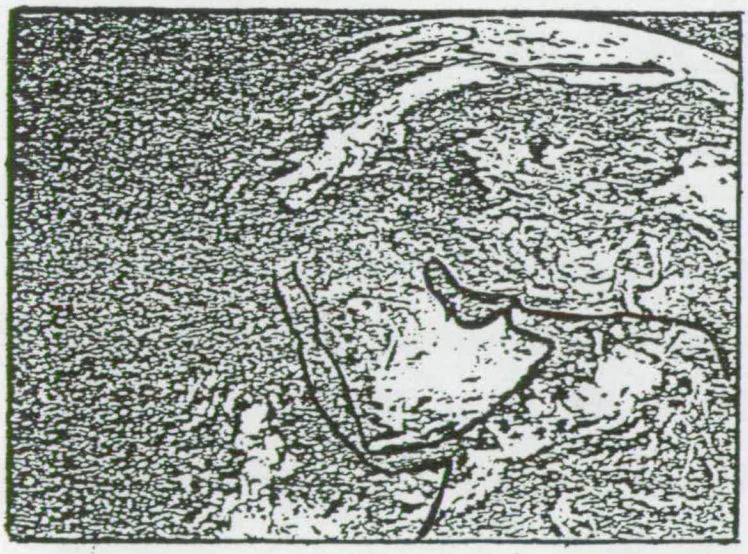

Figure 7.2b Enlargement of the above image, showing the Iraq/Middle East area and neighbouring countries.

these parameters. These analyses suggest that water vapour would be of particular help over Middle East remote regions where conventional data is very sparse. In addition, the large area, synoptic coverage afforded by the satellite in conjunction with these water vapour data, should be helpful in providing insight regarding the interconnection of tropical and mid-latitude systems which are manifested in the upper troposphere.

Furthermore, the improvement of the model of estimating daily rainfall over Iraq can be done if the orbiting satellite images are used (figure 7.1) and the geostationary satellite images of GOES.I.O. (figures 7.2a and b). Because these satillite will considerably reduce the slight curvature which the METEOSAT-1 images showed over the Middle East area, which the author could not avoid; this is considered as a defect in this model.

The Iraqi Meteorological Office will definitely improve the meteorological services by using satellite data and develop the skill of local observations and forecasting in the Middle East zone.

This improvement of observations and forecasting would doubtlessly be of value in providing more accurate observations, nowcasting and forecasting

regularly to other neighbouring and remote meteorological offices, which would be beneficial for global atmospheric studies and circulation.

REFERENCES

Air Ministry, M.O. (1962) Weather in the Mediterranean, General Meteorology, Vol. I and II. London:HMSO., 237p

Akvilonova, A.B., Krylova,M.A., Kutuza,B.G., and Mitnik, L.M. (1971) SHF radiometric characteristics of frontal cloudiness as measured from COSMOS-243, Advance in Satellite Meteorology, Wiley & Sons, New York.

Alder, R.F., and Rodgers, E.B. (1977). Satellite-observed latent heat release in a tropical cyclone. Mon. Weath, Rev. 105, pp. 956-963.

Allison, L.J., Steranka,J. and Hisenrath,E. (1972). Meteorological applications of NIMBUS-4 THIR 6.7 micron channel data. Bull. Amer. Met. Soc., pp. 526-535.

Allison, L.J., Rodgers,E.B. White T.T. and Fett,R.W. (1974) Tropical cyclone rainfall measured by the NIMBUS-5 ESMR. Bull. Amer. Met. Soc. 55, pp. 1074-1089.

Anekeeva, L.A. (1968) Use of cloud data obtained by meteorological satellite for an objective analysis of wind field. Proc. of the HMC. Vol. 36 (English Copy). pp. 1-6.

Barrett, E.C. (1970). The estimation of monthly rainfall from satellite data. Mon. Weath.Rev., Vol. 98, pp. 322-327.

Barrett, E.C. (1971) The tropical Far East: ESSA satellite evaluation of high season climatic patterns. Geogr. J., Vol. 137, pp. 535-555.

Barrett, E.C. (1972) Estimation of daily and monthly rainfall from weather satellite data. "Paper given at Bristol". Symp. on remote sensing of Man's Env. University of Bristol, October, 1972.

Barrett, E.C. (1973) Forecasting daily rainfall from satellite data. Mon. Weath. Rev. Vol. 101, pp. 215-222.

Barrett, E.C. (1974) "Climatology from satellites". Methuen (London) and Barnes and Noble New York. 418P.

Barrett, E.C. (1975) Rainfall in Northern Sumatra analyses of conventional and satellite data for the planning and implementation of the Krueng Jreue/Krueng Baro irrigation schemes. Final Rep. for Binnie and Partners. (Consulting Engineers), London, 50P.

Barrett, E.C. and Martin, D.W. (1981) The use of satellite data in rainfall monitoring. Academic Press. London, New York, Toronto, Sydney, San Francisco. 340P

Bizzarri, B. (1975). The scientific aspect of METEOSAT. European Space Agency (ESA) Bull. No. 3, pp. 52-59.

Bjerknes, J. and Solberg, H. (1921). Meteorological conditions for the formation of rain. Goefysiske Publikationev, 2, 3, pp. 1-60.

Booth, L. and Taylor, V.R. (1969). Meso-scale archive and computer products of digitized video data from ESSA satellite. Bull. of the American Met. Soc., 50. pp. 431-438.

Browning, K.A. (1979). The FRONTIERS plan: a strategy for using radar and satellite imagery for very short-range precipitation forecasting. Met. Mag. No. 1283, Jun. Vol. 108. pp. 161-183.

Browning, K.A. (1980). Radar as part of an integrated system for measuring and forecasting rain in the U.K: Progress and plan. Weather, 35, pp. 94-104.

Committee on Space Research (1967). Status report on the application of space technology to the World Weather Watch. COSPAR working group, London, 144P

Cracknell, A.P. (1981). Remote sensing in Meteorology, Hydrology and Oceanography. Ellis Harwood L.T.D. New York, Chichester, Brisbane and Toronto. 542P.

Dennis, A.S. (1963). Rainfall determination by meteorological satellite radar. Final Rept. SR14080., Stanford Res. Inst. Menlo Park, Calif. 105P

Eigenwillig and Fischer, H. (1980) Determination of wind vectors from METEOSAT water vapour channel data. Advances in Space Research. Vol. 1, No. 4, A. Bewersdoff, Ed., Pergamon Press, pp. 129-132.

Essenwangen, O. and Haggard. (1960) The relation between cloud cover and relative humidity. Final Rep. Project order R-65-O-99856-SC-O1-91, National Weath. record centre. U.S. Weath. Bureau, A. Sheville, N.C. 73OP.

European Space Operation Centre. (ESOC) (1978) Introduction to the METEOSAT System. Issue-1 ESOC (Compiled by MDMD - Met.) pp. 1-111.

Fischer,H., Eigenwillig, N. and Muller,H. (1981). Information content of METEOSAT and Nimbus/THIR water vapour channel data: Altitude Association of Observed Phenomena. J. Appl. Met., 20, pp. 1344-1352.

Fletcher, N.H. (1962) The physics of rain clouds. Cambridge University Press. Cambridge, 386P.

Follansbee, W.A. (1973) Estimation of average daily rainfall from satellite and cloud photographs. NOAA Tech. Memo. NESS 44. 39P.

Follansbee, W.A. and Oliver, V.J. (1975) A comparison of infrared imagery and video pictures in the estimation of daily rainfall from satellite data. NOAA Tech. Memo. NESS 62, 14P

Follansbee, W.A. (1976) Estimation of daily precipitation over China and the USSR using satellite imagery. NOAA Tech. Memo. NESS 81, 3OP.

Fujita, T.T., Watanabe, K. and Izawa, T. (1969) Formation and structure of equatorial anticyclones caused by large scale corss-equatorial flows determined by ATSI photographs. J. Appl. Met. 8, pp. 649-667.

Fujita, T.T. Pearl, E.W. and Shenk, W.E. (1975) Satellite-tracked cumulus velocity. J. Appl. Met.14, pp. 407-413.

Gaby, D.C. (1967) Cumulus cloud lines versus surface winds in equatorial latitude. Mon. Weath. Rev. 95, pp. 203-208.

Gaby, D.C. and Potent, K.O. (1973) ATS-3 satellite-derived low level wind: a provisional climatology. J. Appl. Met. pp. 1054-1061.

Galway, J.G. (1956) The lifted index as a prediction of latent heat instability. Bull. Amer. Met. Soc. Lancaster, Pa., 37, 528P

Gerrish, H.P. (1970) Satellite and Radar analyses of meso-scale features in the Tropics. Final Rep. ECOM-0205-F, U.S. Army Elect. Command, New Jersey, 45P.

Griffith, G.G., Woodly, W.L., Gruber,P.G., Martin, D.W., Stout,J. and Skidar, D.N. (1978). Rain estimation from geostationary satellite imagery-visible and infrared studies. Mon. Weath. Rev., 106, pp. 1153-1171.

Gruber, A. (1971) Estimation of rainfall in regions of active convection. Paper presented at the 7th Tech. Conf. on hurricanes and tropical meteorology, Barbados, West Indies.

Hamilton, M.G. (1973) Satellite studies of the Asian summer monsoon. Ph.D. Thesis. University of Bristol, (England)

Handbook of Weather Forecasting (1975) "HWF" Three volumes. Met.0.875. Meteorological Office, (Bracknell)

Hess, S.L. (1959) Introduction to theoretical meteorology. Halt, Rinehart & Winston, New York. 352P.

Hope, J.R. (1966) Path of heavy rain photographed from space. Bull. Amer. Met. Soc. Vol. 47, No. 5, pp. 371-373.

Houghton, J.T. (1979a) The role of satellite in tropical observation system. R. Met. Soc. Trop. Ocean. Bracknell. pp. 211-273.

Houghton, J.T. (1979b) The future role of observation from meteorological satellites. Presidential Address, Q.J.R. Met. Soc. 105, pp. 1-20.

Hubert, L.F. (1976) Wind determination from geostationary satellite. Proceeding of the symposium in meteorology observation from space: their contribution to the FGGE, COSPAR,, pp. 211-213.

Hunt, G.E., Saunders, R.W., Rumball, D.A., and Marriage, N. (1981) Some quantitative meteorological measurements from geostationary satellite. Weather, 36, pp. 96-104.

Johnson, H.M. (1969) The role of the tropics in the global circulation of the atmosphere. (G. Gaby, Edit.), 113P. R. Met. Soc. London.

Karein, A.D. (1979) The forecasting of cyclogenesis in the Mediterranean region. Ph.D. Thesis. 159P. University of Edinburgh.

Kastner, M. and Fischer, H. (1980) Wind determination from NIMBUS-5 observation in the 6.3 μm water vapour band, J. Appl. Meteor. 19, pp. 409-418.

Kellogg, W.W., Buettner, K.J.K. and Mary, E.C. (1964). Meteorological satellite observation of thermal emission. RM4392-NASA, p. 87. Rand Corp., Santa Monica, Calif.

Kessler, E. and Atlas, D. (1959) Model precipitation distributions. Aerospace Eng. 18, No. 12. pp. 36-40.

Kilonsky, B.J. and Ramage, C.S. (1976) A technique for estimating tropical open-ocean rainfall from satellite observations. J. Appl. Met. 15, pp. 972-975.

Kuettner, J.P. (1959) The band structure of the atmosphere. Tellus, 11, pp. 211-273.

Leese, J.A., Novak, C.S., and Clark, B.B. (1971). An automated technique for obtaining cloud motion from geostationary satellite data using corss correlation. J. Appl. Met. 10, pp. 118-132.

Lethbridge, M. (1967) Precipitation probability and satellite radiation data. Mon. Weath. Rev. Vol. 95, pp. 487-490.

Lethbridge, M. and Panofsky, H.A. (1969) Satellite radiation measurement and synoptic data. Final Rep. Grant, No. WBG-48, Pennsylvania State University, 35P.

Lovejoy, S. and Austin, G.L. (1979) The delination of rain areas from visible and infrared data for GATE and Mid-latitudes. Atmospheric-ocean 17. pp. 77-92.

Lovejoy, S. and Austin, G.L. (1980) The estimation of rain from satellite-borne microwave radiometers. Q.J.R. Met. Soc. 106, pp. 225-276.

Lyons, W.A. and Fujita, T.T. (1968) Mesoscale motions in oceanic stratus as revealed by satellite data. Mon. Weath. Rev. Vol. 96, pp. 304-314.

Malkus, J.S. and Riehl, H. (1964) Cloud structure and distribution over tropical ocean. University of California Press, Berkeley and Los Angeles, 230PP.

Martin, F.L., and Salomonson, V.V. (1970) Statistical characteristics of sub-tropical jetstream features in terms of MRIR observations from NIMBUS-2. J. Appl. Met., 9. pp. 508-520.

Martin, D.W. and Scherer, W.D. (1973) Review of satellite rainfall estimation methods. Bull. American Met. Soc. 54, pp. 661-674.

McClain, E.P. (1966) On the relation of satellite-viewed cloud conditions to vertically integrated moisture field. Mon. Weath. Rev. Vol. 94, pp. 509-514.

McIntosh, D.H. and Thom. A.S. (1975). "Essentials of Meteorology". The Whkeham Sciences Series. Wykeham Publication (London) Ltd. 24 OP.

Morgan, J. (1978) METEOSAT-1 in orbit. World Meteorological Bulletin, Vol. 27, No. 4. pp. 250-253.

Morgan, J. (1979) Operational extraction of cloud-motion wind from METEOSAT data. (ESA) Bull. No. 20, Nov. pp. 14-19.

Rackliff, P.G. (1962) Application of instability index to regional forecasting. Met. Mag. London, Vol. 91, pp. 113-120.

Rao, M.S., Abbot, W.V. and Theon, J.S. (1976). Satellite-derived global oceanic rainfall atlas (1973 & 1974), NASA SP-410, Scientific and Tech. Info. Office NASA Goddard Space Flight Centre, Greenbelt, MD, 186P.

Raschke, E. and Bandeen, W.R. (1967) A quasi-global analysis of troposphere water vapour content from TIROS-4 radiation. J. Appl. Met. 6, pp. 468-481.

Reynolds, D.W., Brown, M.L., Smith, A.E. and Vonder Haar, T.H. (1978). Cloud type separation by spectral differencing of image pairs. Mon. Weath. Rev. 106, pp. 1214-1218.

Roulleau, M. (1978) Remote sensing of the atmosphere: Inversion methods and applications. (Fymat, L.A. Edt.) Developments in Atmospheric Science. Vol. 9, 372P. Oxford-New York.

Scherer, W.D. and Hudlow, M.D. (1971) A technique for assessing probable distributions of tropical precipitation echo lengths for X-band radar for NIMBUS-3 HRIR data. BOMEX Bull. No. 10, BOMAP Office, NOAA, Rockville Maryland, pp. 63-68.

Scofield, R.A. (1977) A scheme for estimating convective rainfall from satellite imagery. NOAA Tech. Memo. NESS86, 47P.

Scofield, R.A., and Oliver, V.J. (1977). Using satellite imagery to estimate rainfall from two types of convective system. Preprints 11th Conf. Hurricanes and Tropical Met. Miami. Amer. Met. Soc. pp. 204-211.

Showalter, A.K. (1953) A stability index for thunderstorm forecasting. Bull. Amer. Met. Soc. 34, No. 6. pp. 250-252.

Simmons, A.J. and Hoskins, B.J. (1979) The downstream and upstream development of baroclinic wave. J. Atmos. Sci., 36, pp. 1239-1254.

Skidar, D.N. and Suomi, VE. (1971) Time variation of tropical energetic from geostationary satellite. J. Atmos. Sci. 28., pp. 170-180.

Skidar, D.N. and Suomi, V.E. (1972) On the remote sensing of mesoscale tropical convection intensity from a geostationary satellite. J. Appl. Met., 11. pp. 37-43.

Smagorinsky, J. (1960) On the dynamical prediction of large scale condensation by numerical methods. Physics of precipitation, Geophysical monograph, No. 5, Amer. Geophys. Union,Wash. D.C., pp. 71-78.

Smith, G.D. and Lidge, M.G.H. (1957) The use of composite radar photograph in synoptic weather analysis. Sci. Rep. 3. Contract AF19 (604)- 1564, the A & M. College of Texas. College Station.

Smith, E.A. and Kidder, S.Q. (1978) A multispectral satellite approach of rainfall estimates. Dept of Atmos. Sci. Colo. State University, Fort Collins, Colo. 80523.

Staelin, D.H., Kunzi, K.G., Pettyjohn, R.L. and Wilcox, R.W. (1976) Remote sensing of atmospheric water vapour and liquid water with the NIMBUS-5 microwave spectrometer. J. Appl. Met. 15, pp. 1204-1214.

Starr, V.P., Peixoto, J.P. and Livadas, G.C. (1958) On the meridional flux of water vapour in the Northern Hemisphere. Geofis. Pura. Appl. 39, pp. 174-185.

Steranka, J. Allison,L.J. and Salomonson, V.C. (1973) Application of NIMBUS-4 THIR 6.7 μm observation to regional and global moisture and wind field analysis. J. Appl. Met. 12, pp. 386-395.

Stepanenko, V.D. (1968) Contrast of radio brightness temperature in clouds and precipitation. Transfer of microwave radiation in the atmosphere. U.S. Dept of Commerce, Springfield, Va.

Stout, J.E., Martin, D.W. and Skidar, D.N. (1979) Estimating Gate rainfall with Geostationary satellite image. Mon. Weath. Rev. 107, pp. 585-598.

Suchman, D. and Martin, D.W. (1976) Wind sets from SMS image: an assessment of quality for Gate. J. Appl. Met. 15, pp. 1265-1278.

Suchman, D. and Martin, D.W. (1977) Deep convective mass transport: an estimate from a geostationary satellite. Mon. Weath. Rev. 105, pp. 943-955.

Suomi, V.E. (1969) Recent development in satellite technique for observing and sensing the atmosphere (Edit. Corby). R. Met. Soc. pp. 222-234.

Szava-Kovats, J. (1938) Verteilung de luftfeuchtigkeit auf der Erde. Ann. Hydro. Maritime Met. 60. pp. 373-378.

Taha, M.F., Harbs, S.A., Nagib, M.K., and Tantawy, A.H. (1981) Climate of the nearest east Climate of Southern and Western Asia. World Survey of Climatology Volume 9. (Takahashi, K. and Arakawa, H. "Ed") Elsevier Scientific Publishing Co. Amsterdam, Oxford, New York, 333P

Ward, H.R., Saunder, R.W. and Hunt, G.E. (1981) A case study of summer thunderstorms over European using METEOSAT. Mon. Weath. Rev. (in press)

Weston, K.J. (1980) An observational study of convective cloud streets. Tellus, 32, pp. 433-438.

Wilheit, T.T. (1975) The electrically scanning Microwave Radiometer (ESMR) experiment. The NIMBUS-6 user guide NASA, Goddard Space Flight Centre, Greenbelt, Md.

Wilheit, T.T. Chang, A.T. Rao, M.S. Rodger,E.B. and Theon, J.F. (1977) A satellite technique for quantitatively mapping rainfall rates over the oceans. J. Appl. Met. 16, pp. 551-560.

Woodley, W.L. and Sancho, B. (1971) A first step towards rainfall estimate from satellite cloud photographs. Weather. 26, pp. 279-289.

Woodley, W.L. Sancho, B. and Miller, A.H. (1972) Rainfall estimation from satellite cloud photographs. NOAA Tech. Memo. ERI- OD-11. 43P.

World Meteorological Organisation (1967) The role of meteorological satellite in the World Weather Watch. WWW Planning, Rept. No. 18, 38P. WMO Geneva.

World Meteorological Organization. (1973) The use of satellite pictures for weather analysis and forecasting. WMO. No. 333. Geneva, Switzerland.

Younkin, R.J., La Rue, and Sanders, F. (1965). The objective prediction of clouds and precipitation using vertically integrated moisture and adiabatic vertical moisture. J. Appl. Metero. Vol. 4. No. 1, pp. 3-17